AN ABSTRACT OF A DISSERTATION

PHYSICOCHEMICAL STUDIES OF EXPANDABLE POLYSTYRENE BEADS AND FOAM AS APPLICABLE IN LOST FOAM CASTINGS

Pravin Kannan

Doctor of Philosophy in Engineering

Expandable polystyrene (EPS) is the preferred raw material for making polystyrene foam patterns that finds use in various applications, including as a construction material for buildings, spacecraft insulation, and as pattern mold in metal casting processes. Thus, information regarding the physicochemical behavior of EPS could be used for material and process development. In this study, the decomposition kinetics and gas diffusion characteristics of EPS foams have been investigated.

The goal of the kinetic study was to understand the effects of heating rate and gaseous environment on the decomposition behavior of EPS. Laboratory-scale kinetic experiments (both *low* and *high* heating rates) were carefully designed to collect pyrolysis data that were later used to estimate values for kinetic parameters, including activation energy and pre-exponential constant. A thorough review of literature on the available kinetic models have been presented and discussed. During the course of this study, a simple, yet effective, *fast* pyrolysis technique has been demonstrated for studying decomposition kinetics of various materials, including polymers and bio-mass.

Diffusion studies focused towards understanding the gas diffusion behavior through expanded polymeric foams from a *multiscale* perspective. An experimental technique was developed to collect gas transmission data for both monolithic polymer films and expanded foams. An existing coarse multiscale model available in the literature was further developed to account for the diffusion anomalies due to certain morphological features of the foam. The experimental data was utilized to validate the multiscale behavior and estimate the fractional contribution of the individual diffusion mechanisms. Results highlight the significance of the multiscale model in exploring and understanding the microstructure of the foam.

PHYSICOCHEMICAL STUDIES OF EXPANDABLE POLYSTYRENE BEADS AND FOAM AS APPLICABLE IN LOST FOAM CASTINGS

A Dissertation

Presented to

the Faculty of the Graduate School

Tennessee Technological University

By

Pravin Kannan

In Partial Fulfillment

of the Requirements of the Degree

DOCTOR OF PHILOSOPHY

Engineering

May 2009

CERTIFICATE OF APPROVAL OF A DISSERTATION

PHYSICOCHEMICAL STUDIES OF EXPANDABLE POLYSTYRENE BEADS AND FOAM AS APPLICABLE IN LOST FOAM CASTINGS

by

Pravin Kannan

Graduate Advisory Committee:

Joseph J. Biernacki, Chairperson — 4-29-09 — date

Donald P. Visco Jr. — 4.29.09 — date

Pedro E. Arce — 4.29.09 — date

Kenneth R. Currie — 4/29/09 — date

Holly A. Stretz — 4/29/09 — date

Approved for the Faculty:

Francis Otuonye

Associate Vice President for Research and Graduate Studies

5/6/09

Date

DEDICATION

To my family

ACKNOWLEDGEMENTS

My dissertation would not have been made possible without my advisor, Prof. Joseph J. Biernacki. Since the time I have worked with him (January 2001), he has provided immense guidance and steered me in the proper direction. Among all the people whom I have/will come across in life, he will always stand out for his kindness, support, understanding, character, dedication, and above all, his simplicity.

I would like to extend my sincere appreciation to Prof. Donald P. Visco, Jr., who has made this research more effective with his invaluable knowledge and guidance. His technical and language comments have made this dissertation look more professional than before. I would also like to thank my committee members, Dr. Pedro E. Arce, Dr. Holly A. Stretz, and Dr. Kenneth R. Currie for their comments and participation.

I wish to thank Mr. Dan Dodson for his technical assistance with the FID. His contribution to the success of this work is priceless. My thanks also extend to Perry Melton for his assistance in machining the parts used in the experiments.

I would also like to thank the Center for Manufacturing Research at Tennessee Technological University, Department of Energy, Oakridge National Laboratories for their financial support.

Finally, above all, to my family and friends without whom this work wouldn't have been made possible. Their unwavering love, support, and encouragement has been my biggest companion and asset during the hard times and saved my life. I am indebted to all of you.

TABLE OF CONTENTS

Page

LIST OF FIGURES viii

LIST OF TABLES xi

GENERAL INTRODUCTION xii

PART

1. A REVIEW OF PHYSICAL AND KINETIC MODELS OF THERMAL DEGRADATION OF EXPANDED POLYSTYRENE FOAM AND THEIR APPLICATION TO THE LOST FOAM CASTING PROCESS 1

1.1. Introduction 1

1.1.1. EPS foam pattern manufacturing process 2

1.1.2. Introduction to the LFC process 3

1.2. Chemistry and mechanism of polystyrene degradation 6

1.3. Review of physical models of foam degradation 8

1.3.1. Zhao's physical model of foam degradation 9

1.3.2. Cai's physical model of foam degradation 10

1.3.3. Molibog's foam decomposition model 11

1.4. Review of kinetic models of polystyrene foam decomposition 13

1.4.1. Westerhout's "*random chain dissociation*" kinetic model 14

1.4.2. Bockhorn's kinetic model 15

1.4.3. Faravelli's kinetic model 16

1.4.4. Liu's kinetic experiment 17

1.4.5. Carniti's kinetic experiment 19

PART Page

1.4.6. Anderson and freeman's kinetic model 20

1.4.7. Simard's kinetic experiment 21

1.4.8. Molibog's kinetic model 22

1.5. Analysis and discussion 23

1.6. Endnotes 34

2. LOW-HEATING RATE KINETICS OF THERMAL DECOMPOSITION OF EXPANDABLE POLYSTYRENE IN DIFFERENT GASEOUS ENVIRONMENTS 36

2.1. Introduction 36

2.2. Literature review 37

2.3. Experimental procedure and analysis 40

2.4. Results and discussion 41

2.4.1. Effect of heating rate on PS degradation 41

2.4.2. Effect of gaseous environment on PS degradation 46

2.4.3. Kinetics of EPS degradation 48

2.5. Conclusions 55

2.6. Endnotes 56

3. FAST PYROLYSIS KINETICS OF EPS 57

3.1. An overview 57

3.2. Introduction 57

3.3. Background of the Technique 58

3.4. Experimental Setup 60

3.5. EPS pyrolysis: - Results and Discussion 69

3.6. Conclusions 90

PART Page

3.7. Endnotes 91

3.8. Appendix 3.1 92

4. A SIMPLE MULTI SCALE TECHNIQUE FOR DETERMINING GAS DIFFUSIVITY THROUGH EPS FOAMS 94

4.1. An overview 94

4.2. Introduction 94

4.3. Literature review 98

4.4. Experimental procedure 104

4.4.1. Flow-zero net pressure gradient diffusion experiment 106

4.5. Mathematical modeling 109

4.6. Results and discussion 114

4.7. Conclusions 121

4.8. Endnotes 123

Summary 125

Vita 126

LIST OF FIGURES

Figure Page

1.1. Schematic representation of the foam pattern manufacturing process 4

1.2. Propagation reactions (a) H-abstraction, (b) β-decomposition, (c) Unzipping reaction 8

1.3. Schematic of the foam degradation process 12

1.4. Comparison of Liu's kinetic predictions and experimental data at various temperatures 27

1.5. Comparison of Carniti's kinetic predictions and experimental data at various temperatures 28

1.6. Plot of fractional conversion and pyrolysis times predicted by various kinetic models at a temperature of 370 ºC 29

1.7. Plot of fractional conversion and pyrolysis times predicted by various kinetic models at a temperature of 400 ºC 30

2.1. TGA curves of EPS degradation at different heating rates in nitrogen 42

2.2. DTG curves of EPS degradation at different heating rates in nitrogen 43

2.3. Multiple TGA runs of EPS degradation in helium at 20 K/min showing good reproducibility 45

2.4. TGA scans of EPS degradation at a heating rate of 5 K/min in different atmospheres 47

2.5. Kinetic analysis using the *modified* Coats-Redfern method for EPS degradation in Nitrogen environment 50

2.6. Activation energies of EPS degradation at different conversion levels in all environments 53

3.1. Experimental setup of the *fast* pyrolysis technique used in this study 61

3.2. A view of the SRI Capillary FID Gas Chromatograph 63

3.3. Dispersion test in the reactor and transfer lines using the gas standard 67

Figure Page

3.4. Effect of reaction temperature on dispersion test 68

3.5. A comparison plot of FID *raw* peak intensities of EPS pyrolysis at different temperatures 70

3.6. A comparison plot of normalized peak intensities of EPS pyrolysis at different temperatures 71

3.7. Reproducibility test; three different FID response curves at reactor temperatures of 511, 513, and 518 ºC 73

3.8. Reproducibility test; Derivative of three different FID response curves at reactor temperatures of 511, 513, and 518 ºC 74

3.9. Comparison of total area under the FID curves at different temperatures experimental 75

3.10. Experimental yields; fraction of volatiles at different reactor temperatures 76

3.11. Validity test for single first order reaction for conversion between 0.05 and 0.95 77

3.12. A simplified illustration of the experimental setup 78

3.13. Comparison plot of experimental and theoretical yield fractions of EPS pyrolysis at 750 K 80

3.14. A comparison plot of theoretical and experimental yield at a heater temperature of 763 K 85

3.15. A comparison plot of theoretical and experimental yield at a heater temperature of 1018 K 85

3.16. Variation of activation energy with reaction temperature 87

3.17. Variation of heat transfer coefficient with temperature 87

3.18. EPS sample temperature at various times during the reaction process for various constant reactor wall temperatures 89

4.1. Schematic representation of the gas diffusion process in EPS foams 95

4.2. A multi-scale representation of the morphology of expanded polystyrene beads 97-98

4.3. Overall methodology of the multiscale technique employed in this study 105

Figure Page

4.4. A view of the diffusion cell 106

4.5. Continuous Flow–Zero net pressure gradient diffusion experimental setup 108

4.6. Schematic of a simplified model of foam architecture proposed in this study .. 112

4.7. Argon gas diffusion through PS films of various thicknesses of 0.03, 0.11, 0.12, and 0.27 mm 115

4.8. Dimensionless gas concentration versus time through PS films of thicknesses, 0.03, 0.11, 0.12, and 0.27 mm 116

4.9. Argon gas diffusion through 1 cm thick EPS foam – Comparison of experimental vs. model predictions 118

4.10. Reproducibility test for film experiments using 0.03 mm film at three individual runs 119

4.11. Reproducibility test for foam experiments using a 1 cm thick EPS sample 119

LIST OF TABLES

Table Page

1.1. Summary of polystyrene decomposition kinetic experiments/models reviewed in this study 24

1.2. Regression coefficient values obtained from the analysis of experimental data provided by Liu et al. [1.18] and Carniti et al. [1.13] for the most commonly used mechanisms summarized by Criado et al. [1.33] 32

2.1. Comparison of experimental EPS peak volatilization decomposition temperature measured in this work versus predicted values using Liu's model in air at various heating rates 44

2.2. Activation energies of EPS decomposition in various environments 51

3.1. Major Composition of the hydrocarbon gas mixture used as a standard in this study 65

3.2. EPS Pyrolysis Study Experimental Matrix 69

3.3. Values of various system and thermal parameters used for calculations 81

3.4. Values of kinetic parameters, heat transfer coefficient, and reactor volume estimated by optimization with their corresponding standard deviations based on a 99% confidence interval 86

3.5. Standard deviations of kinetic parameters, heat transfer coefficient, and reactor volume based on statistical error (S.E) and experimental error (E.E) 90

4.1. Experimental diffusivity values of argon diffusion in polystyrene films 116

GENERAL INTRODUCTION

Expandable polystyrene (EPS) is the preferred *raw* material for making polystyrene foam patterns that finds use in various applications, including as a construction material for buildings, spacecraft insulation, and as pattern molds in metal casting processes. A common metal casting technique, for example, is the *lost* foam casting (LFC) process wherein knowledge of gas diffusion through expanded polystyrene (EPS) foam, and foam decomposition kinetics may lead to new and improved practices. Foundry trials have shown that when the foam is purged with helium before casting, the foam pyrolysis efficiency and the quality of the cast part is improved significantly. However, the role of the gaseous environment in purging and during casting is not yet understood. These and similar challenges form the basis and motivates the present research on diffusion in EPS foam.

In this study, the decomposition kinetics and gas diffusion characteristics of EPS have been investigated. While diffusion studies would help to understand the gas diffusion behavior through expanded polymeric foams from a *multiscale* perspective, kinetic studies would serve to understand the effects of heating rate and gaseous environment on the decomposition behavior of EPS.

This dissertation has been divided into four parts. Part 1 provides a brief introduction to the synthesis of EPS, *Lost foam* casting technique, and a thorough review of the most recent research on polystyrene decomposition kinetics and models. Parts 2 and 3 discuss the experimental techniques employed for both the low heating rate non-isothermal, and the isothermal fast pyrolysis decomposition studies performed as part of

this research. Finally, Part 4 focuses on the development of the experimental setup and multiscale model used for data collection and analysis respectively for the diffusion studies.

PART 1

A REVIEW OF PHYSICAL AND KINETIC MODELS OF THERMAL DEGRADATION OF EXPANDED POLYSTYRENE FOAM AND THEIR APPLICATION TO THE LOST FOAM CASTING PROCESS

1.1. Introduction

One of the most widely used methods of metal casting involves the liquid metal displacement of refractory coated expendable foam patterns by means of thermal decomposition. This technique is referred to by several terms including expendable pattern casting (EPC), evaporative pattern casting, lost foam casting (LFC), full mold process, Castyral process, Replicast process and Policast process [1.1]. In the remainder of this dissertation, this process will be referred to as lost foam casting or by the acronym LFC. The LFC process is widely employed by the automotive industry for making engine components [1.1]. Aluminum and iron castings are the most common; however, magnesium castings could be a potential replacement in high temperature applications because of its improved strength-to-weight ratio.

This thesis provides a brief introduction to the LFC process and the importance of polystyrene foam decomposition to process productivity. Herein the authors review the most recent research on polystyrene decomposition kinetic models, though provide a more comprehensive list of citations going back to 1949.

1.1.1. Expanded Polystyrene (EPS) Foam Pattern Manufacturing Process

Expandable polystyrene is the raw material used for the molding of expanded polystyrene foam patterns. Styrene monomer, water, initiator and suspending agents are charged to the polymerization reactor in which the monomer is dispersed in water by the suspending agents throughout the reaction. Suspending agents mainly consist of insoluble inorganic salts such as magnesium carbonate, which are added to prevent the monomer droplets from coalescing. As the reactor is heated, polymerization takes place within the droplets at a controlled reactor temperature and pressure. After polymerization, the polymer-water slurry is cooled and centrifuged to separate the water from the polymer beads. The beads are then dried, size-distributed, and stored in tanks. The beads, along with water and a blowing agent like pentane or butane, are added to the impregnation reactor. The blowing agent dissolves in the polymer melt and about 5-7% of the blowing agent is entrapped inside the polymerized beads [1.2]. At this stage, the sizes of the beads are about 0.1 inch in diameter [1.2]. The slurry is again washed, dewatered, dried, and mixed with additives to improve the processing characteristics. These beads are referred to as expandable polystyrene beads.

The term 'expanded polystyrene' (EPS) refers to a closed-cell, lightweight, rigid plastic foam [1.2]. It is usually produced by a process known as steam molding. The expandable polystyrene beads are loaded into a pre-expander and steam is introduced to heat and soften the polymer and expand the entrapped gaseous blowing agent. Control of density and bead distribution is critical. After pre-expansion, the beads are stored in stabilization tanks to eliminate excess water contained in and on the surface, which

otherwise is detrimental to the molding process. The mold cavity is preheated, filled with the beads, and again heated by steam. This causes the pre-expanded beads to further expand into the voids and fuse together into a rigid mold. This rigid mold, called expanded polystyrene, is patterned into a desired shape and used in the LFC process as a casting pattern. Figure 1.1 is a schematic representation of the expanded foam pattern manufacturing process.

1.1.2. Introduction to the LFC Process

The LFC process, first introduced by M. C. Flemmings in 1964 [1.2], was modified from the full mold process originally developed by H. F. Shroyer in 1958 [1.2]. The LFC process is distinguished from the full mold process by the use of unbonded sand as opposed to the bonded sand in the latter. The expanded polystyrene pattern is coated with a layer of refractory slurry by spraying, dipping, or pouring. Significant care is taken in controlling the coating thickness as thickness affects coating permeability and performance [1.1]. The coating serves the following functions: (1) provides a barrier for avoiding metal penetration into the sand, (2) prevents sand collapse into the gap between the metal and the foam, and (3) provides stiffness to the pattern to help minimize distortion. The coated pattern is dried and placed into a flask, which is then filled with unbonded sand that is compacted using a vibration table. The metal is liquefied and poured into the mold at a prescribed rate; rapid enough to prevent mold collapse, but

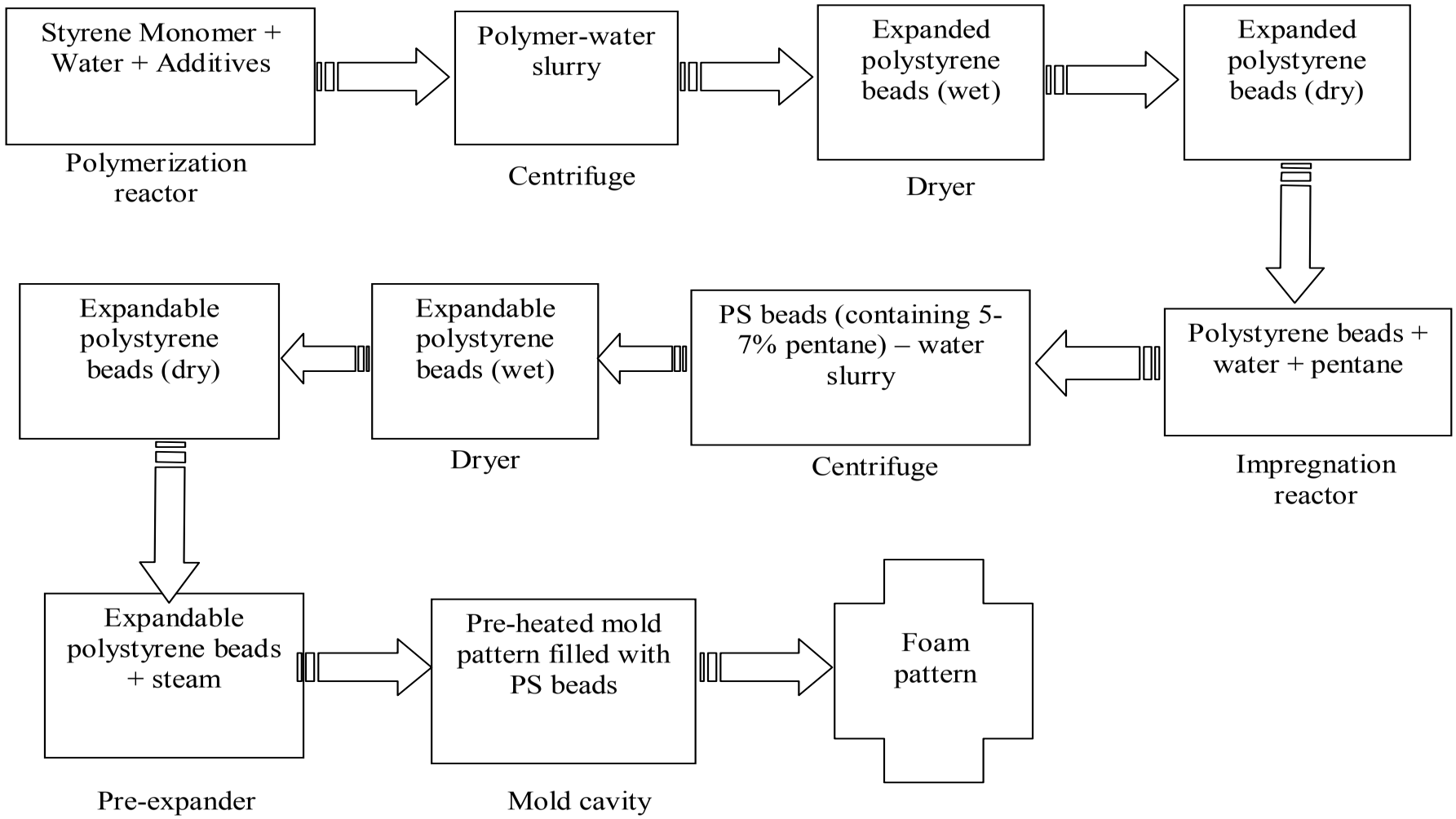

Figure 1.1: Schematic representation of the foam pattern manufacturing process

sufficiently slow to allow decomposition products to escape through the coating and the sand. The foam is degraded through a series of reactions and the metal replaces the foam to yield the casting after solidification.

Although LFC was thought to provide improved casting accuracy, dimensional control, repeatability, and process flexibility as compared to conventional *Green sand* casting techniques [1.3], it was soon found that lost foam castings contained numerous defect forms, mostly associated with incomplete removal of the foam material [1.3]. Advances in LFC are expected to include design of foam microstructure, chemical modification of the polymer, inclusion of decomposition aids, optimization of coating formulations, and development of engineering models that describe the casting process [1.3]. The latter of these, engineering models, if accurate in predicting the metal fill, solidification, and defect formation, could be used to optimize the process and, hopefully, significantly reduce production time and cost [1.4]. Unfortunately, existing computer codes do not include all of the physics and chemistry necessary to define the casting process, i.e. the kinetics of foam degradation and, hence, cannot predict the process performance over a wide range of conditions. The major problem faced by modelers is the lack of data availability on the metal/pattern exchange process [1.4]. This, in part, is due to the challenges of setting up a lab-scale experiment that adequately mimics the conditions of the commercial casting process. Most of the available data, including heat transfer parameters, material degradation parameters, chemistry, and mechanism of foam decomposition are scattered throughout the literature and frequently seem conflicting. This dissertation aims to review, summarize, and discuss the chemistry and kinetic aspects of polystyrene foam degradation for the aluminum lost foam casting process.

1.2. Chemistry and Mechanism of Polystyrene Degradation

EPS foam used in the LFC process is an amorphous, linear polymer composed of 92% carbon and 8% hydrogen by weight [1.5] and has a molecular weight ranging from 300,000 to 500,000. The physical properties of polystyrene beads typically used in aluminum castings include a density of .02 to .026 g/cm^3 and an average bead diameter of 1.4 mm (.055 in). A polystyrene bead, when subjected to thermal decomposition, softens at about 120 ˚C, melts at 160 ˚C, and completely volatilizes between 470 and 500 ˚C [1.6]. Softening is accompanied by a decrease in the bead size from its expanded size to the unexpanded size. The average heat of degradation of the EPS foam has been estimated to be 800 J/g (191.08 cal/g) [1.5]. Results from other differential scanning calorimetric (DSC) experiments [1.6] have proved that the initial bead structure and polymer density does not have a significant effect on the heat of degradation. It has been observed that the rate of molecular weight decrease is very high at the initial stages of the reaction and slower at later stages, accompanied by the evaporation of the low molecular weight fragment species [1.7]. This process takes place regardless of the original form of the polystyrene. Since this study looks at the rate of decomposition of polymer from a foamed precursor, it will be referred to as "foam decomposition," not inferring that the foamed form is present during decomposition, but rather that the polymer was originally in a foamed state. Degradation refers to the reduction in molecular weight of the polymer [1.8].

The thermal stability of polystyrene depends on a number of parameters including the presence of additives, number of weak bonds, method of synthesis, etc. [1.9]. For

instance, polystyrene is more stable thermally when prepared in the presence of oxygen than in the absence [1.9]. Upon thermal decomposition, polystyrene yields the styrene monomer and various saturated and unsaturated fragments. Literature suggests that the styrene monomer is the major product among the decomposition species when complete depolymerization takes place below 500 ˚C [1.8]. At temperatures above 500 ˚C, the oligomers undergo further defragmentation and form low molecular weight gaseous species, including toluene, benzene and significant amounts of partially depolymerized viscous residue, containing dimer, trimer, tetramer and other oligomers of styrene [1.10].

The ratio of gaseous to liquid products increases at temperatures above 750 ˚C, implying more polymers degrade into the gaseous phase at those temperatures as the exposure time increases [1.11]. The degradation of polystyrene occurs by a radical chain process characterized by three consecutive steps: (1) initiation, (2) propagation and (3) termination. Since most of these reactions involve a C-C bond cleavage, the thermal stability of polystyrene depends on the strength of its C-C bond. Initiation reactions can either occur by random scission or by C-C bond chain-end cleavage resulting in the production of radicals. Sometimes an external initiator such as bromine is added during the synthesis of PS [1.1]. Results have shown that the presence of bromine in the PS matrix promotes cleavage of the polymer chain into smaller units and, thus, increases the depolymerization rate significantly [1.11]. Propagation reactions consist of the sequence of H-abstraction and β-decomposition or unzipping reactions (refer Figure 1.2 for illustrations). The free radicals formed react with polystyrene to produce short chain radicals. Hence, the rate of the propagation step is dependent on the concentration of free radical sites. Termination usually occurs by the recombination of two radical chains with

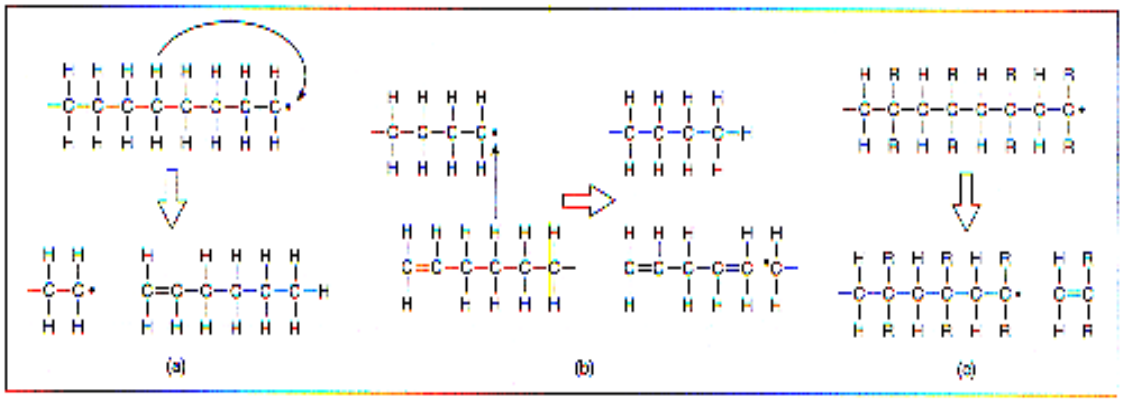

Figure 1.2 [1.12]: Propagation reactions (a) H-abstraction, (b) β-decomposition, (c) Unzipping reaction.

or without the formation of an unsaturated end. The propagation step is considered the most predominant step in the radical chain process

1.3. Review of Physical Models of Foam Degradation

Physical models explain the foam degradation process that occurs when the liquid metal transfers heat energy to the solid foam. They include the formation and elimination of the foam decomposition products from the reaction site to the surroundings, temperature losses in the liquid metal due to heat transfer, permeability of the refractory coating and sand, metal flow behavior, etc. On the other hand, kinetic models describe the rate of formation of decomposition products and/or the rate of elimination of the reactants. A number of physical models have been put forth. The salient and common features of these models, which deal with the gas formation and elimination phenomena, are discussed in this section.

1.3.1. Zhao's Physical Model of Foam Degradation [1.3] (2002)

Zhao proposed the presence of an organic gas-liquid phase between the advancing liquid metal and the retreating solid foam pattern, comprising of a mixture of PS decomposition products. Since the boiling point of polystyrene is about 300 Cº less than the metal temperature, liquid metal is always separated from liquid PS by the gaseous decomposition products. Hence, polystyrene foam gasification cannot be avoided throughout the casting process. According to Zhao's model, initially when the molten metal is poured on to the foam mold, direct contact between the metal and the solid foam occurs. Due to the highly endothermic nature of the degradation process, a significant amount of heat flux occurs during the initial contact phase resulting in immediate vaporization/gasification of the foam. Hence, during the casting period, the contact time is very small and heat transfer by direct contact is one of the predominant modes of heat transfer [1.4].

As the process proceeds, radiation becomes the dominant mode of heat transfer because of the gas layer build up. The radiant heat softens, collapses, and melts the foam, which flows outward, away from the progressing metal front, towards the coating/sand interface where it coalesces and adheres to the coating surfaces. The advancing metal envelopes the coalesced foam products, referred to as "plastic globs" by Zhao. The thermal conductivity of polystyrene is very low; hence, huge temperature gradients exist across the plastic globs. Scanning electron microscopic analysis of the remains of the coating revealed that the temperature at the coating substrate (coating/sand interface) would be less than 150 ºC, and at the plastic/melt interface would be nearly 440 ºC, just

less than the boiling point of PS. Thus, gasification occurs at the melt-plastic interface, which forces the plastic globs to shrink in all directions. As it shrinks, it uncovers the permeable coating through which the gaseous products escape into the sand. The coating, well ahead of the advancing metal front, is undisturbed and is essentially non-permeable because of the plastic globs. Thus, the decomposed gaseous products could escape only through the uncovered coating region between the advancing metal and the retreating foam. Within this region, the gases escape as soon as they are formed and, hence, gasification controls the metal fill rate. Elsewhere, the gas layer builds up due to limited escape paths, and gas removal through the coating controls the mold fill rate. The latter case is particularly true during the initial stages of the process when very little coating substrate is uncovered compared to the volume of gas produced. The liquid metal cools down by transferring heat to the sand and the plastic globs, and begins to solidify. The total pressure, i.e., the sum of gas pressure and metallostatic pressure, increases and forces the ungasified plastic globs into the coating substrate. Partially decomposed plastic globs that were not completely removed from the metal after solidification may be present as defects.

1.3.2. Cai's Physical Model of Foam Degradation [1.11] (2002)

According to Cai et al., the composition of the mixture of degradation products is a function of the time that the products reside in the interface before escaping out through the coating and the sand. The longer that the products remain inside the system, the greater the extent of long chain fragmentation allowing low molecular weight fragments

to build up. By investigating the degradation products resulting from short thermal exposures, Cai et al. proposed an explanation of the physical phenomena of the foam degradation process. Since the majority of the degradation products at the metal front are liquefied polystyrene, physical and chemical properties of the liquefied polystyrene were obtained. The liquid products were mostly recovered from the coating and the sand near the molten metal front. This facilitated the study of EPS foam degradation at the early transient state. From a mass balance and a molecular weight analysis of the thermal degradation products, the following physical model was presented. As the metal advances, it radiates heat to the foam and breaks the long polystyrene chains into smaller chains. The gaseous products escape through the coating and into the sand. The liquid products of low molecular weight species get absorbed into the coating and, when sufficient heat from the metal accumulates in the coating, the absorbed organics decompose into smaller fragments and volatilize. This condensation-volatilization process continues in the sand until the liquid metal loses heat and solidifies.

1.3.3. Molibog's Foam Decomposition Model [1.4] (2001)

A schematic of the physical model of foam degradation proposed by Molibog et al. is shown in Figure 1.3. Explanations concerning the formation and elimination of degradation products are more or less similar to Zhao's physical model [1.3]. According to Molibog et al., a three-phase *kinetic zone* comprising of the solid polymer, liquid polymer, and the gaseous products of foam pyrolysis is formed between the metal and the

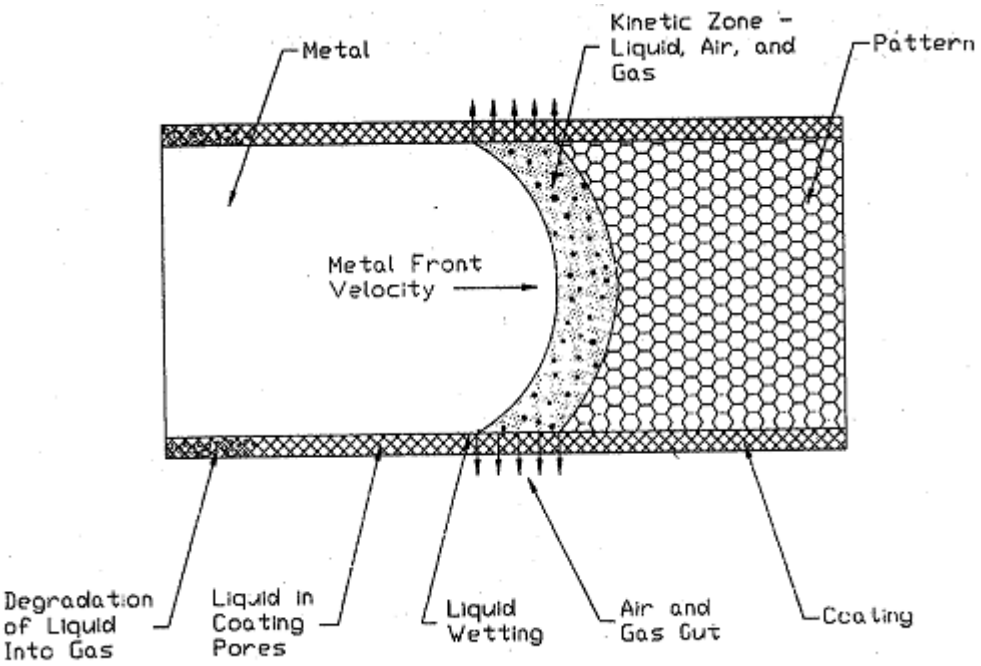

Figure 1.3 [1.5]: Schematic of the foam degradation process.

pattern. In this zone, mass transfer and chemical reactions occur at the same time when heat is exchanged between the metal and the foam during the degradation process. It was argued that the width of this *kinetic zone* and the shape of the metal front dictates the rate of formation and elimination of the pyrolysis products, respectively. Depending on the width of the kinetic zone, the heat transfer from the metal to the pattern varies, consequently varying the amount of energy supplied to the foam. As the width increases, the rate of heat transfer decreases and the gas layer starts to build up. Due to this decrease in heat transfer, the rate of gas generation also decreases until the gaseous products escape from the kinetic zone, thus, starting the process cycle again.

Molibog et al. also believed that the shape of the metal front has a strong effect on the rate of removal of pyrolysis products from the kinetic zone. A convex-shaped metal

front would assist the highly viscous residue to move towards the coating from the center and escape from the kinetic zone. They hypothesize that the shape of the metal front could be controlled by designing foam patterns with density gradients allowing more rapid melt infiltration in some regions and slow infiltration in others.

1.4. Review of Kinetic Models of Polystyrene Foam Decomposition

Most of the kinetic models of PS degradation were developed by researchers working on plastics recycling processes. The processing conditions in the plastics recycling process are similar to that of the casting processes, as the major step in plastics recycling is the pyrolysis of the polymers; however, at a much lower temperature than the former. A temperature range of 250 to 500 ºC was usually selected for these studies as the polymer completely volatilizes in this temperature range. While some experiments were carried out at conditions that favor the production of a particular species, i.e. styrene monomer, because of its rich chemical value, others focused on reducing the pollution caused by the plastics recycling pyrolysis process [1.13]. These experiments used polystyrene in powder or liquid form, different from the actual PS rigid foam. Between each of the PS beads present in the foam pattern, there might be significant differences in physical and chemical properties, like density, entrapped cell gas composition, etc. This is because some PS beads comprising the foam pattern might have been synthesized and exposed to different environmental conditions. Due to this heterogeneity in the foam pattern, the thermal degradation behavior of PS beads and, accordingly, the foam itself cannot be interpreted from earlier experiments. Also, though these experiments provide

kinetic parameters of PS degradation, their application to higher temperatures (600 to 1000 ºC) required by the casting process is questionable due to the lack of experimental data in this temperature range. It is worth noting here that the temperature range in aluminum casting is 800 to 1000 ºC and much higher in iron castings [1.1]. The salient features of some models developed for the plastics recycling process are discussed below.

1.4.1. Westerhout's "Random Chain Dissociation" Kinetic Model [1.7] (1997)

This model explains the kinetics of decomposition of polystyrene by considering the effects of both the physical and chemical processes simultaneously. The physical process refers to the evaporation of the species while the chemical process refers to the actual breakage of chemical bonds. The primary reason for differentiating these processes is because all of the chemical bonds that are broken do not lead to the evaporation of the species. In most other kinetic experiments, heat and mass transfer limitations are not completely accounted for. Hence, the measured kinetic parameters do not reflect the intrinsic kinetic data. The random chain dissociation (RCD) model proposed by Westerhout et al. overcomes these limitations by incorporating a statistical reaction pathway model originally developed by Wagenaar et al. [1.14]. In Westerhout's model, each bond type in the polymer structure is associated with a particular rate constant and activation energy. The rate of change of the number of each bond type, N_i, is given by

$$\frac{\partial N_i}{\partial t} = -k_{0i} \cdot e^{\left(\frac{-E_{ai}}{RT}\right)} \cdot N_i = -k_i \cdot N_i \qquad (1.1)$$

where k_{0i} and E_{ai} are the rate constant and activation energy of the bond type 'i', respectively, and T is the temperature. It was argued that polymer fragments whose chain length is greater than a certain value L_c, which is a function of temperature and pressure, would not evaporate at the given conditions of temperature and pressure. The value of L_c estimated from the boiling points of normal alkanes and alkenes, the length and extent of branching of the polymer chain calculated from initial molecular weight, and the structure of the polymer were provided as input parameters to the model. Based on these values, the conversion was calculated by determining the number and weight of fragments having chain length less than L_c. This model proved to be valid for the entire conversion range, unlike the previously used first order model that was applicable only at high conversions [1.7]. Unfortunately, this RCD model could only be applied at temperatures below 400 ºC, as experimental data could not be obtained at higher temperatures.

1.4.2. Bockhorn's Kinetic Model [1.15] (1998)

Bockhorn et al. used an isothermal "gradient-free" reactor to study the kinetics of gasification of PS in the plastics incineration process. The sample, preheated in a platinum crucible, was introduced quickly into the reaction chamber. The sample is then heated to the desired temperature by mixing the reactor contents using a small gas turbine. The sample was processed and the gas products were analyzed by using an on-line quadrupole mass spectrometer.

From the mass spectrometer data, the experimental conversion was calculated. The kinetic parameters obtained from isothermal kinetic experiments were used to develop a rate equation for PS degradation. Based on a radical chain mechanism, the theoretical degree of conversion was given by the following equation:

$$\alpha(t) = 1 - (k \cdot t \cdot (n-1) + 1)^{1/(1-n)} \qquad (1.2)$$

where $\alpha(t)$ is the degree of conversion, k is the rate constant, t is the reaction time, and n is the apparent reaction order. Using the method of least squares, the degree of conversion obtained from the model is fitted to the experimental degree of conversion by varying k and n. The activation energy and the pre-exponential factor were calculated from the Arrhenius temperature dependency plot. The reaction was found to be first order with respect to the formation of volatiles for a temperature range of 360 to 410 ºC.

1.4.3. Faravelli's Kinetic Model [1.16] (2001)

Faravelli et al. assumed that thermal degradation occurs only in the liquid phase and that gas phase cracking reactions are negligible. In addition, this model incorporates the differences in starting material and a wide range of reaction conditions (i.e., heating rates and temperatures). Based on Faravelli et al.'s previous kinetic models developed for polyethylene and polypropylene thermal degradation [1.17], they calculated the kinetic parameters and volatile distributions for PS degradation. The rate constants were evaluated for each of the individual reactions in the radical chain process. The kinetic

parameters that describe the radical chain reactions were evaluated based on structural contributions as well as similarity and analogy rules [1.18]. Due to the inhibition of molecular rotations of large C-C segments in the condensed phase, available gas phase kinetic data could not be applied directly for the liquid phase degradation. Hence, significant corrections were applied to the gas phase pyrolysis rate constants for the different initiation, propagation and termination radical chain reactions. By using a lumping procedure, the global concentrations of all the radicals were calculated. By relating the chain length of the formed species to temperature and pressure, boiling temperatures for species with different carbon atoms were also determined. All of the decomposition products were categorized into five families and mass balance equations were formulated. The concentrations of various products were computed by numerically integrating the system of ordinary differential mass balance equations. When the product distribution was compared with the experimental data, the model showed little variation with temperature. The concentration increase of some species like 1,3 diphenylpropane, with temperature, could not be accounted for, as additional experimental data was needed to better characterize the model.

1.4.4. Liu's Kinetic Experiment [1.19] (1999)

Liu et al. investigated the kinetics of PS pyrolysis at temperatures ranging from 370 to 500 ºC using the sequential pyrolysis gas chromatography technique. The sample used in this study was a solution of PS (2μL) in chloroform (30 mg/mL). A thin coating of the sample inside a quartz tube is rapidly heated to the desired pyrolysis temperature

using a platinum coil-heating element. The temperature is maintained and the sample was pyrolyzed several times sequentially until fully decomposed. Liu et al. grouped the decomposition products into three categories: low, medium, and high boiling fractions, according to their respective boiling points. The experimental data was fit to a first order rate equation:

$$d\xi / dt = k(1 - \xi) \tag{1.3}$$

where $\xi = m/m_o$, m is the mass of the sample volatilized, and m_o is the initial mass of the sample. Rearranging and integrating the above equation yields

$$-\ln(1 - \xi) = kt \tag{1.4}$$

where t is the reaction time (pyrolysis time). From the experimental data, Liu et al. observed a linear relationship between $-\ln(1-\xi)$ and t for each of the products indicating that the kinetics of formation of volatile products from PS decomposition followed an apparent first order mechanism. A hypothesis for PS decomposition was postulated and the model was simulated using the experimental rate constant data obtained for the three groups of decomposition products. Based on the relative ratios of the rate constants, a parallel reaction pathway for the formation of the three volatile groups was proposed.

1.4.5. Carniti's Kinetic Experiment [1.13] (1989)

Carniti et al. studied the kinetics of formation of radicals of PS degradation by means of direct determination through electron spin resonance (ESR) spectroscopy. The sample, in powder form, was packed and sealed in glass tubes and immersed in a fluidized alumina bath. The temperature of the alumina bath was varied from 360 and 420 ºC for various kinetic runs. The tubes were then cooled, and the contents of the tubes were dissolved in acetone and analyzed by gas chromatography. Since the reaction was carried out in sealed tubes, the escape of gases from the tubes was minimized, although gas phase reactions were still possible.

From kinetic experiments, the weight fractional conversion of PS to volatile products was calculated for various reaction temperatures and times. The kinetic rate parameters were calculated by using the method of least squares to minimize the sum of squared error between the experimental and theoretical weight fractions. The theoretical weight fraction was calculated using the following equation:

$$y = 1 - e^{-k_1 t} \tag{1.5}$$

where y is the theoretical weight fraction of the volatile products. In contrast to all other experiments found in literature, only small quantities of styrene were found because of the experimental conditions employed.

1.4.6. Anderson and Freeman's Kinetic Model [1.20] (1961)

One of the major constraints in using an isothermal TGA experiment for a kinetic study is accounting for the uncertainties of possible chemical reactions during the heating period. In order to overcome this disadvantage, Anderson and Freeman utilized a non-isothermal method to determine the kinetic parameters of the thermal decomposition of polystyrene. This method involved the use of a continual increase in the sample temperature (temperature scanning) to obtain the thermo-gravimetric curves. These curves were differentiated to obtain the following rate equation:

$$\Delta \log\left(\frac{dW}{dt}\right) = n\Delta \log W_t - \left(\frac{\Delta E}{2.3 \cdot R}\right) \cdot \Delta\left(\frac{1}{T}\right) \qquad (1.6)$$

where dW/dt represents the reaction rate, E_a the activation energy, R the gas constant, T the absolute temperature, and W_t is proportional to the amount of reactant. The reaction order, n, and activation energy were calculated as the slope and intercept, respectively, from a plot of $\Delta\log (dW/dt)$ versus $\Delta\log W_t$ for values of $\Delta (1/T)$. From the temperature dependency plot, Anderson and Freeman showed that the decomposition reaction follows zero order kinetics during the initial stage of the reaction, up to 10% weight conversion. Between 15 and 95% weight loss, it follows first order kinetics and the activation energy increases. The results indicate the presence of at least two different mechanisms of polystyrene degradation, one below 370 ºC and the other above 370 ºC.

1.4.7. Simard's Kinetic Experiment [1.21] (1995)

Simard et al. studied the recovery of styrene monomer by thermolysis of PS in a nitrogen atmosphere between 368 and 407 ºC. Polystyrene, in powder form, was placed in a reactor fitted with a four necked lid, a heating mantle and a mixing paddle. Heating rates of 20 to 40 ºC/min were employed. The volatiles were condensed and collected in a rotating vessel equipped with six receiving flasks. The vessel was sequenced during the experiment to allow staged collection of off-gas as a function of reaction time. The liquid fractions were analyzed by gas chromatography/gas chromatography-mass spectroscopy and the residues by cryoscopy and nuclear magnetic resonance to determine the composition and molecular weight, respectively. From plots of volatile yield as a function of reaction time for different reaction temperatures, it was concluded that the rate of volatile generation follows a first order mechanism for most of the reaction time. A simple expression identical to Equation (1.3) can be inferred from their figures and text.

Simard et al. also reviewed a number of earlier works [1.13, 1.21-1.29] and noted that polystyrene decomposition reactions have been described as zero–order kinetics, first-order kinetics, or both, based on the weight loss, monomer generation, or other variables including molecular weight and free radicals generation. In one particular case [1.27], it was even found that the activation energy is independent of the order of the decomposition reaction.

1.4.8. Molibog's Kinetic Model [1.30] (2002)

Molibog's attempt to model the metal/pattern exchange phenomena in the LF casting process is not only very significant in understanding the decomposition process better, but also seems to be one of the first realistic lab-scale experiment which closely mimics the foundry casting process. There is little doubt that his work will provide a foundation for future developments in the modeling of the metal/pattern exchange process in LF castings.

Molibog assumed that the kinetics of polystyrene foam decomposition follows a zero order reaction. In other words, it was assumed that the conversion of the foamed polymer to liquid and gaseous products is proportional to the reaction time and hence the rate of gas generation was presumed to be only a function of the temperature. This can be expressed as $\alpha = K(T)\ t$, where α is the conversion, K is the reaction rate, T is the temperature and 't' the reaction time. Differentiating the above equation, it follows that

$$R_v = \frac{d\alpha}{dt} = K(T) \tag{1.7}$$

where R_v is the gas generation rate. Assuming an Arrhenius type relationship, the integrated form of the above equation can be written as

$$\log(R_v) = \log(K_0) - \left[\frac{E}{R \cdot \ln(10)}\right]\frac{1}{T} \tag{1.8}$$

The activation energy was reported as 113.3 KJ/mole and was found to be about 40% less than the literature values. Molibog attributed the discrepancy to the insulating effect of the gas film, which creates a temperature difference between the foam surface and the heater surface.

A summary of all the above-discussed kinetic models is presented in Table 1.1.

1.5. Analysis and Discussion

The primary aim of this work is to review the available polystyrene decomposition kinetic models and to assess their applicability for the LFC process. Most of the aforementioned kinetic experiments measure the weight loss during the degradation process and determine the fractional weight conversion of the initial sample or the fractional yield of the volatiles over a period of time at some fixed temperature. Bockhorn [1.14] quantified the product gases using on-line mass spectrometry and reported experimental conversion on a normalized scale. Bockhorn defined degree of conversion as the mass of gas products evolved at times ‘t‘ divided by the total mass of evolved gas products when the sample was pyrolyzed completely. Simard [1.20] condensed and measured the volatiles and reported kinetic data in terms of product yield, which was defined as the ratio of the weight of condensate to the weight of initial polystyrene. Liu’s [1.18] technique involved pyrolysis of the sample several times sequentially for the same length of time until no gaseous products are evolved from the sample. The cumulative amounts of the gaseous products were measured and the weight

Table 1.1: Summary of polystyrene decomposition kinetic experiments/models reviewed in this study

Author	Sample conditions	Processing conditions	Experimental technique	Measured parameter	Calculated parameter	Model proposed?	Activation energy KJ/mol
Anderson [1.19]	Powder PS, MW=360000	30-500 ºC, 5 ºC/min, vacuum	Non-isothermal TGA	Weight loss	Weight conversion	Yes	193 - 273
Bockhorn [1.15]	PS, MW=186000	360-410 ºC, 0.6-1.5 ºC/min, helium	Sample introduced into a preheated reactor coupled with online MS	Total ion current	Weight conversion	Yes	168 -176
Carniti [1.14]	Powder PS	360-420 ºC, vacuum	Tubes filled with PS and heated in a fluidized alumina bath	Amount of volatile products	Weight conversion	Yes	195
Liu [1.18]	Solution of PS in chloroform	370-500 ºC, 13-26 ºC/min, nitrogen	Thin coating of PS evaporated on the sample holder placed in a pyrolyzer equipped with GC	Amount of volatile products	Yield fraction	Yes	71.3
Molibog [1.30]	Polystyrene foam	600–800 ºC, nitrogen	Sample pushed against a heated plate at constant velocity	Weight loss	Gas fraction	Yes	113.3
Simard [1.20]	Powder PS, MW=138000	370-420 ºC, 20-40 ºC/min, nitrogen	Sample heated in a reactor vessel and volatiles collected in receiving flasks	Amount of volatile products	Yield fraction	No	166.5
Westerhout [1.8]	Less than 3mg of PS	365-400 ºC, nitrogen	TGA	Weight loss	Weight conversion	Yes	204

fractional yields were calculated for each pyrolysis temperature. Faravelli [1.16] modeled the degradation process and reported volatilization or conversion on a normalized scale similar to Bockhorn. Carniti [1.13] measured the sample weight loss and defined conversion based on the initial sample weight. As seen above, authors have either used initial sample weight or the total mass of evolved gas products to define degree of conversion. Interestingly, Carrasco et al. [1.31] found that there is very little carbonaceous residue left when polystyrene is completely decomposed. Hence, it could be safely assumed that the value of the total evolved gas products upon complete pyrolysis would be the same as the initial sample weight. This assumption is the basis for Figures 1.4-1.7 discussed in this section.

In this review work, two different pyrolysis temperatures, 370 and 400 ºC, were selected as the basis for analysis and comparison. Experimental kinetic data published by different researchers are available at these two temperatures and hence is the reason for selecting these temperatures in this review. All the experimental data were collected from the kinetic plots presented by the mentioned authors. Model data were obtained from simulation of the kinetic equations using their respective kinetic parameters. For example, Liu's model data was collected by simulating Equation (1.4), with the values 1.16E04 sec^{-1} and 71300 J/mol for the pre-exponential constant and activation energy, respectively. Figures 1.4 and 1.5 compare the fractional yield of volatiles over different pyrolysis times obtained from Liu's and Carniti's kinetic model and experiments. As seen from both the figures, the Carniti model prediction is quite good whereas there is minor deviation in Liu's model prediction. Figure 1.6 compares the results from different kinetic models and experiments for which the fractional conversion of polystyrene versus

pyrolysis times at 370 ºC could be determined. Figure 1.7 compares the kinetic data from various experiments and models at a temperature of 400 ºC. The time scale in Figure 1.7 is very much smaller than the one used in Figure 1.6 as smaller time intervals are employed to decompose the polymer at the higher temperature [1.19]. It could be seen from Figures 1.6 and 1.7, that Liu et al. achieved a much higher decomposition reaction rate and conversion compared to others, which could be attributed to the sequential pyrolysis technique employed in the experiment.

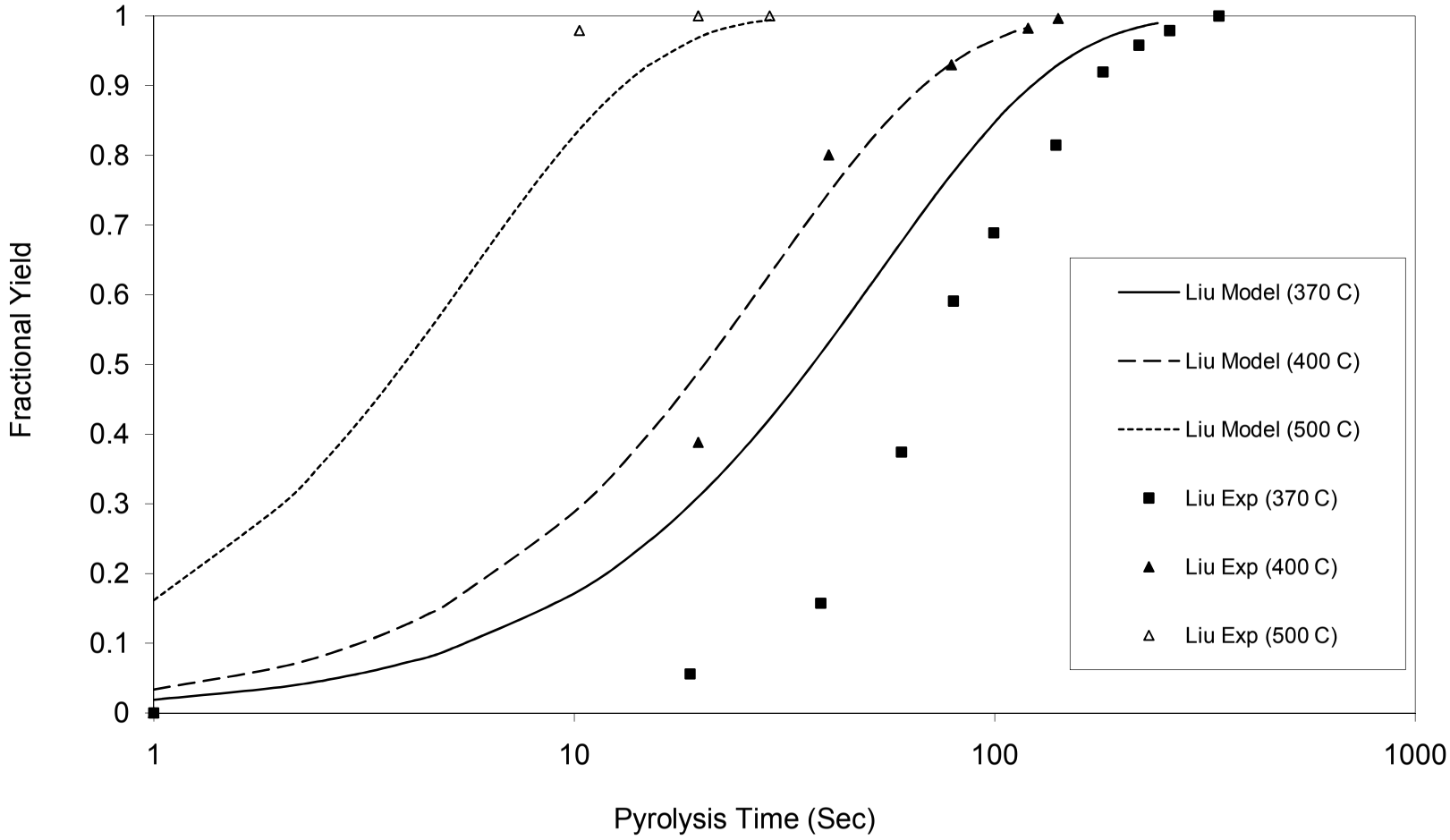

Figure 1.4: Comparison of Liu's kinetic predictions and experimental data at various temperatures.

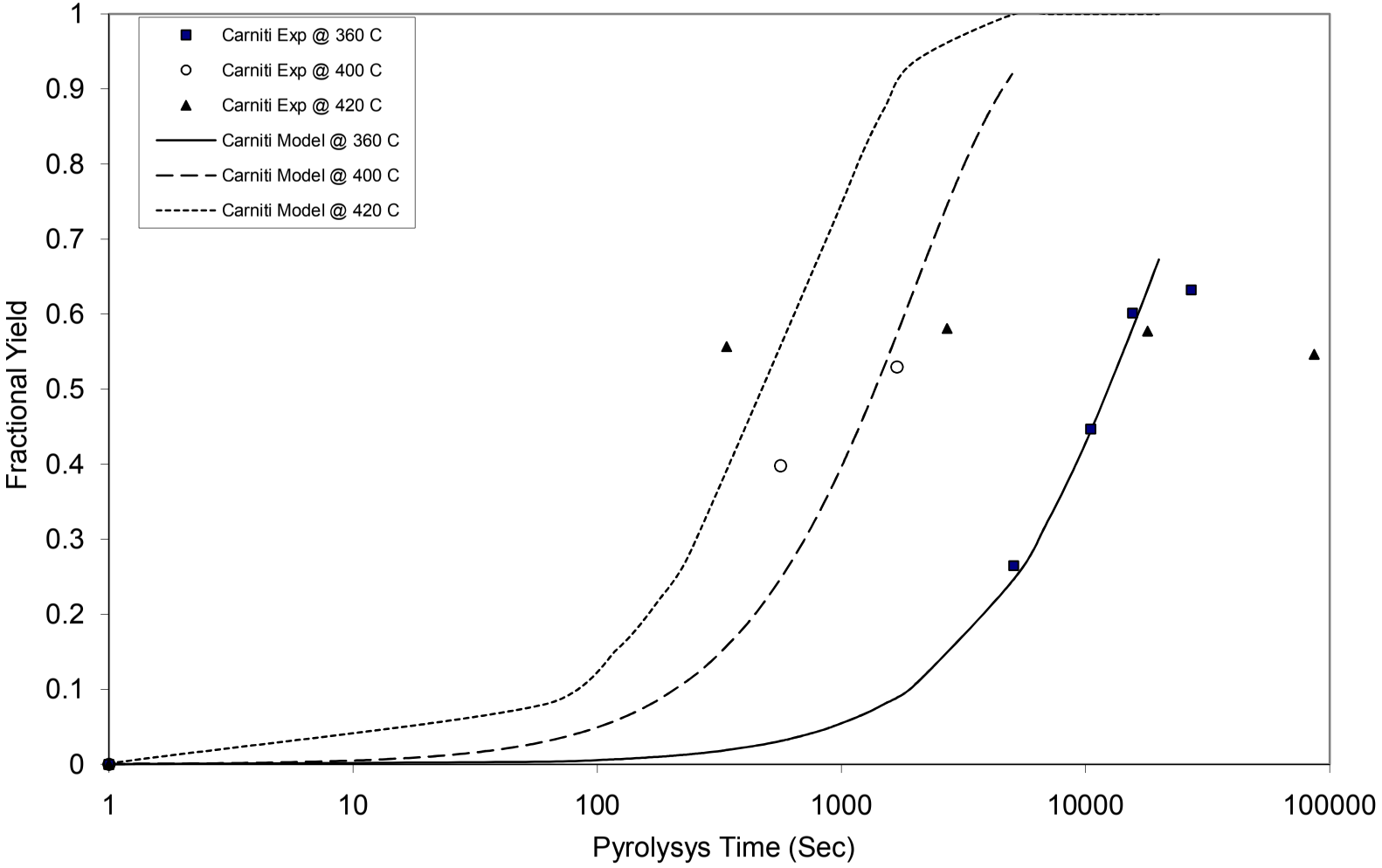

Figure 1.5: Comparison of Carniti's kinetic predictions and experimental data at various temperatures.

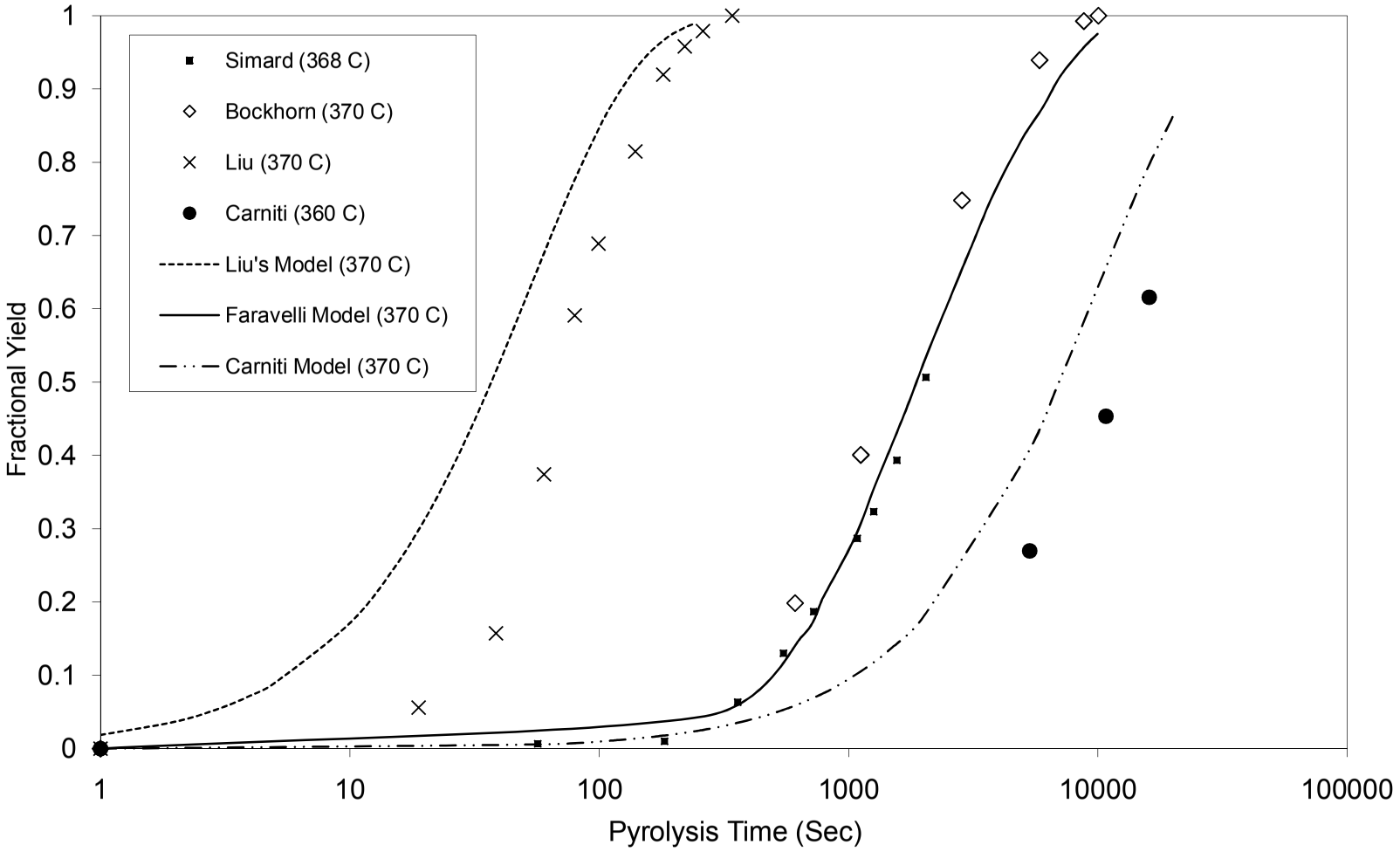

Figure 1.6: Plot of fractional conversion and pyrolysis times predicted by various kinetic models at a temperature of 370 ºC

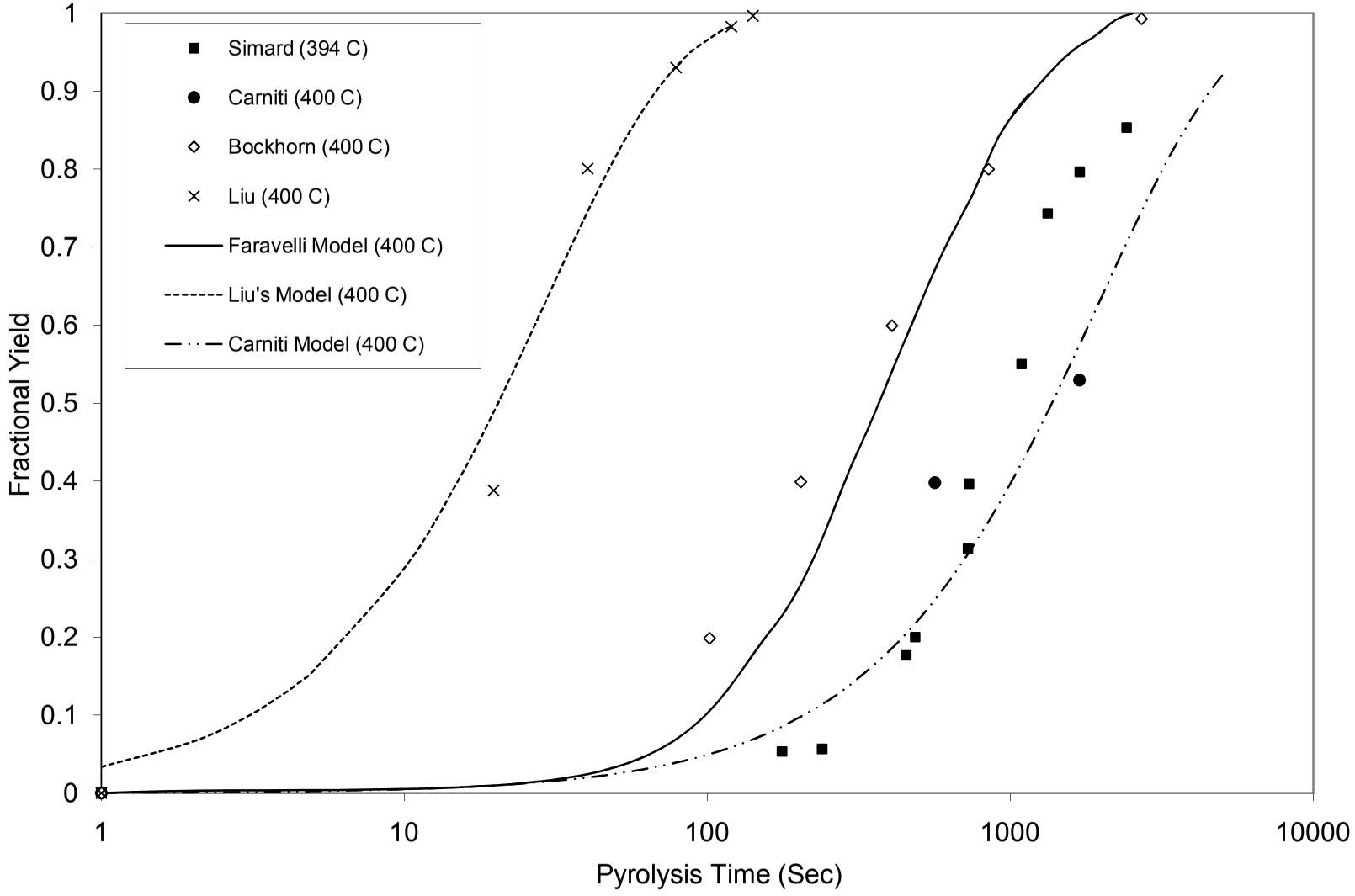

Figure 1.7: Plot of fractional conversion and pyrolysis times predicted by various kinetic models at a temperature of 400 ºC.

It is evident from the figures that each kinetic model is consistent only with its corresponding experimental data set. None of the models is flexible enough to predict the degradation when carried under different operating conditions. The disagreement between the models, and even between the experimental results, likely reflect differences in synthesis conditions of the starting material, molecular weight of the polymer, sample processing conditions, and the method of data collection.

The findings of Tanaka et al. [1.32] and Criado et al. [1.33] suggests that experimental kinetic data for solid-state reactions can be equally well described by virtually any one or many reasonable rate laws available in literature for solid–state decompositions. If this hypothesis is true for a particular solid-state reaction, then it becomes very difficult in selecting the appropriate integral function that describes the actual mechanism of the reaction. In other words, the kinetic parameters, namely the activation energy and pre-exponential constant, become independent of the kinetic equation of the solid-state reaction. This hypothesis was tested for polystyrene decomposition experimental data of Liu et al. and Carniti et al. The conversion-time data was fitted to different mechanistic functions summarized by Criado et al. Table 1.2 shows the regression coefficient values obtained from the analysis of Liu et al.'s and Carniti et al.'s kinetic data. It is obvious that the data fits well to at least more than one of the integral functions considered and the authors Liu et al. and Carniti et al. have failed to consider this hypothesis. The conclusion is that it is difficult to predict the correct reaction order for the polystyrene foam decomposition reaction just based on any of the above-discussed kinetic models alone.

Table 1.2: Regression coefficient values obtained from the analysis of experimental data provided by Liu et al. [1.18] and Carniti et al. [1.13] for the most commonly used mechanisms summarized by Criado et al. [1.33].

Mechanistic Integral Function	**Linear Regression Coefficient**	
	Liu et al.	**Carniti et al.**
α	.9564	.9045
$2(1-(1-\alpha)^{1/2})$	.9807	.9207
$3(1-(1-\alpha)^{1/3})$	.9869	.9253
$-Ln(1-\alpha)$	.9953	.9330
$(-Ln(1-\alpha))^{1/2}$	.9742	.8673
$(-Ln(1-\alpha))^{1/3}$	.9617	.8152
α^2	.9882	.9392
$(1-\alpha)\ Ln(1-\alpha) + \alpha$	.9948	.9409
$(1-(1-\alpha)^{1/3})^2$	.9936	.9413
$(1-2\alpha/3) - (1-\alpha)^{2/3}$	.9955	.9412

Although the pyrolysis experiment designed by Molibog captured the relevant physics of the LF casting process; it is not ideally suitable as a kinetic experiment. It was reported that the heater surface temperature fluctuated by about ± 50 °C during the entire run of each foam pyrolysis [1.34]. It is well-known in the field of reaction engineering that the reaction rate doubles for every 10 °C increase in temperature [1.35]. Hence, better temperature control that keeps the fluctuations to a minimum and/or heaters that

could provide sufficient heat flux for the pyrolysis reaction are needed to collect more meaningful kinetic data.

The very high heating rates and high temperatures employed in the LFC process would further increase the model deviation resulting in poor agreement between the model prediction and experimental results. Therefore, none of the aforementioned models or experiments can be used to predict the LFC decomposition process accurately. It is important to mention again that all of these kinetic experiments were developed for the plastics recycling industries wherein the processing conditions are much different than for the LFC industry. Polystyrene decomposition would not be the same for these processes and hence the authors suggest that a more rigorous and intrinsic kinetic experiment depicting the actual foundry conditions is necessary to develop a model that describes the foam degradation kinetics.

1.6. ENDNOTES

1.1 C.E. Bates, J. Griffin and H. Littleton, Expendable Pattern Casting-Process Manual, AFS publication, 1 (1994) p. 1.

1.2 www.huntsman.com/polymers/media/EPS1-1.0.pdf, Introduction to Expandable Polystyrene, Huntsman technical Bulletin 1-1.0, (2001), p. 1.

1.3 Q. Zhao, T.W. Gustafson, M. Hoover and M.C. Flemings, AFS Transactions 112 (2004) p. 1145.

1.4 T.V Molibog and H. Littleton, AFS Transactions 109 (2001) p. 1523.

1.5 S. Shivkumar and B. Gallois, AFS Transactions 95 (1987) p. 791.

1.6 S. Mehta, S. Biederman and S. Shivkumar, J. Mater. Sci. 30 (1995) p. 2944.

1.7 R.W.J. Westerhout, J. Waanders, J.A.M. Kuipers and W.P.M. van Swaaij, Ind. Eng. Chem. Res. 36 (1997) p. 1955.

1.8 V.R. Gowariker, Polymer Science, New age international (P) ltd., publishers, (2000).

1.9 S.L. Madorsky, Thermal Degradation of Organic Polymers, Polymer reviews, Interscience, 7, (1964).

1.10 S. Shivkumar, X. Yao and M. Makhlouf, Scripta metallurgica et materialia 33 1 (1995) p. 39.

1.11 M. Cai, J. Siak, B.R. Powell, G. Nouaime and S.J. Swarin, AFS Transactions 02-094 (2002) p. 1463.

1.12 C.L. Beyler and M.M. Hirschler, Thermal Decomposition of Polymers, in: SFPE Handbook of Fire Protection Engineering, 2nd edn., (1995).

1.13 P. Carniti, P.L. Beltrame, M. Armada, A. Gervasini and G. Audisio, Ind. Eng. Chem. Res. 30 (1991) p. 1624.

1.14 B. M. Wagenaar, The Rotating Cone Reactor for Rapid Thermal Solids Processing; University of Twente: Enschede, The Netherlands, (1994).

1.15 H. Bockhorn, A. Hornung and U. Hornung, in: The Twenty-seventh International Symposium on Combustion/The combustion institute, (1998), p. 1343.

1.16 T. Faravelli, M. Pinciroli, F. Pisano, G. Bozanno, M. Dente and E. Ranzi, J. Anal. Appl. Pyrol. 60 (2001) p. 103.

1.17 T. Faravelli, G. Bozzano, C. Scassa, M. Perego, S. Fabibi and M. Dente, J. Anal. Appl. Pyrol. 52 (1999) p. 87.

1.18 Y. Liu, S. Guo and J. Qian, Petroleum Science and Technology 17 (1999) p. 1089.

1.19 D.A. Anderson and E.S. Freeman, J. Polym. Sci. 54 (1961) p. 253.

1.20 Y.D.M. Simard, J. Polym. Sci. 58 (1995) p. 843.

1.21 H. H. G. Jellinek, J. Polym. Sci. 4 (1949) p. 13.

1.22 S. L. Madorsky, J. Polym. Sci. 9 (1952) p. 133.

1.23 L. A. Wall, S. Straus, J. H. Flynn, D. McIntyre, and R. Simha, J. Phys. Chem. 70 (1966) p. 1.

1.24 D. H. Richards and D. A. Salter, Polymer 8 (1967) p. 127.

1.25 G. G. Cameron, W. A. J. Bryce, and I. T. McWalter, J. Eur. Polym. 20 (1984) p. 563.

1.26 B. V. Kokta, J. L. Valade, and W. N. Martin, J. Appl. Polym. Sci. 17 (1973) p. 1.

1.27 B. Dickens, Polym. Deg. Stab. 2 (1980) p. 249.

1.28 P. Carniti, A. Gervasini, and P. L. Beltrame, J. Polym. Sci. 27 (1989) p. 3865.

1.29 K. Marc, Thermo-Chemical Recovery of Polystyrene from Polymer Waste, M. Eng. Thesis, McGill University, (1992).

1.30 T. Molibog, Modeling of Metal/Pattern Replacement in the Lost Foam Casting Process, Doctoral Dissertation, University of Alabama, Birmingham, (2002).

1.31 F. Carrasco and P. Pages, J. Appl. Polym. Sci. 61 (1996) p. 187.

1.32 H. Tanaka, S. Ohshima, and H. Negita, Thermochim. Acta. 53 (1982) p. 387.

1.33 J. M. Criado, M. Gonzalez, A. Ortego, and C. Real, J. Thermal Anal. 29 (1984) p. 243.

1.34 T. Molibog, Experimental Modeling of the Metal/Pattern Exchange Mechanism in the Lost Foam Casting Process, M. Eng. Thesis, University of Alabama, Birmingham, (1999).

1.35 H. S. Fogler, Elements of Chemical Reaction Engineering, 3rd Ed. Prentice Hall of India p. 72.

PART 2

LOW-HEATING RATE KINETICS OF THERMAL DECOMPOSITION OF EXPANDABLE POLYSTYRENE IN DIFFERENT GASEOUS ENVIRONMENTS

2.1. Introduction

Expandable polystyrene (EPS) is used as a rigid foam in numerous applications including metal casting patterns [2.1], building insulation, and non-weight bearing architectural structures [2.2]. EPS is subjected to extreme thermal and environmental conditions in these applications and hence the behavior of EPS in such environments must be well understood and characterized for any process or product development. Thermal degradation of EPS depends on both process and sample conditions, including heating rate and gaseous environment, as well as the conditions under which the foam was synthesized, molecular weight of the polymer, and type and amount of blowing agent present in the foams [2.3]. Among the process variables, the gaseous environment in which the sample degrades plays a significant role in the polymer decomposition process. Recent empirical investigations by Currie et al. [2.4] provided some interesting information on the effect of a helium environment that had been left unexplored until this time. Their qualitative tests, conducted on the *casted* products, revealed new insights on the pyrolysis efficiency of the non-oxidizing environment. Thorough lab-scale experimental work, however, was needed to understand the process better, thus forming the motivation for this project. In this study, an attempt was made to revisit the thermal behavior of individual EPS beads under different oxidizing and non-oxidizing environments and to propose a reasonable explanation for the differences in the observed

kinetic behavior. The objective of the present study is to determine the activation energy of the EPS decomposition process in various oxidizing and non-oxidizing environments, and to demonstrate a methodology for kinetic interpretation of EPS decomposition using thermogravimetric data.

2.2. Literature Review: - Low Heating Rate Kinetics of EPS degradation

In general, the thermal degradation of expandable polystyrene can be represented by the following "reaction" process:

$$\textbf{EPS} \rightarrow \textbf{gas and liquid decomposition products + residue} \qquad (2.1)$$

Exploring the kinetics of EPS decomposition at lower heating rates and in a highly controlled environment serves to understand the general decomposition mechanism, and to explore the effects of various factors that affect the process. This low heating rate kinetic experiment could be efficiently done using a thermo gravimetric analyzer (TGA) or similar analytical-scale instrumentation.

In a recently published work by Jun et al. [2.5], kinetic data of thermo and thermo-oxidative decomposition of expandable polystyrene has been presented and a kinetic model for foam decomposition that also accounts for the oxygen concentration in the gaseous environment has been proposed and is shown below:

$$\frac{d\alpha}{dt} = A\exp\left(\frac{-E}{RT}\right)\cdot(1-\alpha)^n\cdot[O_2]^m \qquad (2.2)$$

Here *A, E* are Arrhenius parameters, *R* is the gas constant, *T* is the absolute temperature, $[O_2]$ is the oxygen concentration in the reaction environment, *n, m* are the reaction orders, *t* is the reaction time, and α is the conversion defined as

$$\alpha = \frac{W_o - W}{W_o} \tag{2.3}$$

with W_o being the initial sample mass and W the instantaneous sample mass at any time *t*.

Thermogravimetric data obtained for PS decomposition was analyzed in various ways by prior researchers, including the use of integral, and differential or isoconversional methods, and the activation energy values thus obtained have been summarized in the literature [2.2, 2.5, 2.6]. The discrepancies in their reported values are likely due to differences in experimental conditions, including sample material, heating rates, gaseous environment, and also the method employed for kinetic analysis. The integral methods are typically based on a single thermogravimetric experiment that is conducted at some particular heating program, i.e., one single heating rate experiment. It has been accepted in the field of thermal analysis that kinetic parameters obtained from single heating rate experiments are not unique, and there could be several kinetic parameter sets that might as well fit the data with equivalent statistical accuracy [2.7]. On the other hand, the differential methods rely on thermograms collected from multiple heating rate experiments. The basic underlying assumption of the differential method is that the reaction model is independent of the TGA heating program. Therefore, most of the differential methods possess the unique ability to predict activation energy without prior knowledge about the functional form of the reaction model.

A review of the literature [2.8, 2.5, 2.6] reveals that the gaseous environment affects polystyrene decomposition kinetics, with the reaction being faster in non-oxidizing environments, although the samples decompose at a much higher temperature than in the presence of oxygen. Although there are some quantitative and qualitative information available on bulk polystyrene thermal decomposition in various environments, information on EPS decomposition kinetics is still not exhaustive. Also, the available information on the effects of various material and process parameters on foam decomposition kinetics is widely scattered across the literature with no work including all of the above-mentioned factors, primarily because of the difficulties encountered in foam material characterization techniques, and the challenge of designing a suitable *lab-scale* experiment to study the kinetics of EPS foam decomposition. Although many researchers have employed a commonly used thermal analysis technique, thermogravimetric analysis (TGA), to monitor sample degradation, only a few have proposed kinetic models to describe the reaction rate and mechanism of the foam decomposition phenomena. Although, for kinetic purposes, TGA has its own limitations with regards to instrument heating rate and sample phase change, it does provide insights about the effects of both sample and process parameters on the behavior of foam degradation. Furthermore, for materials such as EPS that produces numerous gaseous decomposition products, thermal analysis techniques like TGA serve as an indispensable and convenient tool to study the reaction kinetics by simply monitoring the changes in the physical properties of the reactant.

In this research, EPS thermal degradation data was collected for various oxidizing and inert environments using non-isothermal TGA. For kinetic interpretations, TGA data

was processed using modified Coats-Redfren multiple constant heating rates integral technique. Mathematical formulation and details of this technique are described elsewhere [2.9].

2.3. Experimental Procedure and Analysis

Low heating rate degradation experiments were carried out in a *TA Instruments SDT 2960* Simultaneous DSC-TGA. Expandable polystyrene beads impregnated with pentane as a blowing agent was supplied by Styrochem Inc. for the experiments. Due to the low density of the sample and the size of the crucible, the foam samples used were limited to a mass of ca. 2 mg. Degradation of the samples was observed in both oxidizing environments with differing oxygen levels (1%, 5%, 21%, 50% oxygen and balance nitrogen in all cases), and non-oxidizing environments (helium, argon, and nitrogen) with gas flow rates greater than 50 SCCM in order to minimize residence time inside the TGA chamber. All TGA experiments used a continuous linear heating rate of 5 to 25 K/min up to a maximum temperature of 600 ^{o}C, after which the sample was held isothermally for 15 minutes and then cooled. When environments other than air were used, the furnace on the TGA was closed and gas was allowed to purge the system for ten minutes prior to starting thermal analysis.

2.4. Results and Discussion

2.4.1. Effect of Heating Rate on PS Degradation

Figures 2.1 and 2.2 illustrate the weight loss and the derivative weight loss curves respectively as a function of temperature for various heating rates (5, 10, 15, 20, 25 K/min) in a nitrogen environment. At first glance, one might be tempted to conclude that these results suggest a single decomposition mechanism. A careful kinetic analysis will show otherwise. Clearly, however, the reaction rate seems to increase with the heating rate. The shift in apparently higher volatilization rates towards lower temperatures for lower heating rates can be attributed to the fact that with lower heating rates, the sample spends a longer time at a certain temperature. With a longer residence time at that temperature, more degradation will occur before the sample reaches the next temperature zone. Liu et al. [2.10] reported a similar trend for TGA data obtained for polystyrene films degraded in an argon environment.

Liu et al. also reported the following empirical relationship between the peak volatilization temperature (T_{pv} in ºC) and the heating rate (R in K/min):

$$T_{pv} = 365.1 R^{0.0565} \tag{2.4}$$

Peak volatilization temperature is the temperature at which the rate of degradation of the sample is at the maximum. Using this relationship in the *current* study, the peak volatilization temperature of the PS foam beads at various heating rates was calculated, and compared with the TGA experimental data. It can be noticed from Table 2.1 that the

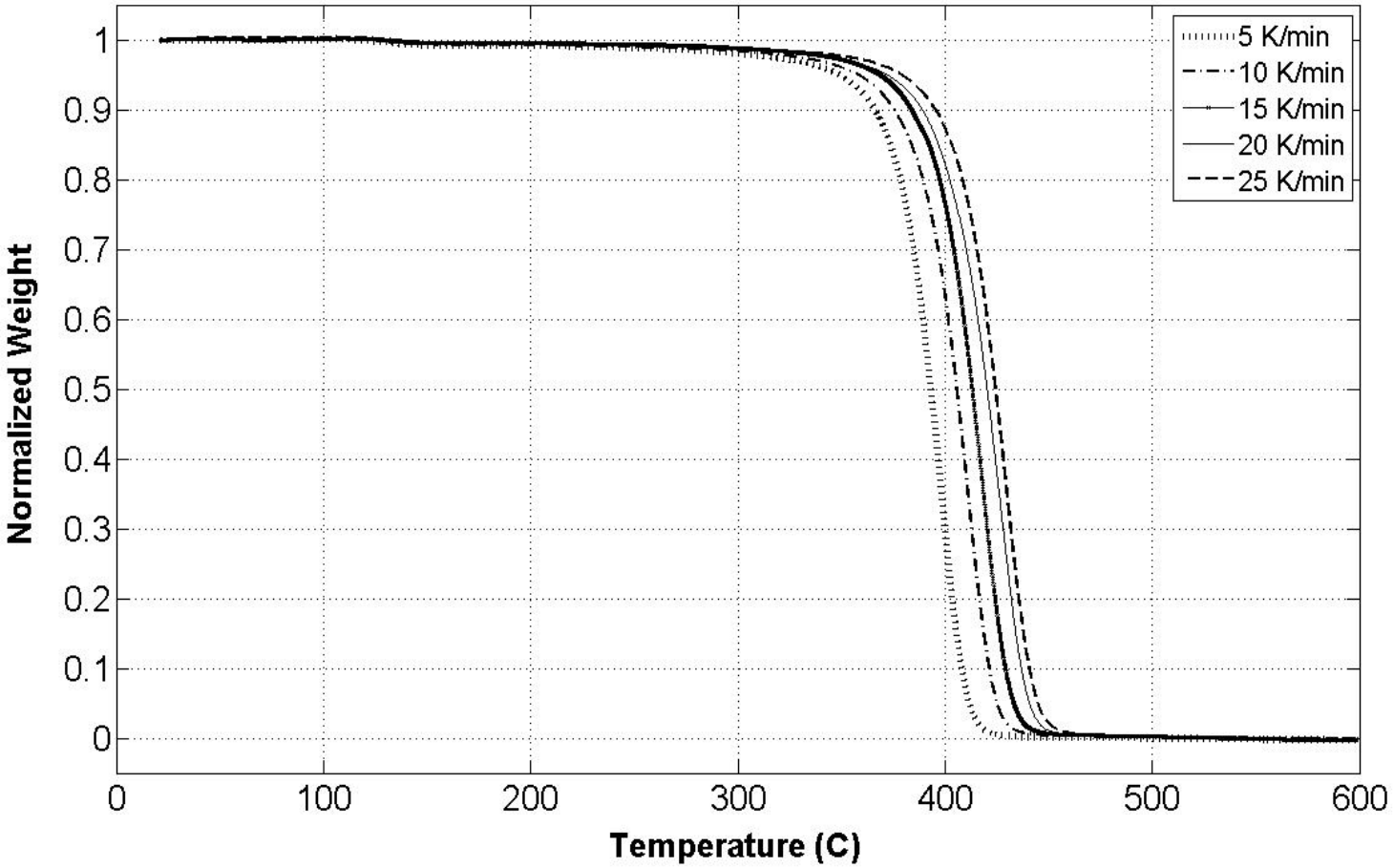

Figure 2.1: TGA curves of EPS degradation at different heating rates in nitrogen.

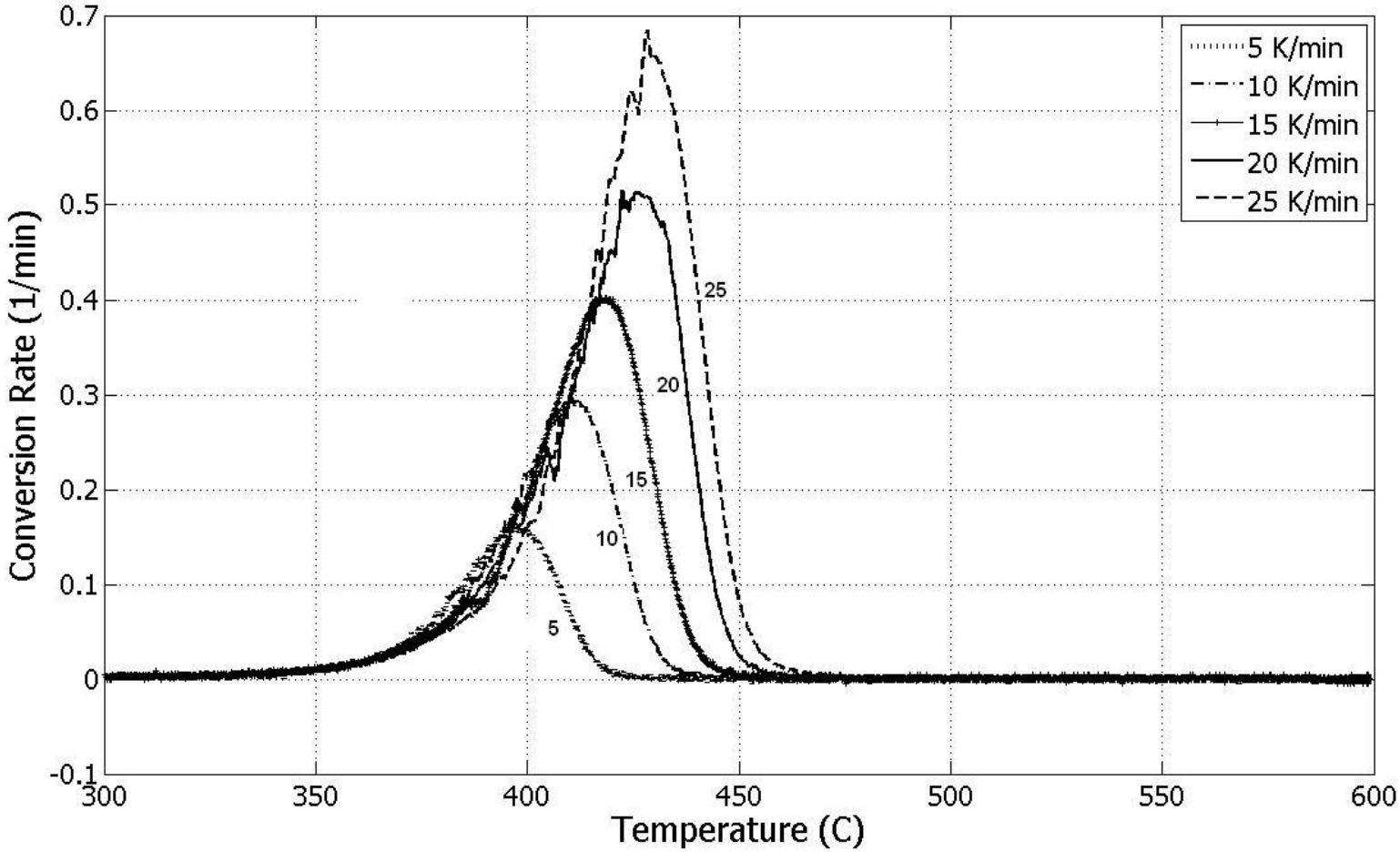

Figure 2.2: DTG curves of EPS degradation at different heating rates in nitrogen.

Table 2.1: Comparison of experimental EPS peak volatilization decomposition temperature measured in this work versus predicted values using Liu's model in air at various heating rates

Heating Rate (K/min)	Peak Volatilization Temperature (°C)	
	Liu et al. [2.10] Model Prediction	current work Experimental
5	399	400
10	415	415
15	425	422
20	432	430
25	437	435

values computed from this experiment are very much in agreement with Liu et al.'s empirical relationship.

To demonstrate reproducibility of the TGA experiment, TGA runs performed on foam samples in a helium environment are shown in Figure 2.3. As can be seen from the results, each individual TGA run is consistent with others with minimum deviations. All TGA curves also exhibit small fluctuations at around 150 °C. A TGA experimental run using *raw* (blowing agent dissolved, but unexpanded) beads showed a pronounced fluctuation in the TGA curve around 135 °C (curves not shown here). However, when the *raw* beads were preheated in an external oven at 150 °C for a period of about 15 minutes, the fluctuations were drastically reduced. Hence it was concluded that the small fluctuations on all TGA curves at around 150 °C is due to the degassing of the blowing

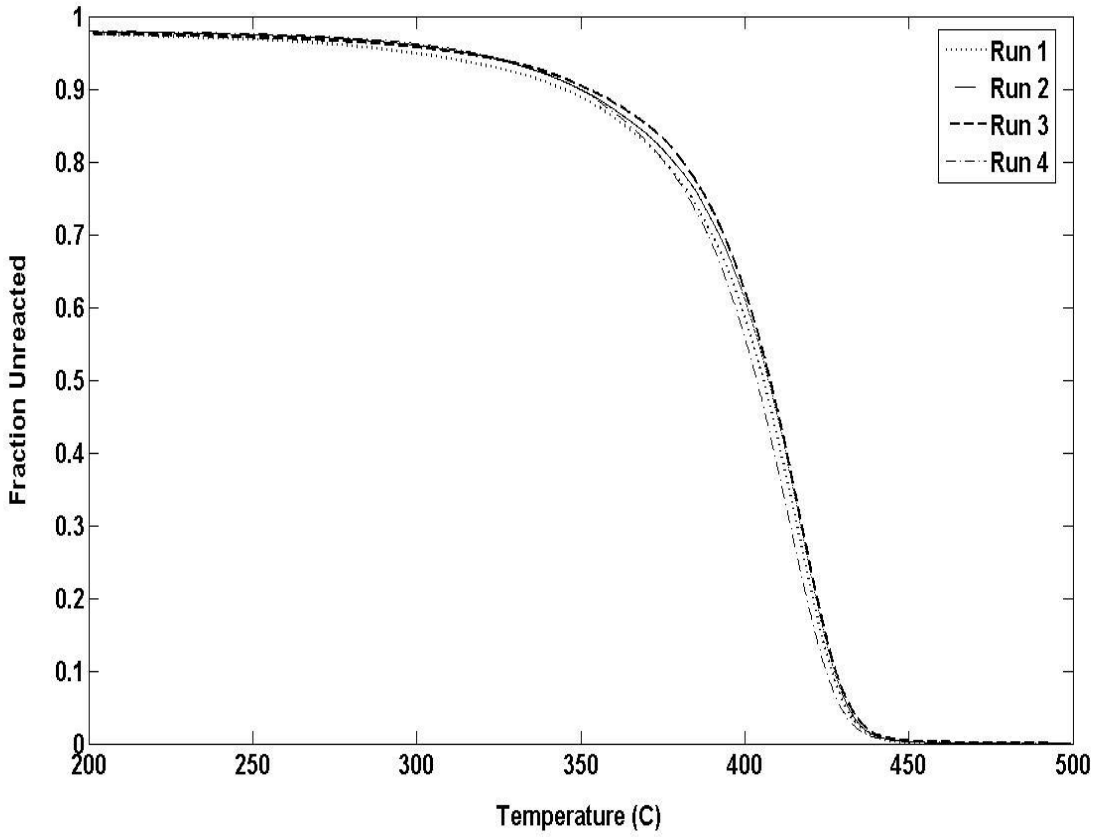

Figure 2.3: Multiple TGA runs of EPS degradation in helium at 20 K/min showing good reproducibility.

agent from the sample. However, this amount is so small that the gas release hardly has any recordable change in sample mass, and therefore the fluctuations are likely due to the buoyancy and movement of the sample instigated by the release of the blowing agent.

2.4.2. Effect of Gaseous Environment on PS Degradation

Figure 2.4 shows a sample TGA plot of EPS degradation under various atmospheric conditions, including 1% oxygen, 5% oxygen, 50% oxygen, air, helium, argon, and nitrogen at a constant heating rate of 5 K/min. In this non-isothermal TGA plot, normalized weight fraction remaining was plotted as a function of temperature. Normalized weight (W_n) was calculated by using the following formula, $W_n = \frac{W_i - W_0}{W_f - W_0}$; where W_o represents the initial mass, W_i represents the instantaneous mass, and W_f represents the final mass of the sample left unreacted (residue). It can be seen that the degradation pathway is similar for all non-oxidizing environments, including nitrogen, helium, and argon. Although these qualitative plots imply a single step mechanism for inert environments, a detailed kinetic analysis, as shown later in Section 4.3, would prove otherwise. When oxygen is present, however, the sample degrades at a much lower temperature and a significant amount of residue remains until the temperature reaches 550 °C. This behavior has been consistently found throughout the literature on different types of PS samples, including monolithic films [2.6] and expandable PS beads [2.5], and expanded PS beads [2.11]. The higher the oxygen content the greater the effect of the secondary reaction as is clearly indicated by the 21% oxygen and 50 % oxygen environment thermograms.

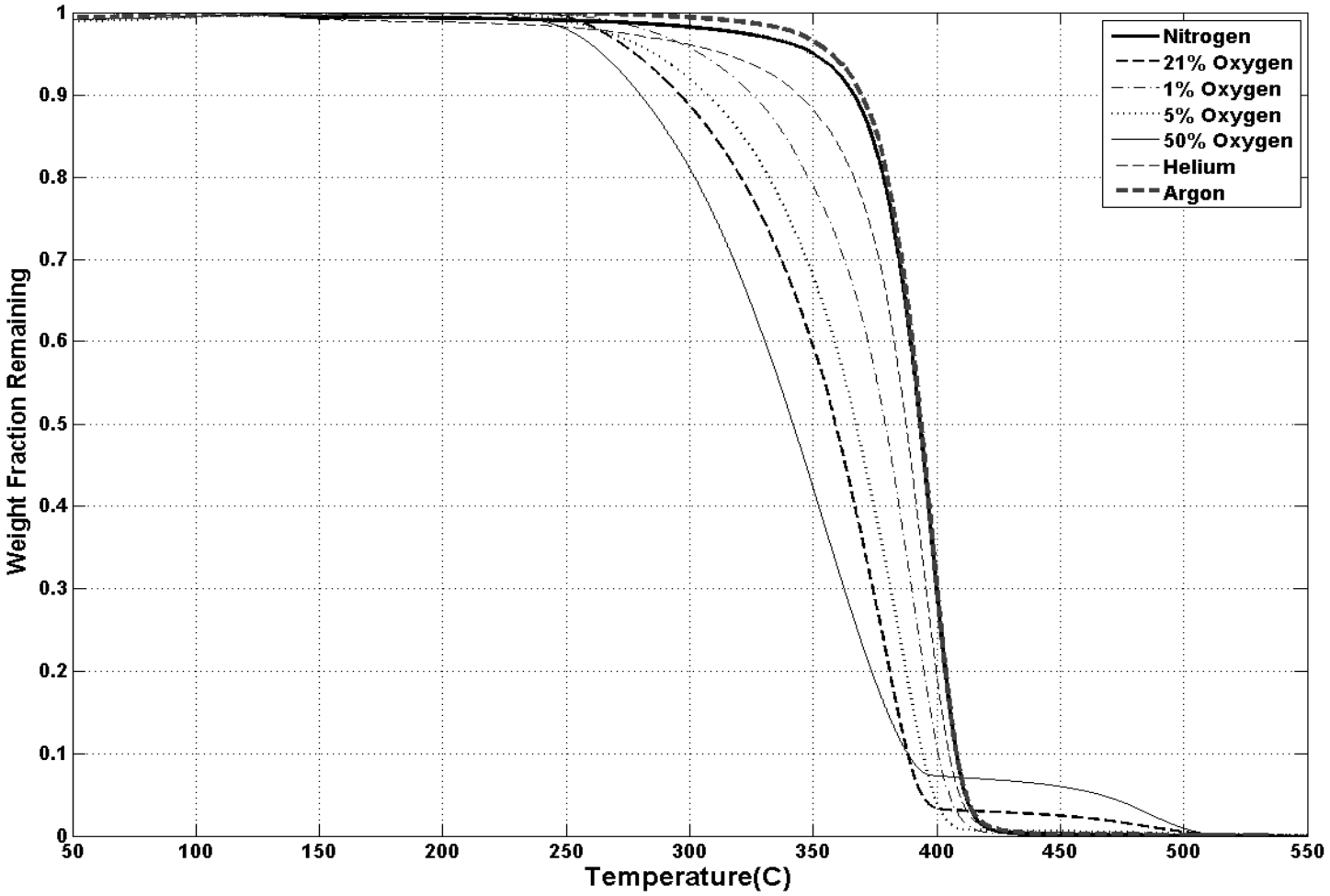

Figure 2.4: TGA scans of EPS degradation at a heating rate of 5 K/min in different atmospheres.

2.4.3. Kinetics of EPS Degradation

The decomposition of expandable polystyrene can be mathematically expressed by Equation (2.5), where r is the rate of reaction, t is time, k is a rate constant, $f(\alpha)$ is a kinetic expression that describes the functional dependence of rate on extent of reaction, A is the pre-exponential factor (frequency factor), E is the activation energy, R is the gas constant, and T is the absolute temperature.

$$r = \frac{d\alpha}{dt} = k \cdot f(\alpha) = A \cdot e^{\frac{-E}{RT}} \cdot f(\alpha) \tag{2.5}$$

The most commonly used functional form of $f(\alpha)$ for solid state decomposition reactions takes the form $(1-\alpha)^n$, n being the order of the reaction with respect to the reactant consumption. α represents the reaction conversion, and is defined by Equation (2.6), thus:

$$\frac{d\alpha}{dt} = -\frac{dw}{dt}\ ;\ \alpha = 1 - \frac{w}{w_o} = \frac{w_o - w}{w_o} \tag{2.6}$$

Over the years, researchers have either used a differential or an integral form of Equation (2.5) to determine the kinetic triplets, namely the activation energy, pre-exponential constant, and the functional form $f(\alpha)$. While some of the techniques depend on the functional form of conversion, $f(\alpha)$, it has also been successfully demonstrated in the literature [2.7] that activation energy values could be estimated without any prior

knowledge of the functional form. These techniques are often referred as "model free" isoconversional techniques that make use of TGA data collected at different heating rates, to predict activation energies at fixed conversion levels. One such method is the modified Coats-Redfern method that has been demonstrated successfully earlier by Burnham et al. [2.12] for the decomposition reaction of calcium carbonate using six experimental TGA runs obtained at different heating rates between 1.8 to 10 K/min. Using the relationship $\beta = {dT}/{dt}$, an approximation for the temperature integral, and linearizing Equation (2.5), gives

$$\ln\left[\frac{\beta_i}{T_i^2\left(1-2RT_i/E_\alpha\right)}\right] = -\frac{E_\alpha}{RT_i} + \ln\left[-\frac{A_\alpha R}{E_\alpha I(\alpha)}\right] \tag{2.7}$$

where the subscript '*i*' refers to a particular heating rate experiment, the subscript 'α' refers to a fixed conversion level, and $I(\alpha)$ refers to the integral value of the function $f(\alpha)$. It can be noticed from Equation (2.7) that irrespective of the form of $f(\alpha)$, at any fixed conversion α and for each heating rate β_i, a plot of the left hand side versus $1/T_i$ yields a straight line with slope equal to $-E_\alpha/R$. Thus, a set of activation energy values was estimated at different conversion levels using the above-mentioned technique. A sample plot of EPS decomposition in nitrogen is shown in Figure 2.5 where seven different conversion levels (0.02, 0.15, 0.30, 0.45, 0.60, 0.85, and 0.98) were considered. The values of activation energy and correlation coefficient are tabulated; refer Table 2.2, for

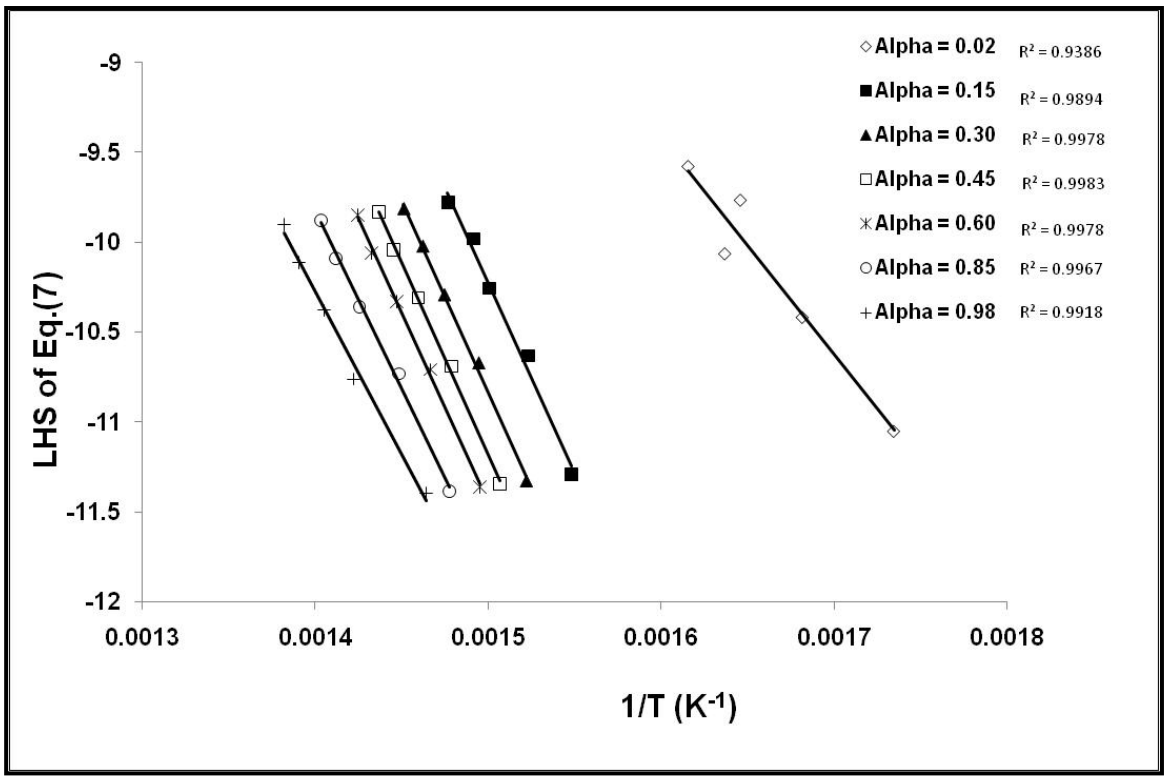

Figure 2.5: Kinetic analysis using the *modified* Coats-Redfern method for EPS degradation in nitrogen environment.

Table 2.2: Activation energies of EPS decomposition in various environments.

Environment	Alpha	Activation Energy (kJ/mol)	S. Error	R^2	Literature	Ref.	Comments
Nitrogen	0.02	100.75	14.88	0.939	136.25	[2.5]	Differential method
	0.15	176.07	10.52	0.989	189-216	[2.13]	Optimization technique
	0.30	176.74	4.79	0.998	145-179	[2.5]	Integral Method
	0.45	176.53	4.21	0.998	200	[2.6]	Optimization technique,
	0.60	174.36	4.75	0.998			sample condition diff.
	0.85	164.07	5.45	0.997			from EPS
	0.98	150.54	7.92	0.992			
Argon	0.02	91.88	36.97	0.755	not available		
	0.15	169.95	5.59	0.998			
	0.30	166.45	4.17	0.999			
	0.45	169.14	4.25	0.999			
	0.60	171.52	4.65	0.999			
	0.85	172.31	3.38	0.999			
	0.98	160.09	1.00	1.000			
Helium	0.02	N/A	4.76	0.499	not available		
	0.15	174.69	19.46	0.976			
	0.30	192.24	12.24	0.992			
	0.45	195.23	8.54	0.996			
	0.60	197.57	6.38	0.998			
	0.85	198.66	6.67	0.998			
	0.98	193.33	14.56	0.989			
Air	0.02	46.25	2.69	0.990	126.52	[2.5]	Differential method
	0.15	62.04	14.24	0.864	100-106	[2.5]	Integral Method
	0.30	70.81	22.34	0.770	125	[2.6]	Optimization technique,
	0.45	83.58	27.33	0.757			sample condition diff.
	0.60	105.12	28.39	0.820			from EPS
	0.85	169.91	24.97	0.939			
	0.98	N/A	30.57	0.419			
1% Oxygen	0.02	121.84	29.34	0.852	not available		
	0.15	102.17	2.45	0.998			
	0.30	128.14	3.50	0.998			
	0.45	145.93	6.32	0.994			
	0.60	156.13	7.47	0.993			
	0.85	169.73	9.37	0.991			
	0.98	169.86	7.49	0.994			
5% Oxygen	0.02	114.56	39.27	0.739	126.25	[2.5]	Differential method
	0.15	109.96	6.46	0.990	107-118	[2.5]	Integral Method
	0.30	127.87	6.20	0.993			
	0.45	146.62	6.45	0.994			
	0.60	161.10	6.59	0.995			
	0.85	179.69	6.79	0.996			
	0.98	172.43	4.16	0.998			
50% Oxygen	0.02	87.80	29.50	0.747	not available		
	0.15	84.51	11.07	0.951			
	0.30	80.31	15.26	0.902			
	0.45	84.69	18.67	0.873			
	0.60	98.69	20.63	0.884			
	0.85	159.47	28.59	0.912			
	0.98	N/A	177.89	0.295			
Vacuum					195	[9]	Sample in powder form

all environments. The values of the regression coefficient are nominally linear for most values of conversion considered. For all unacceptable values of correlation coefficient, activation energy values are not taken into consideration, which is indicated by 'N/A' in Table 2.2. The reported standard error values on the activation energy were estimated based on a 99% confidence interval.

It was pointed out earlier from qualitative results that thermal decomposition of EPS in inert gas seemed to be a single step phenomenon, while thermo-oxidative decomposition indicated a multiple step process. In order to better investigate and understand the process mechanism, a plot of activation energy versus conversion was made for all environments, see in Figure 2.6. It is evident that in the case of non-oxidizing environments, activation energy remains constant during the initial and mid conversion levels; the activation energy value at $\alpha = 0.45$ is 176, 169, and 195 kJ/mol for nitrogen, argon, and helium, respectively. However, after the reaction has attained about 60 to 85% conversion, the activation energy drops by ca. 10 to 15 kJ/mol. This is an indication of a possible secondary mechanistic step. Marcilla et al. [2.13] suggested that in nitrogen, PS decomposes via a two-step mechanism involving the formation of an intermediate species with activation energy of about 220 kJ/mol followed by the decomposition of the intermediate to gaseous products with corresponding activation energy of ca. 185 kJ/mol.

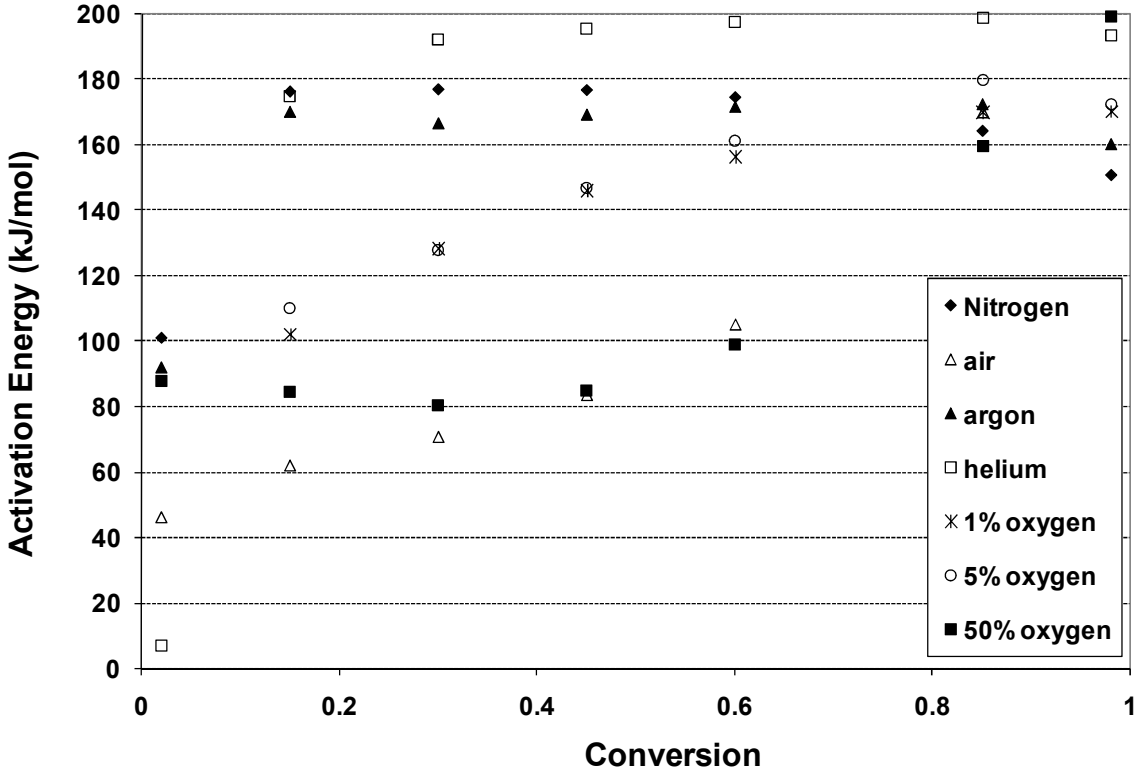

Figure 2.6: Activation energies of EPS degradation at different conversion levels in all environments.

In the case of low concentration oxidizing environments, including the 1% and 5% oxygen, the reaction process looks more complex as evidenced by increasing activation energy values with increasing extent of reaction. As the concentration of oxygen in the environment increases to 21% and 50% oxygen levels, the activation energy remains constant at about 85 kJ/mol until alpha = 0.60. After that point, it was found to increase sharply to ca. 160 kJ/mol consistent with that for non-oxidizing environment, thereby suggesting a secondary reaction. Literature [2.6] suggests that the thermo-oxidative reaction is initiated by the formation of polymer radicals with corresponding activation energy of about 80 - 110 kJ/mol that reacts with oxygen to form a peroxy radical intermediate. In the later stages, this peroxy radical decomposes and accelerates the oxidation process yielding more polymer radicals. The hydro peroxide decomposition step has activation energy of ca. 200 kJ/mol [2.14] and is considered to be the rate limiting step in the EPS thermo-oxidative decomposition process. Hence, it can be concluded that thermo-oxidative decomposition is a two-step process indicated by two different activation energies. This could be also evidenced from the thermograms where it can be noticed that there is a sharp decrease in sample weight during the initial and mid conversion levels when compared to the gradual decrease at higher conversions. However, the weight loss rate in an oxidizing environment during the initial and mid conversion levels is not as sharp as encountered for a non-oxidizing environment; refer Figure 2.4, where the weight loss could be correlated to the evaporation of high and medium molecular weight fragments

2.5. Conclusions

From the TGA experiments, it can be concluded that the parameters investigated, namely the heating rate and the gaseous environment, affect EPS foam decomposition kinetics. As expected, at higher heating rates, the degradation shifts to a higher reaction temperature accompanied by an increase in the rate of weight loss. The effect of heating rate on degradation is very significant as the peak volatilization temperature of the PS sample is dependent on the heating rate. It was found that EPS starts to degrade at a much lower temperature in air than in any non-oxidizing environments, including helium, nitrogen, or argon, and that the rate of degradation in non-oxidizing environments may depend on the thermal conductivity of the gaseous environment. A "model free" isoconversional method based on multiple heating rate experiments served as a useful tool to interpret kinetics from the experimental TGA data. Kinetic studies revealed that the major difference in decomposition mechanism between non-oxidizing and oxidizing environments is probably due to the difference in initiation mechanism at the start of the reaction, after which they both follow similar pathways. The reaction is completed by the formation and evaporation of low molecular weight gaseous products. Finally, even though the activation energies for non-oxidizing environments are higher than the oxidizing environment, complete decomposition occurs at a relatively lower temperature in inert environments. This maybe advantageous, for example, in lost foam casting applications where there is presently a huge challenge to reduce casting defects that are attributed to incomplete degradation of the polymer.

2.6. ENDNOTES

2.1. P. Kannan, J. J. Biernacki and D. P. Visco Jr., J. Anal. App. Pyrolysis, 78 (2007) p. 162.

2.2. F. Carrasco, Thermoch. Acta, 23 (1993) p. 115.

2.3. L. Bu, Y. Wan, H. E. Littleton and J. W. Mays, Am. Chem. Soc., 40 (1999) p. 689.

2.4. K. Currie, G. Walford, M. Abdelrahman, F. Vondra and M. Renfro, AFS Trans., 05-102 (2005) p. 1.

2.5. H. Jun, S. C. Oh, H. P. Lee and H. T. Kim, Korean J. Chem. Eng., 23 (2006) p. 761.

2.6. J. D. Peterson, S. Vyazonkin and C. A. Wight, Macromol. Chem. Phys., 22 (2001) p. 775.

2.7. M. Criado, A. Ortega and F. Gotor, Thermochim. Acta., 157 (1990) p. 171.

2.8. S. Shivkumar, X. Yao and M. Makhlouf, Scripta Metallurgica et Materialia, 33 (1995) p. 39.

2.9. A. K. Burnham and R. L. Braun, Energy Fuels, 13 (1999) p. 1.

2.10. Y. Liu, S. I. Bakhtiyarov and R. A. Overfelt, Proceedings of 2001 ASME International Mechanical Engineering Congress and Exposition, NY, 255 (2001) 9.

2.11. S. Shivkumar and B. Gallois, AFS Transactions, 95 (1987) p. 791.

2.12. M. E. Brown, M. Maciejewski, S. Vyazovkin, R. Nomen, J. Sempere, A. Burnham, J. Opfermann, R. Strey, H. L. Anderson, A. Kemmler, R. Keuleers, J. Janssens, H. O. Desseyn, Chao-Rui Li, T. B. Tang, B. Roduit, J. Malek and T. Mitsuhashi, Thermochim. Acta., 355 (2000) p. 125.

2.13. A. Marcilla and M. Beltran, Polym. Degrad. Stab., 50 (1995) p. 117.

2.14. L. Reich and S. S. Stivala, "*Autooxidation of hydrocarbons and polyolefins*", M. Dekker, New York 1969, p. 50.

PART 3

FAST PYROLYSIS KINETICS OF EPS

3.1. An Overview

Fast pyrolysis of polymers, biomass, and other substances is of great interest in various applications. For example, in the lost foam casting process, kinetic information about EPS decomposition in extremely high heating rate conditions is essential for any process development. In this study, a simple laboratory scale *fast pyrolysis* technique has been developed and demonstrated for the study of EPS decomposition kinetics. Pyrolysis experiments were performed at different reaction temperatures. The cumulative gaseous yields were determined using a flame ionization detector (FID) connected in series with the reactor. The governing equations for a semi-batch reactor type were modified and applied to obtain kinetic parameters (the activation energy and the pre-exponential rate constant) for the EPS decomposition process.

3.2. Introduction

The primary advantage of fast pyrolysis is extremely high heating rates which elevate the sample to high temperature prior to complete volatilization. The main utility of the technique is that it enables decomposition to be observed at elevated temperatures that are otherwise difficult or impossible to attain with conventional techniques, such as thermogravimetry. Results obtained from such a study are considered by others to be "more generic, yet accurate" and hence, could be easily extended for other similar applications [3.1]. The basic underlying idea behind this technique is to rapidly take the

sample to the elevated target temperature and minimize its exposure to the lower temperatures that might influence the reaction sequence. In theory, this permits a more direct and simpler correlation between reaction rate and the process conditions, including thermal and environmental factors. Such a technique is demonstrated here for studying EPS decomposition kinetics and is discussed in the following sections.

3.3. Background of the Technique

A summary of the kinetic models and conventional experimental approaches available for EPS decomposition has already been presented in Part 1 [3.2]. The present section briefly discusses literature findings on fast pyrolysis experimental techniques and kinetic data interpretation. *Fast* pyrolysis is ordinarily achieved by using a small amount of sample mass in a suitable form representative of the original and a very high heating rate. Under such conditions, high rates of heat transfer and excellent instrumentation and control, are required to capture the dynamics of kinetic events that are later interpretable.

Liliedahl and Sjostrom [3.1] employed a laboratory-scale *fast* pyrolysis technique for the study of coal pyrolysis kinetics. Their design consisted of a pyrolysis chamber connected in series with a gas chromatograph that is fitted with a flame ionization detector. The pyrolysis chamber was a quartz tube packed with a small quartz wool plug to trap the sample. The quartz tube was placed inside a furnace that continuously heats the tube to maintain an isothermal condition. Coal samples in powder form were quickly introduced into the tube using a solids injector. As the sample pyrolyzes, the carrier gas continuously sweeps the off-gas out of the furnace and into the chromatograph. The

chromatograph was slightly modified by replacing the lengthy GC capillary column with a short and empty column. The design facilitates transfer of the volatiles from the furnace exhaust port directly into the flame ionization detector (FID) with virtually zero residence time delay. This limits the dispersion of the volatiles and does not obscure the fast reaction dynamics at the elevated temperatures.

The response of an FID is directly attributed to the mass of hydrocarbon molecules and the number of carbon-hydrogen bond. The response is less sensitive to the carbon-oxygen bond, inert or halide group bonds. A carrier gas, usually an inert such as helium or nitrogen, ushers the pyrolysis off-gas through the "empty" GC and into the FID. Before the gas effluent enters the FID jet, it is mixed with hydrogen, making it combustible. It is then ignited in the presence of air into the FID where it produces both positive and negative ions. The negative ions are collected and amplified with an electrode, and a corresponding analog signal is generated that is recorded. The response from the FID represents a quantitative combined representation of both the mass and the number of hydrocarbon molecules eluted into the flame. The sensitivity of the instrument depends on several factors, including the stability of the flame. Hence, the ratio of air and hydrogen must be properly adjusted and maintained to provide the stable flame necessary for sample ionization.

To obtain relevant kinetic information, the FID data has to be processed so that it relates the reaction rate with time and temperature. Liliedahl et al. [3.1] monitored devolatilization rates over time at different isothermal temperature conditions and correlated the same to both single and multiple reaction kinetic models. Because coal samples pyrolyze *via* a complex set of multiple reactions, the kinetic approaches were

found to be mathematically cumbersome. Hence, an empirical model was formulated based on a Gaussian distribution to relate the devolatilization rate to the instantaneous amount of volatile matter present in the effluent gas sample. By combining this model with an equation that incorporates the heat transfer rate to the particle, the normalized total devolatilization rate as a function of pyrolysis time (t) and gas temperature (T) was derived:

$$-\frac{dm'}{dt} = a\,\exp(bT)\left[\frac{2t^2}{a\exp(bT)t^4+2}\right]^{1.5} \tag{3.1}$$

where m' is the normalized volatile mass, a and b are numerical rate constants that are specific for a given coal specimen.

Although this technique cannot be used to reveal the mechanistic details of the reaction, it suggests a useful methodology to correlate rate data based on the overall volatile yield.

3.4. Experimental Setup

The design of the pyrolysis apparatus is similar to the one employed by Liliedahl and Sjostrom [3.1], refer Figure 3.1, and consists of a tubular reactor that is connected in series with an FID equipped gas chromatograph. The tubular reactor is a 0.1 cm ID, 50 cm long quartz tube and a muffle furnace. Carrier gas (helium) from the storage cylinder

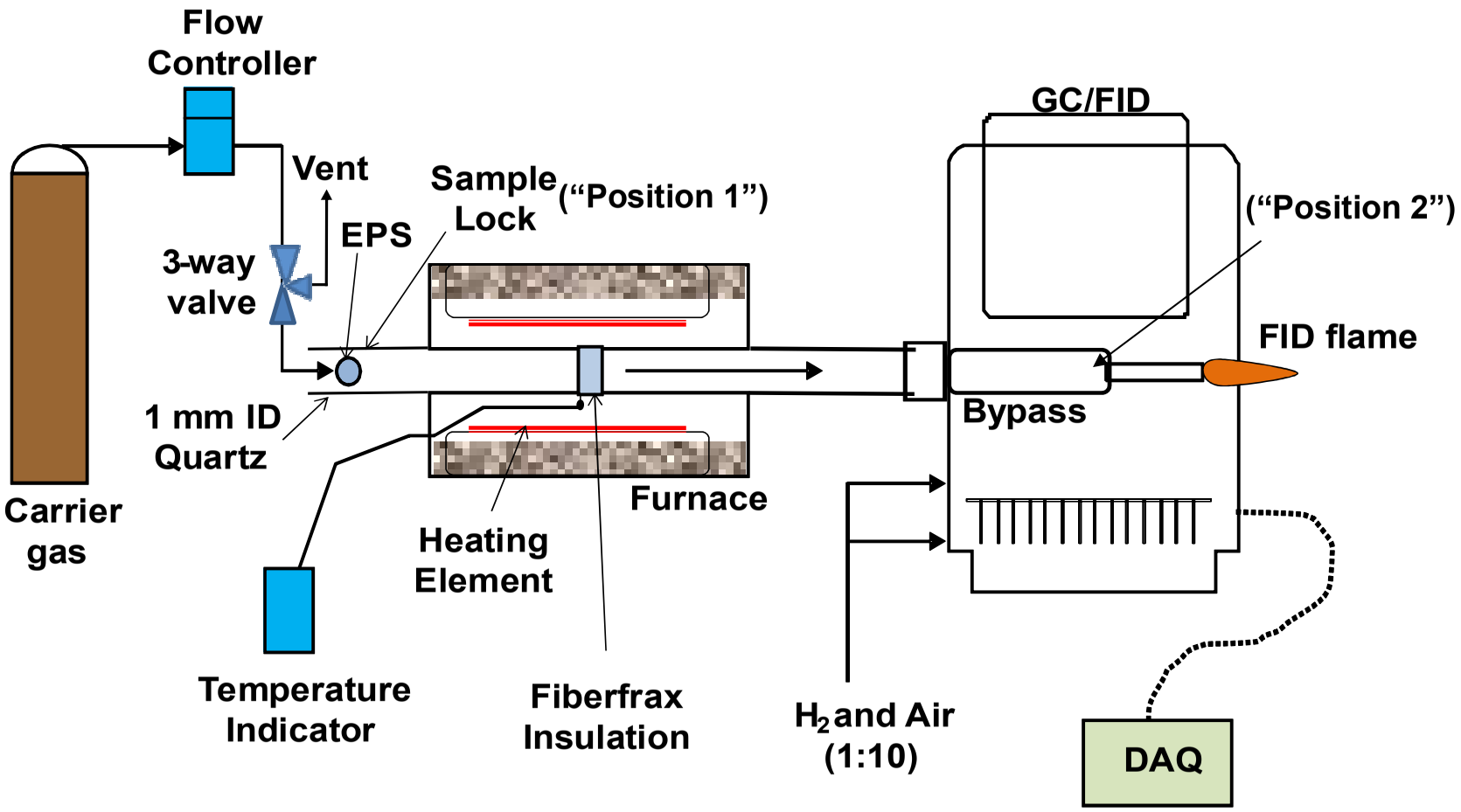

Figure 3.1: Experimental setup of the *fast* pyrolysis technique used in this study.

flows into the reactor through a flow controller and a 3-way valve. The carrier gas serves three purposes: 1. to transport the sample EPS bead into the hot zone, 2. to transfer the volatiles from the reaction zone and into the FID, and 3. to provide a gaseous environment for the reaction. It is very important to choose a proper carrier gas flow rate such that it not only minimizes the transfer time of both the sample and the volatiles, but also to provide a stable FID flame. After many trials, a flow rate of 50 sccm was chosen for all the experimental runs. Between the reactor and the flow controller, a 3-way valve was installed. This permits gas to be diverted to vent while loading a sample into the sample lock. This permits gas to continue to flow, maintaining a consistent upstream pressure. Upon sample injection, the 3-way valve is switched so that gas flows through the reactor tube, thereby carrying the sample into the hot zone of the reactor. A small piece of Fiberfrax insulation was inserted into the quartz tube that serves to trap the EPS bead. The quartz tube was positioned inside the furnace such that the trap is in the middle of the furnace where the temperature is most uniform and highest. A *K* type thermocouple was mounted on the top of the reactor tube just above the insulation trap to indicate the reaction temperature. For gas analysis, a *SRI Capillary FID GC* with *built-in* hydrogen generator as shown in Figure 3.2 was employed. The FID is equipped with an electrometer amplifier with adjustable gain. The *built in* hydrogen generator option was not utilized in this study, and both air and hydrogen were supplied from an external storage tank to fuel the FID flame. The flow rates of air and hydrogen were controlled using FID's electronic pressure controllers that were preset at a prescribed rate. The instrument has a wide detection range from 0.1ppm to 100% for most hydrocarbons and

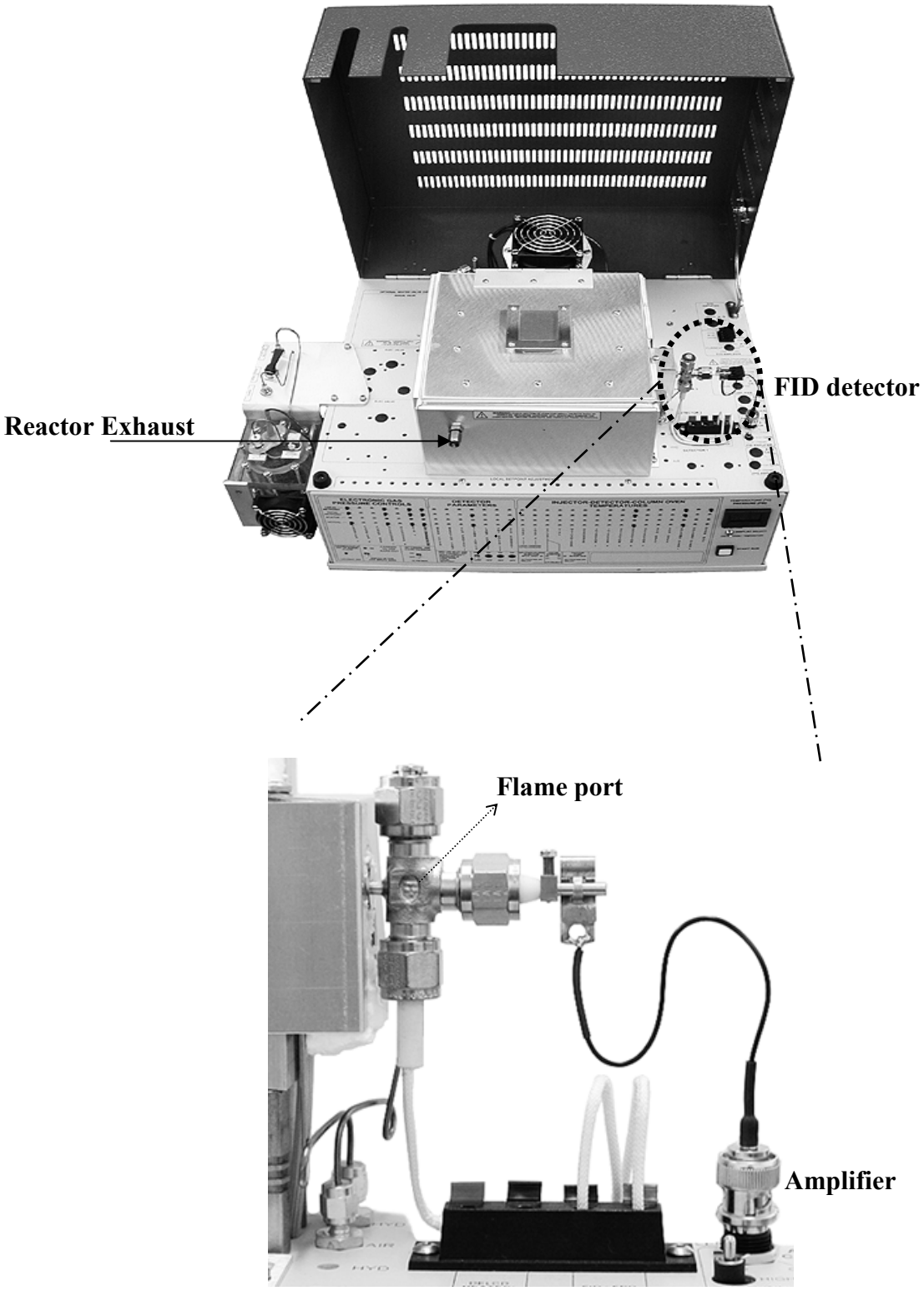

Figure 3.2: A view of the SRI Capillary FID Gas Chromatograph.

can sample at a maximum rate of 50 Hz. The design inside the GC was slightly modified by replacing the entire GC capillary column with a short (ca. 25 cm) empty 1/16" OD stainless steel tube. One end of this tube is attached directly to the reactor quartz tube, and the other end connected to the injection port of the detector using Swagelok fittings.

Expandable polystyrene beads or pre-expanded beads impregnated with pentane as a blowing agent were supplied by Styrochem Inc. Nominally spherical EPS beads of ca. 0.5 mm diameter were selected and carefully weighed in a *TA Instruments SDT 2960* Simultaneous DSC-TGA equipped with a microbalance. Although the balance sensitivity was on the order of 1 μg, disturbances from external factors limited the accuracy to ca. 5 μg. Under these circumstances, it was found that most of the selected EPS beads of the above-mentioned dimensions weighed between 24 to 28 μg ± 5.

At the start of the experiment, the quartz tube was placed inside the furnace and heated to the target temperature. After obtaining a stable FID flame, a single EPS bead was placed in the lock at one end of the quartz tube as shown in Figure 3.1. This end is positioned far from the hot zone and so the temperature in the lock is not hot enough to initiate thermal changes in the sample. After attaining a stable carrier gas flow in the bypass line, the 3-way valve was switched to permit flow into the reactor tube. The EPS bead is immediately carried into the reaction zone by the gas flow, and trapped in the hot insulation wool where pyrolysis occurs. The volatiles that are formed are quickly transported out of the hot zone by the carrier gas and into the FID. The FID records the signal and transfers the data to the external data acquisition device.

Table 3.1: Major Composition of the hydrocarbon gas mixture used as a standard test gas in this study.

Component	Volume Fraction	Weight Fraction
Pentane	0.002	0.004
Pentene	0.002	0.004
Butane	0.002	0.004
Butene	0.004	0.007
Isobutane	0.103	0.188
Propane	0.007	0.010
Propylene	0.008	0.010
Ethane	0.020	0.019
Ethylene	0.020	0.018
Nitrogen	0.832	0.735

Prior to the EPS pyrolysis runs, a set of controlled experiments was also conducted with a standard hydrocarbon gaseous mixture (see Table 3.1) in order to study dispersion and detector response dynamics as a function of furnace temperature and carrier gas flow rate.

The total residence volume from the one end of the reactor tube to the FID jet was estimated to 1.13 cc. At a carrier gas flow rate of 100 sccm, the sample transit time from the sample lock to the FID flame is ca. 0.5 s. A simple experiment was performed to quantify the gas phase dispersion in the reactor and transfer tube lines by injecting the gas standard at two different points along stream. First, about 10 μL of the standard was injected through a septum into a flowing carrier gas stream with the use of a syringe near the sample lock ("Position 1"), refer Figure 3.1. The 10 μL volume was chosen based on

the theoretical total volatile yield of a single EPS bead pyrolyzed at 973 K. The yield of mixed gases from EPS pyrolysis at 973 K is ca. 200 cc per gram of EPS [3]. Assuming a bead mass of 45 μg (an upper limit), the total gas yield was calculated to be around 9 μL. Next, the experiment was repeated by injecting a sample at "Position 2" very close to the FID jet and hence by-passing the entire reaction zone and transfer lines. Figure 3.3 shows a comparison of the FID response over time between the two different positions. A value at time = 0 represents the sample injection time into the system. The abscissa on the response curve for Position 1 has been shifted by 0.5 s to adjust for the sample transit time. This time adjustment provides a time basis for comparison of the two responses with respect to only dispersion. It could be clearly noticed that the response curve of Position 1 is somewhat broader than that of Position 2 indicating some sample dispersion in the system. Since the actual kinetic event is expected to be at least one order of magnitude longer, the modest amount of dispersion shown here, will not significantly affect subsequent interpretations.

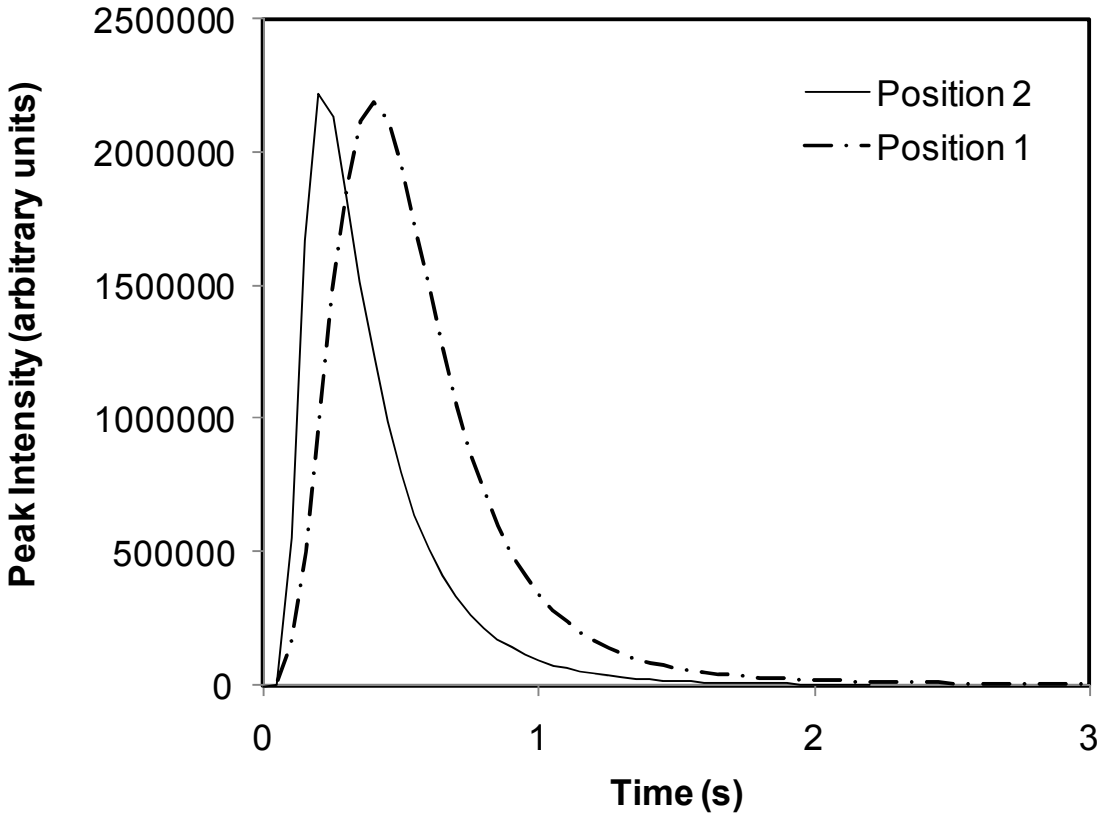

Figure 3.3: Dispersion test in the reactor and transfer lines using the gas standard.

To study the effect of temperature on dispersion, the test gas was injected at Position 1 for three reactor temperatures and the effluent was analyzed with the FID, refer Figure 3.4. The resulting FID response curves exhibit similar dynamics, thereby illustrating that temperature has little or no effect on the observed dispersion.

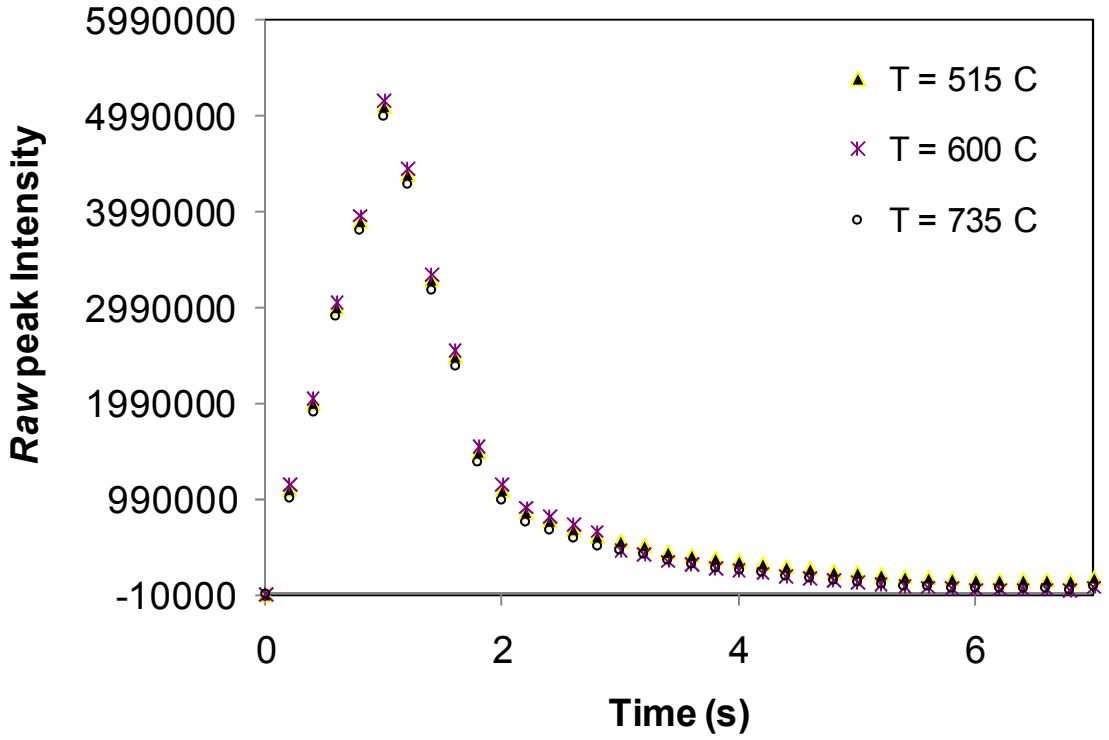

Figure 3.4: Effect of reaction temperature on dispersion test.

Since EPS volatilization temperatures range from 270 to 500 C, a series of pyrolysis experiments were conducted in and above this temperature interval. The entire experimental matrix is shown in Table 3.2. It was subsequently found that at temperatures below 465 ºC, the signal to noise ratio from the FID was very low and hence, a temperature range of 460 to 750 ºC was considered for kinetic study.

Table 3.2: EPS Pyrolysis Study Experimental Matrix (including preliminary tests)

S.No	Sample	Temperature (°C)	Test for
1	Test gas	Room	dispersion
2	Test gas	Room - 750	dispersion
3	EPS	460 - 750	pyrolysis
4	EPS	510	reproducibility

3.5. EPS Pyrolysis: - Results and Discussion

Figure 3.5 shows the *raw* (unprocessed) peak intensities collected using FID for EPS pyrolysis runs at different temperatures and Figure 3.6 shows the corresponding normalized FID peak intensity against pyrolysis time for various reactor temperatures. The normalized values for each temperature were calculated using the relationship, $I^* = \frac{I - I_{\min}}{I_{\max} - I_{\min}}$, where I represent raw peak intensity value at any time, and I_{min} and I_{max} represent the minimum and maximum peak intensities, respectively, at that particular temperature. The small peak noticeable during early reaction times, refer Figure 3.5 and 3.6, corresponds to the evolution of the blowing agent (pentane) that is dissolved in the EPS during the synthesis step.

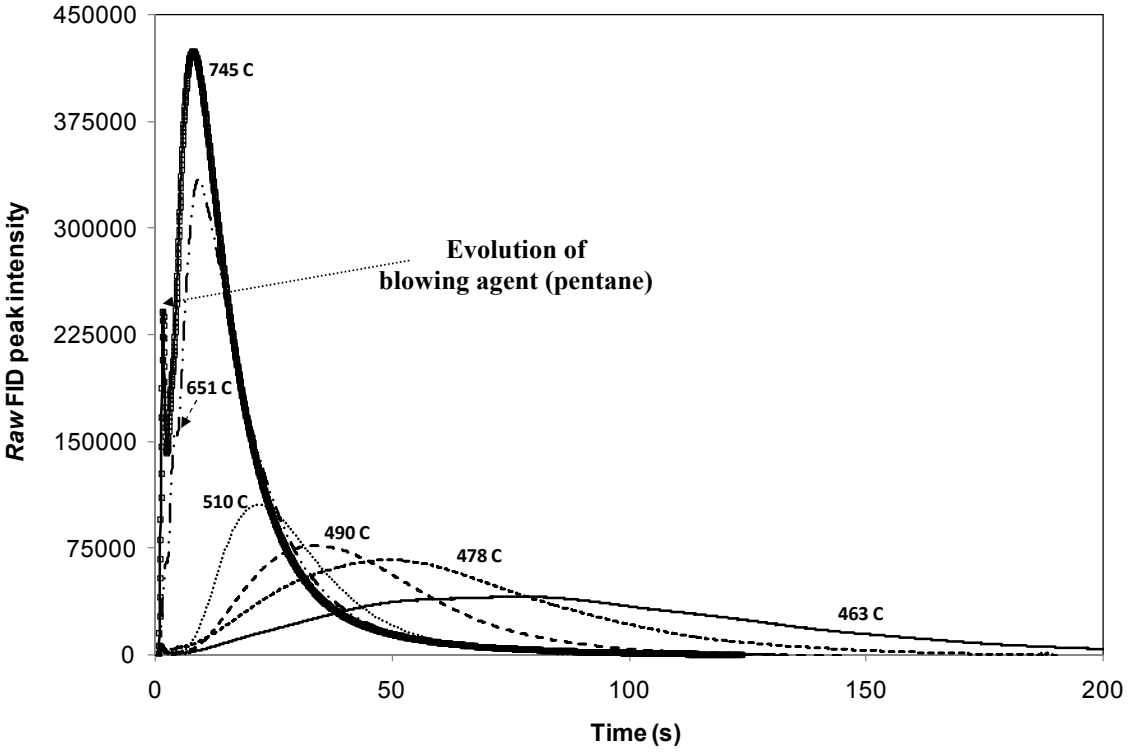

Figure 3.5: A comparison plot of FID *raw* peak intensities of EPS pyrolysis at different temperatures.

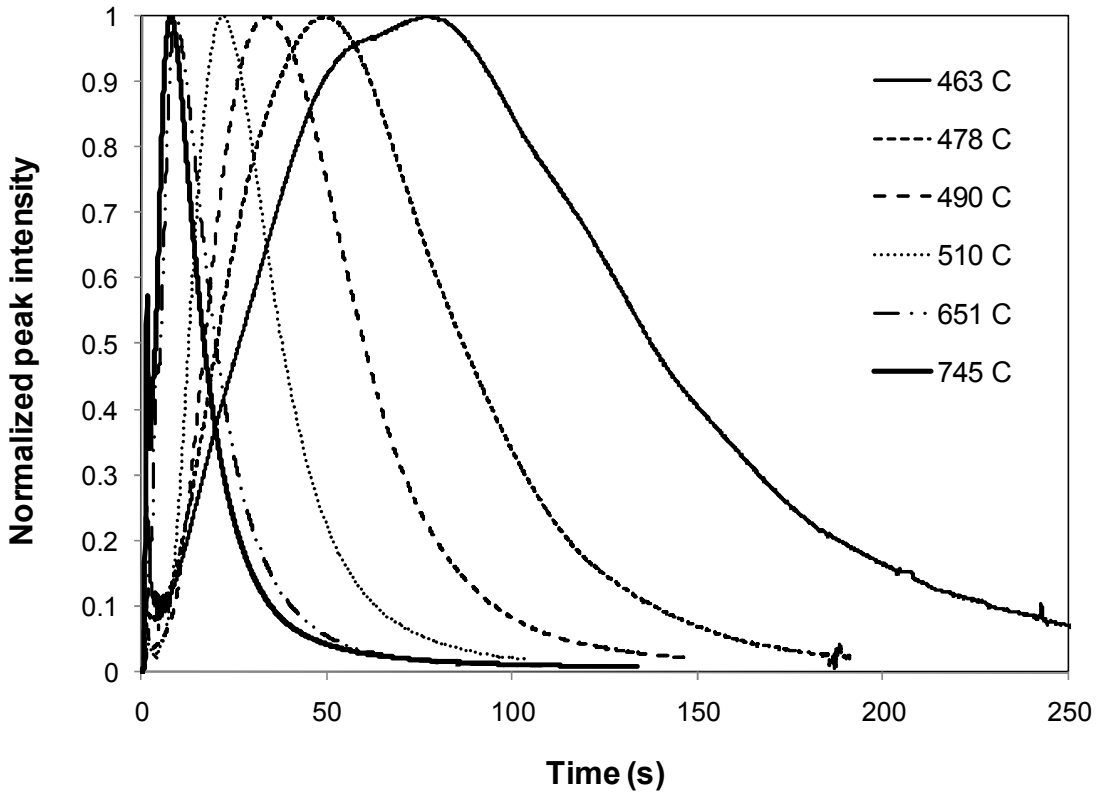

Figure 3.6: A comparison plot of normalized peak intensities of EPS pyrolysis at different temperatures.

The raw peak intensity (ion current) detected by the FID at any instant is proportional to the number of carbon atoms present in the volatiles [3.4]. It is possible to retrieve some important kinetic information based on the total yield of the pyrolysis products. The area under the curve at any instantaneous time is proportional to the cumulative amount of the volatiles generated by the pyrolysis reaction. By forming the ratio of the instantaneous value to the total area under the curve, the experimental reaction yield $Y(t)_{exp}$, defined as the ratio of the cumulative mass of volatiles formed until time t to the initial mass of the reactant could be determined. This could be mathematically expressed as shown below:

$$Y(t)_{\exp} = \frac{\int_0^t I(t)dt}{\int_0^\infty I(t)dt} \tag{3.2}$$

To test the repeatability of the experiment, three different pyrolysis runs were performed at reactor temperatures of 511 ºC, 513 ºC, and 518 ºC. It could be seen from Figure 3.7 and Figure 3.8 that the variation between each run is minimal, and the deviations observed can likely be attributed to uncertainty in reaction temperatures. The experimental yield curves for various temperature was constructed using Equation (2) while the normalized derivative values in Figure 3.8 are estimated using the normalized intensity values as described before.

Prior to any interpretations, the relative variation of the area under the raw FID curves for different temperatures and the replicates were compared and analyzed. The area under the raw FID curve divided by the initial bead mass is proportional to the volatile product yield. Since the mass of a EPS bead used in all experimental runs is nominally constant, a plot of raw FID peak area *vs*. temperature is an indicator of how volatile yield varies with reaction temperature. Figure 3.9 shows a plot of total area under the curve estimated using the denominator in Equation (2) *vs.* reaction temperature. The error bar shown on the data point at a temperature at ca. 514 ºC is based on the statistical average of the three replicates at 511, 513, and 518 ºC. It could be concluded that the differences in area under the curves shown in Figure 3.5 for different temperatures are within the range of deviations between individual experimental runs though a suggestion

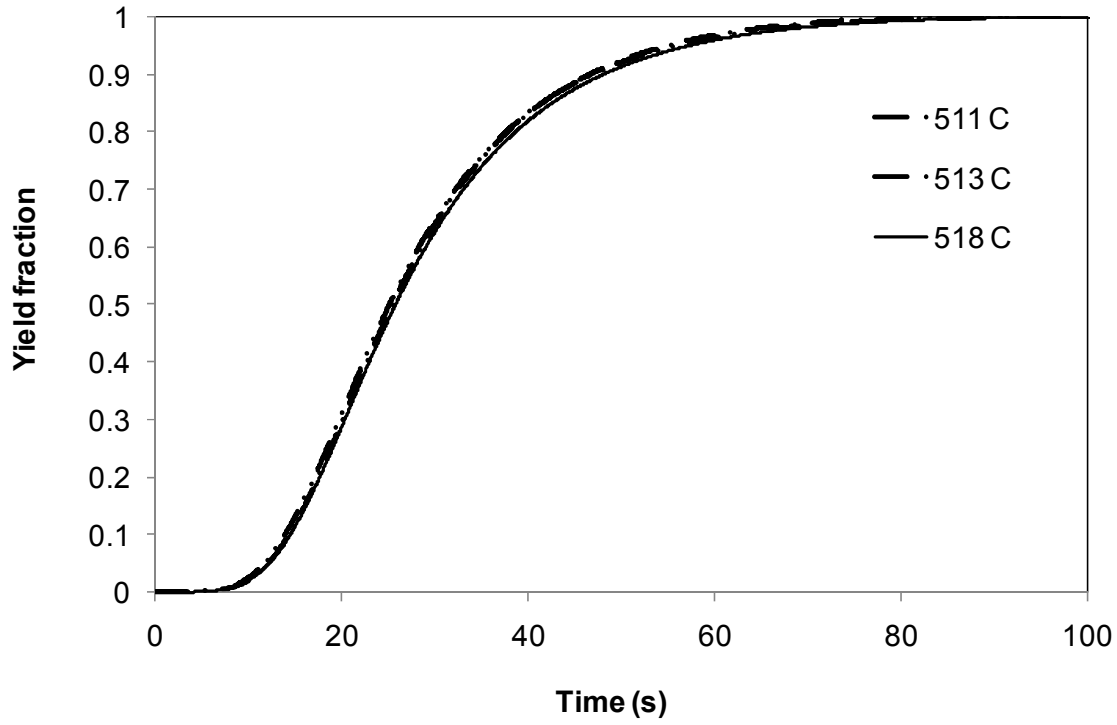

Figure 3.7: Reproducibility test; three different FID response curves at reactor temperatures of 511, 513, and 518 ºC.

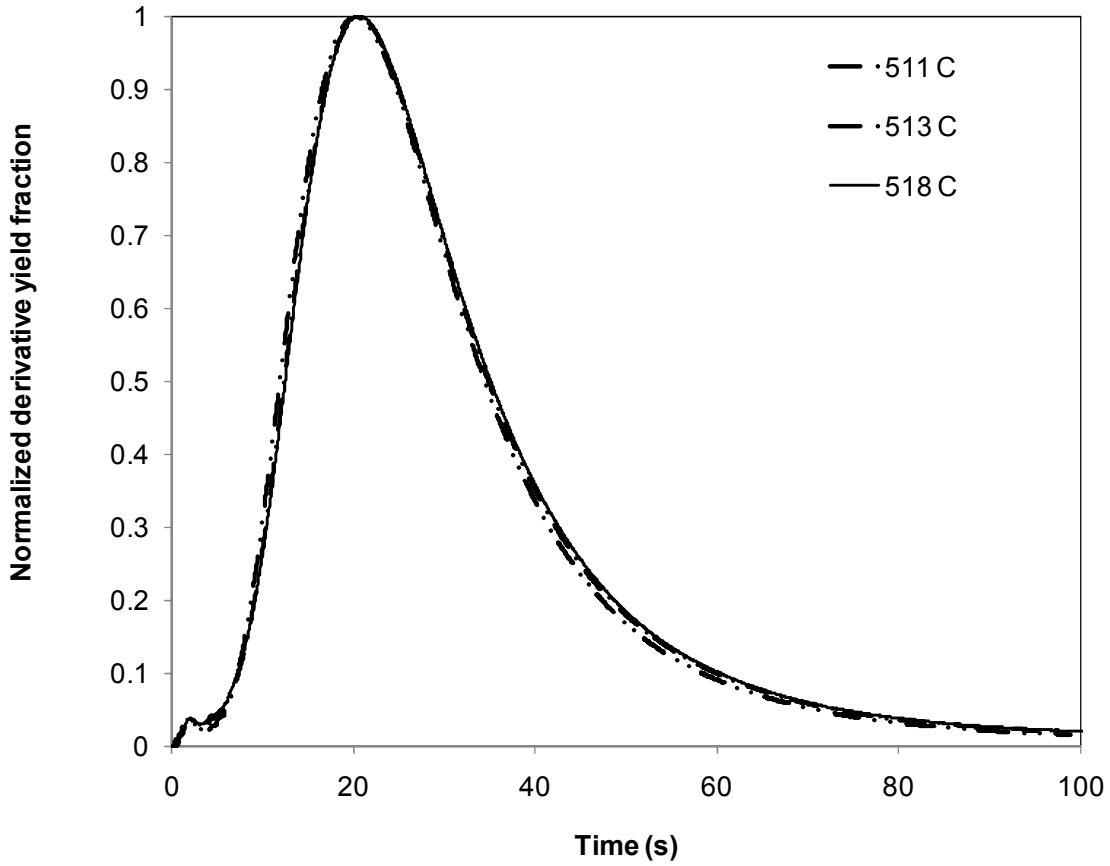

Figure 3.8: Reproducibility test; Derivative of three different FID response curves at reactor temperatures of 511, 513, and 518 ºC.

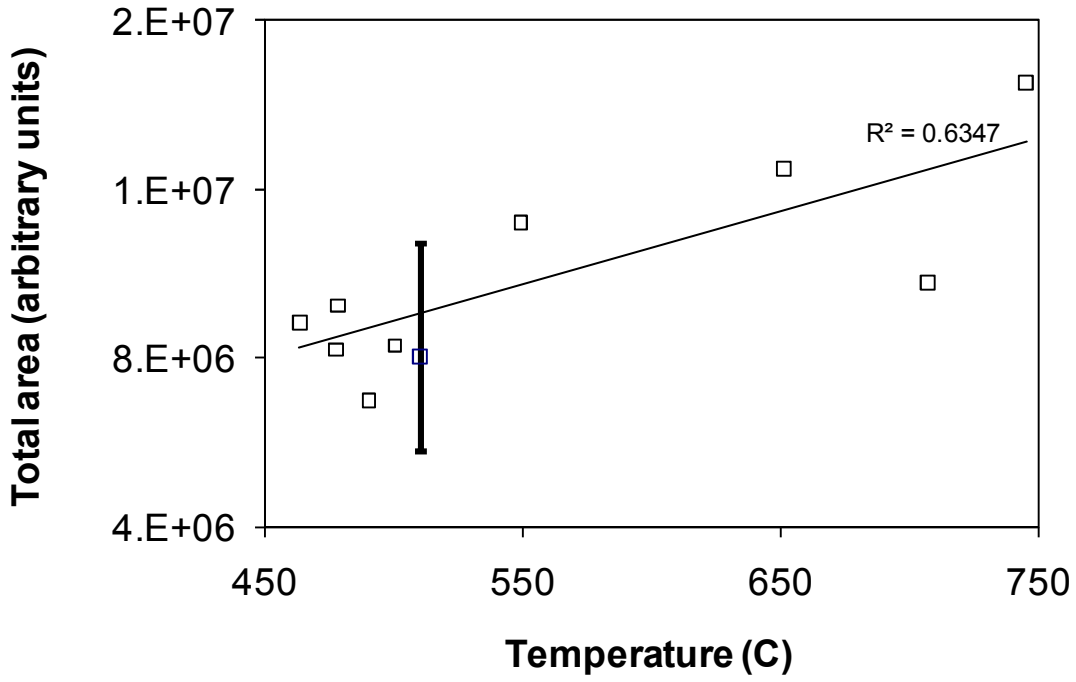

Figure 3.9: Comparison of total area under the FID curves at different temperatures experimental.

of an increasing trend is noted. One might conclude that the volatile yield increases with reaction temperature, though the statistical confidence is low.

Figure 3.10 shows a plot of experimental yield fraction *versus* reaction temperatures. The shape of the pyrolysis curve is also indicative of heat transfer influence. At short times, all pyrolysis curves exhibit hindered pyrolysis. During this period, the sample is heating, thus pyrolysis is non-isothermal. This is more apparent at low temperatures. As temperature increases, the reaction rate increases until ca. 520 ºC as shown by increasingly faster yield rates. A thorough discussion on the effects of heat transfer phenomena is presented in the later sections.

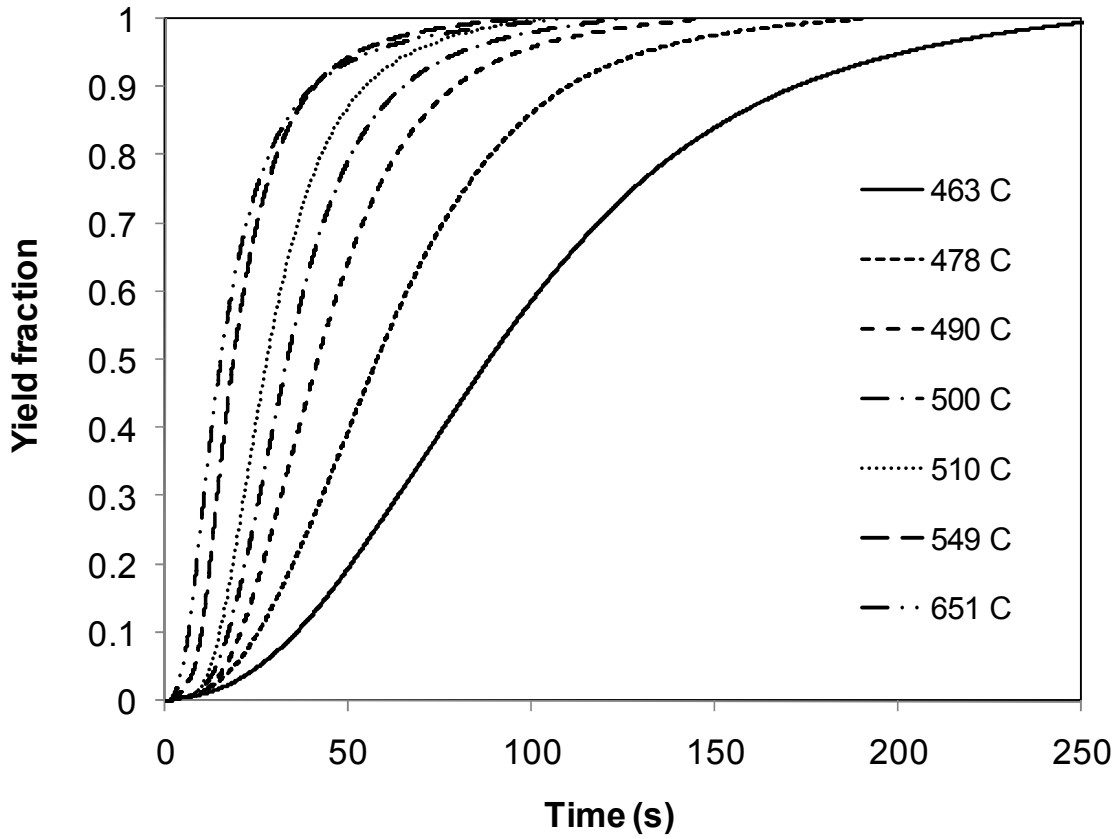

Figure 3.10: Experimental yields; fraction of volatiles at different reactor temperatures.

For a single first order reaction, a plot of $\ln(1/(1-Y(t))$ versus time should yield a straight line. A plot of this test for yield fraction between 0.05 and 0.95 at various reaction temperatures is shown in Figure 3.11. The linearity of this relationship is evident from the value of the regression coefficient ($R^2 = 0.95$). Hence, it can be assumed that the entire reaction can be suitably modeled as a single first order reaction.

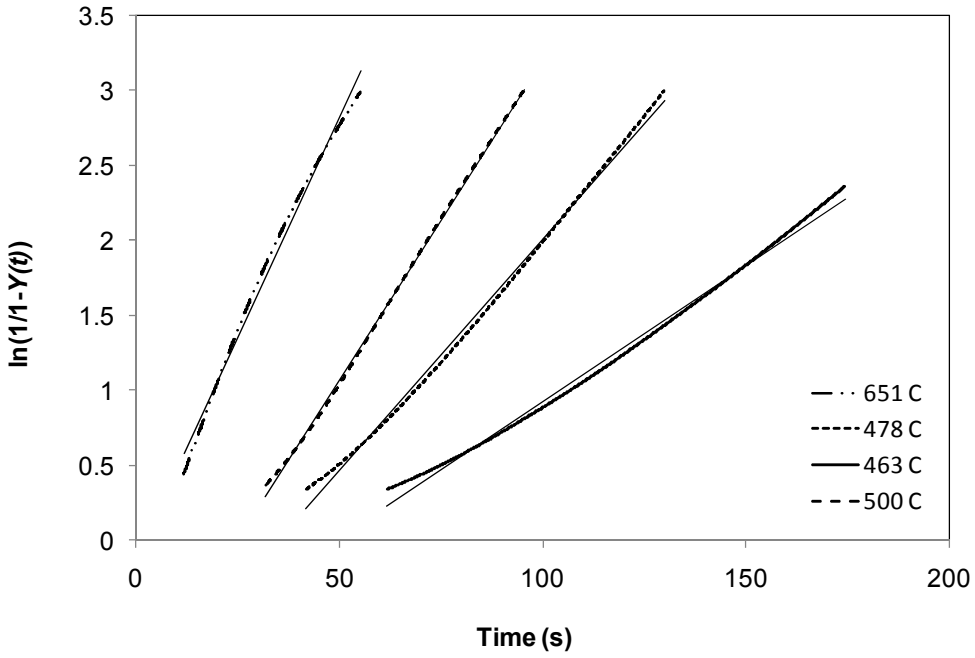

Figure 3.11: Validity test for single first order reaction for conversion between 0.05 and 0.95.

The reactor system was modeled as a continuous stirred semi-batch reactor. Figure 3.12 shows a simplified illustration of the experimental reactor setup, wherein the solid lines represent the system and the dotted lines represent the control volume. The notations V_R and T_R indicate the volume and temperature of the reactor respectively. An overall mass balance on volume V_R for the system depicted in Figure 3.12 is represented by Equation (3.3).

Rate of mass generated within the reactor	=	**Rate of mass accumulated within the reactor**	+	**Rate of mass out from the reactor**	(3.3)

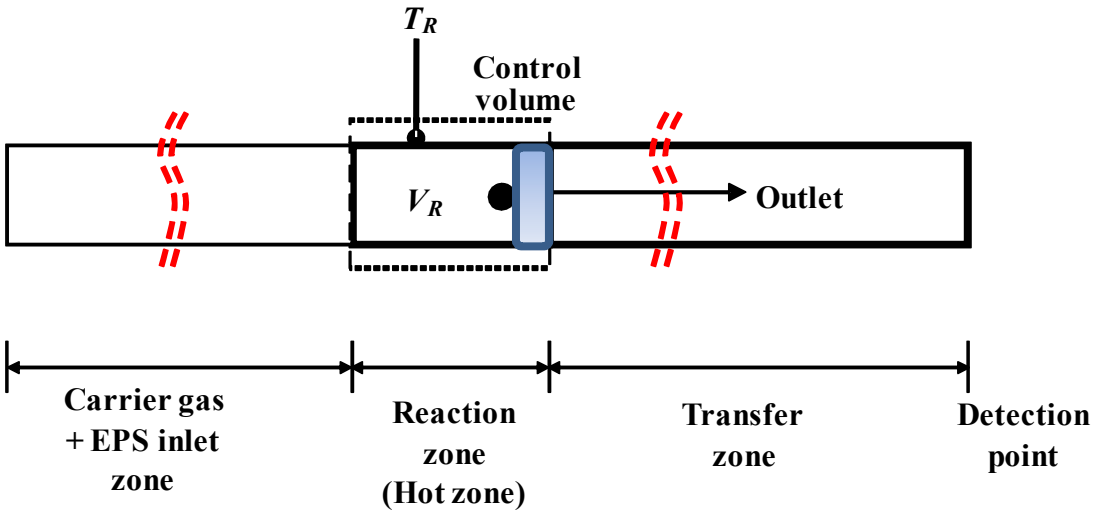

Figure 3.12: A simplified illustration of the experimental setup.

Let $m_v(t)$ denote the instantaneous mass of total volatile content and m_0 denote the initial mass of EPS. The mass balance equation can then be expressed in a mathematical form as shown below:

$$\left.\frac{dm_v(t)}{dt}\right|_{Rxn} = \left.\frac{dm_v(t)}{dt}\right|_{Acc} + \left.\frac{dm_v(t)}{dt}\right|_{Out} \tag{3.4}$$

The reaction rate for a single first order reaction could be expressed as a function of the mass of sample remaining and is given by

$$\left.\frac{dm_v(t)}{dt}\right|_{Rxn} = k\,(m_o - m_v(t)) \tag{3.5}$$

Also, the theoretical yield could be defined as $Y(t)_{\text{mod}} = m_v(t)/m_o$. Substituting in the above equation yields

$$Y(t)_{\text{mod}} = 1 - \exp(-k\,t) \tag{3.6}$$

where k is the rate constant that is assumed to follow an Arrhennius type relationship shown in Equation (3.7).

$$k = A\,\exp\left(\frac{-E}{R\,T_s}\right) \tag{3.7}$$

The mass outflow rate could be expressed as a function of $m_v(t)$, volumetric flow rate (Q) and volume of the reactor as $Q.m_v(t)/V_R$. Finally, after substituting for the individual terms into the mass balance equation, an analytical solution for $Y(t)_{\text{mod}}$ yields

$$Y(t)_{\text{mod}} = \frac{-k}{k + Q/V_R}\left[-1 + \exp\left(-t\left(k + Q/V_R\right)\right)\right] \tag{3.8}$$

Since it is not possible to determine the effective reactor volume (control volume) theoretically, the parameters k and V_R were optimized such that the objective function γ, defined as, $\gamma = \dfrac{\sum_0^t \left(Y(t)_{\text{exp}} - Y(t)_{\text{mod}}\right)^2}{n}$ was minimized for each temperature, n being the total number of time steps. Figure 3.13 shows a comparison plot of the experimental and theoretical yield fraction of the volatiles pyrolyzed at a temperature of 750 K.

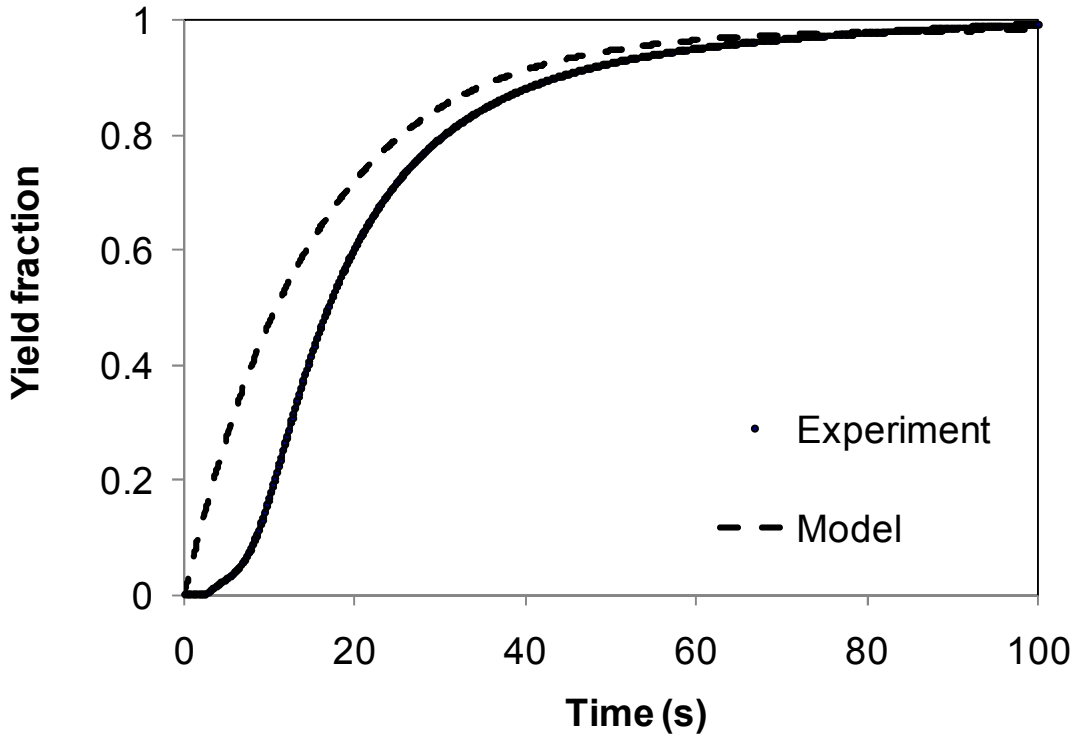

Figure 3.13: Comparison plot of experimental and theoretical yield fractions of EPS pyrolysis at 750 K.

It can be noticed that the model is not able to predict the entire decomposition behavior since it assumes isothermal conditions and, hence, does not account for the heat transfer effects occurring at early times. Therefore, before deducing and interpreting the kinetic information, it was important to account for the sample heat transfer rate by incorporating appropriate heat transfer equations into the overall kinetic model. Values of various parameters used for heat transfer calculations have been tabulated, see Table 3.3.

Table 3.3: Values of various system and thermal parameters used for calculations.

	EPS	Heater tube	Helium	Units
Diameters	0.0005	0.001	NA*	m
Thermal conductivities	0.03	NA	0.1713	W/m/K
Specific heats	1.3	NA	5193.2	J/kg/K
Emissivities	0.01	0.93	NA	unitless
Vol. flow rate	NA	NA	0.83	cc/s
Densities	7	NA	0.173	kg/m^3

*NA = not applicable

The heat necessary for the pyrolysis reaction is transferred to the sample by combined gas phase convection-conduction and radiation and by solid phase conduction. In order to determine the dominating heat transfer mechanism, both external and internal heat transfer parameters were computed and compared.

Since the calculated N_{Re} was less than 10 for all reaction temperatures, the temperature of the gas (T_g) surrounding the sample was calculated for fully developed laminar flow using the following equation [3.5]:

$$\frac{T_w - T_g}{T_w - T_a} = 0.692e^{(-5.78\pi/Gz)} + .131e^{(-30.5\pi/Gz)} + 0.0534e^{(-74.9\pi/Gz)} + ... \qquad (3.9)$$

where T_w is the wall temperature, T_a is the inlet gas temperature, and Gz is the Graetz number defined as follows:

$$Gz \equiv \frac{Q \rho_g C_g}{k_g L} \tag{3.10}$$

where ρ_g is the gas density, C_g is specific heat capacity of the gas, k_g is the thermal conductivity of the gas, and L is the length of the hot section that was measured to be ca. 0.1 m. Based on the value of Graetz number and hot section length, the temperature of the gas phase around the sample was found to be equal to wall temperature at all temperature conditions.

The convective heat transfer coefficient (h_c) between a flowing fluid and the surface of a single spherical particle is given by [3.6]

$$\frac{h_c D_p}{k_g} = 2.0 + 0.60 \left(\frac{D_p G}{\mu_g} \right)^{0.50} \left(\frac{C_p \mu_g}{k_g} \right)^{0.33} \tag{3.11}$$

where D_p represents the particle diameter, G is the mass velocity, and μ_g is the gas viscosity. Using the values shown in Table 3.3, the value of h_c was calculated to be ca. 700 W/m^2 K.

Assuming grey surfaces for both the quartz and the sample, the radiation heat transfer coefficient (h_r) for $T_w >> T_p$ is given by [3.7]

$$h_r = 4 \varepsilon \sigma_b T_w^{\ 3} \tag{3.12}$$

where σ_b is Stefan-Boltzman constant and ε is the overall interchange factor calculated using the individual emissivities (ε_1 and ε_2) and surface areas (A_1 and A_2) using the following relationship [3.8]:

$$\varepsilon = \frac{1}{1/\varepsilon_1 + \frac{A_1}{A_2}\left(1/\varepsilon_2 - 1\right)} \tag{3.13}$$

The combined heat transfer coefficient (h) was found by trial using the following equation [3.8]:

$$h = h_c \left(\frac{h_c}{h + h_r} \right)^{1/3} \tag{3.14}$$

From the computed values of heat transfer coefficients, the Biot number was estimated to be in the range of 4 to 5 indicating an external heat transfer controlled process. Hence, the heat transfer process seems to be dominated by combined gas phase convection and radiation. Thus, the unsteady-state heat balance equation based on particle temperature is given by

$$m_p C_p \frac{dT_p}{dt} = h_c S\left(T_g - T_p\right) + S\varepsilon\sigma_b\left(T_w{}^4 - T_p{}^4\right) \tag{3.15}$$

where m_p is the mass of the particle and S is the surface area of the particle. Solution of the unsteady-state heat balance equation for the particle yields a relationship for determining the average particle temperature (T_p) in terms of sample properties and heat transfer coefficients [3.10].

$$T_p = T_a \exp(-Bt) + A(1 - \exp(-Bt)) \tag{3.16}$$

where the coefficients A and B are given by

$$A = \frac{h_c T_g + 4\varepsilon\sigma_b T_w^{\,4}}{h_c + 4\varepsilon\sigma_b T_w^{\,3}} \qquad B = \frac{S}{m_p C_p}\left(h_c + 4\varepsilon\sigma_b T_w^{\,3}\right) \tag{3.17}$$

Combining Equations (3.7), (3.8), and (3.15) and discretizing, the theoretical volatile yield was estimated by optimizing kinetic parameters, including activation energy and pre-exponential constant, reactor effective volume (V_R), and heat transfer coefficient (h_r). Figures 3.14 and 3.15 show a representative comparison plot of experimental and theoretical yield fraction as a function of time for two reaction temperatures. It can be seen from the sample plots that the theoretical and experimental yield curves are in very good agreement. This is further evidenced by the values of the regression coefficient for all temperature conditions, refer Table 3.4. In all cases, the 99% confidence interval was constructed using Excel's nonlinear solver toolbox.

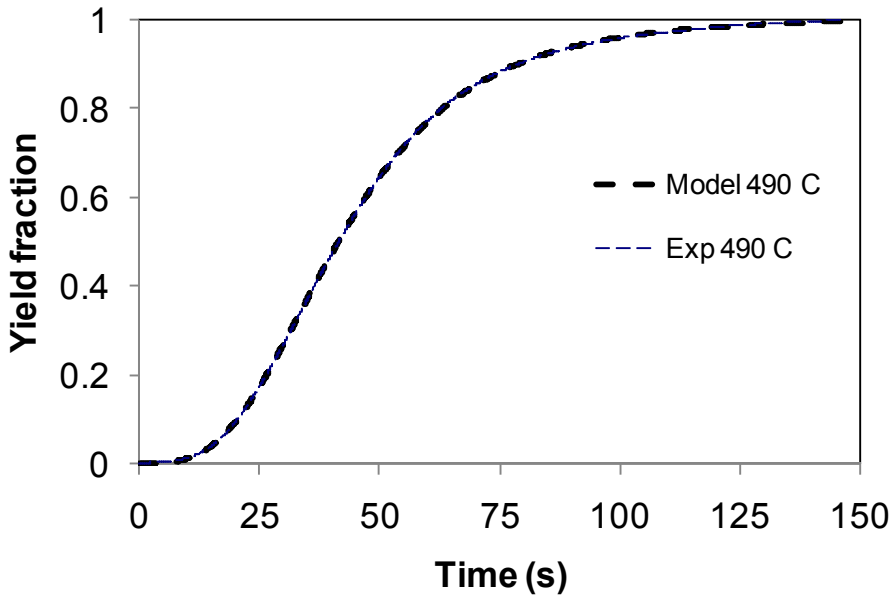

Figure 3.14: A comparison plot of theoretical and experimental yield at a heater temperature of 763 K (490 ºC).

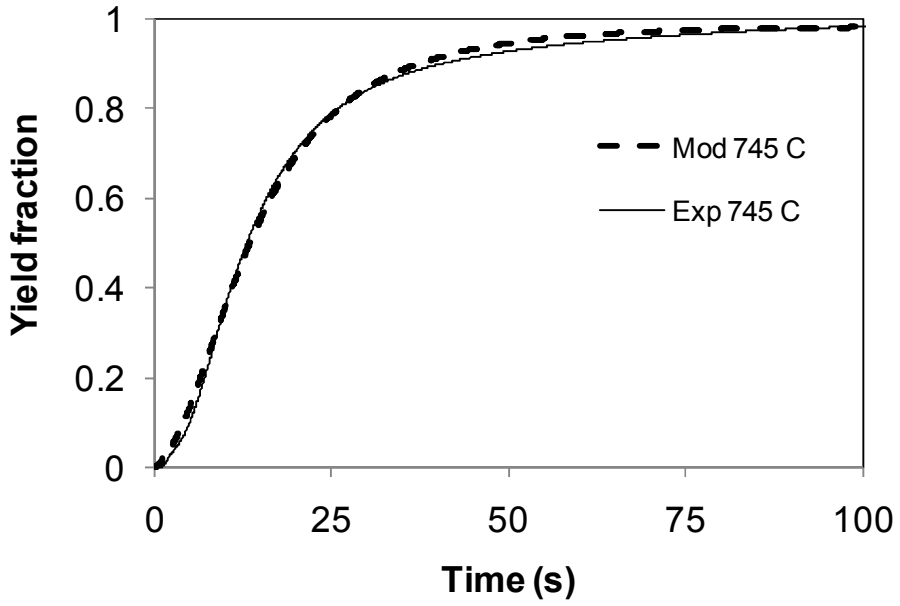

Figure 3.15: A comparison plot of theoretical and experimental yield at a heater temperature of 1018 K (745 ºC).

Table 3.4: Values of kinetic parameters, heat transfer coefficient, and reactor volume estimated by optimization with their corresponding standard deviations based on a 99% confidence interval.

T_w (°C)	E (J/mol)	A (1/s)	h_c (W/m^{2}K)	V_R (cc)	R^2
463	25023 ± 13	41.6 ± .144	31 ± .06	.031 ± 4.4E-05	0.99
477	29360 ± 12	125.9 ± .186	52 ± .03	.027 ± 9.9E-07	0.99
478	29814 ± 17	120.7 ± .2	51 ± .05	.027 ± 4.2E-06	0.99
490	37516 ± 45	290.8 ± 1.41	97 ± .19	.028 ± 1.9E-05	0.99
500	41722 ± 194	412.2 ± 5.5	143 ± 1.3	.029 ± .0002	0.99
510	42623 ± 382	395 ± 6.3	182 ±3.9	.031 ± .0006	0.99
511	37095 ± 329	238.6 ± 8.6	162 ± 2	.029 ± .0002	0.99
549	29045 ± 307	54.1 ± 1.3	194 ± 4	.028 ± .0001	0.99
651	17724 ± 81	6.07 ± .5	181 ± 7	.029 ± .0009	0.99
707	19094 ± 125	6.7 ± .5	189 ± 9	.029 ± .0008	0.99
745	13633 ± 125	3.12 ± .3	162 ± 7	.029 ± .0009	0.99

Figures 3.16 and 3.17 are an illustration of the variation of activation energy and heat transfer coefficient respectively with respect to reaction temperature. The process seems to have relatively higher activation energy (ca. 35,000 J/mol) at low temperatures compared to high reaction temperatures (ca. 15,000 J/mol). At a first glance, the values of activation energy indicates that the process might be heat transfer control rather than reaction controlled. To test this case, the reaction functional form in Equation (3.4) was modified from a simple first order relation to one that is representative of a heat transfer controlled process, refer Appendix 3.1. At lower temperatures, the resulting model equation disproves a heat transfer controlled process. However, at higher temperatures, it seems to be a heat transfer controlled process, as shown by the lower values of activation

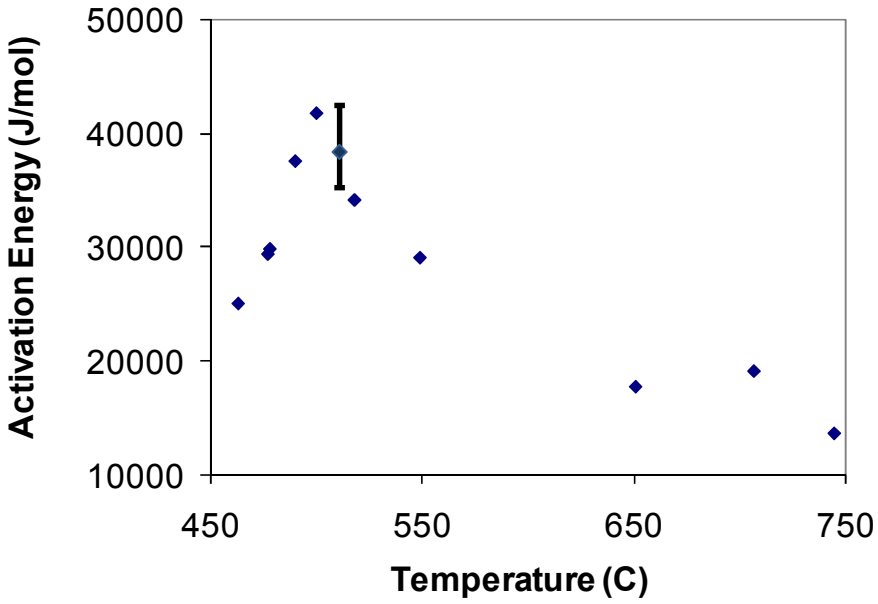

Figure 3.16: Variation of activation energy with reaction temperature.

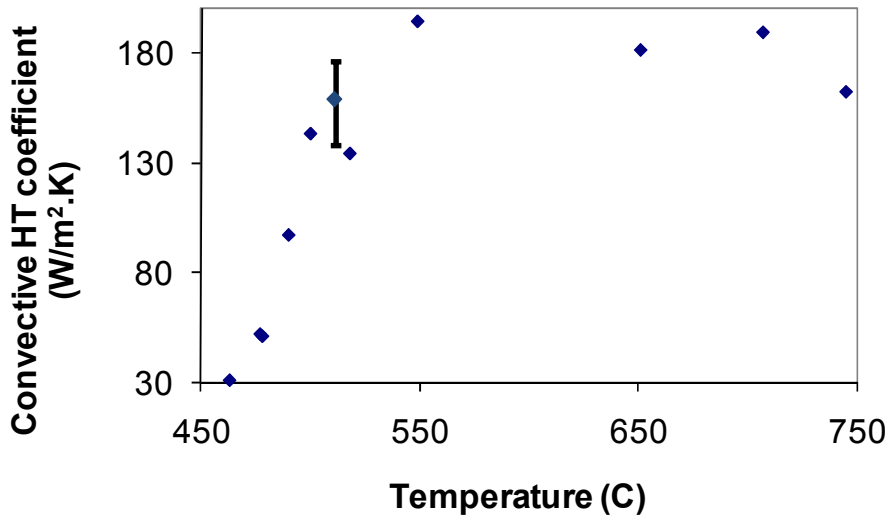

Figure 3.17: Variation of heat transfer coefficient with temperature. (The error bars at 511 ºC represent experimental error calculated based on three replicates at nominally the same temperature).

energy. Hence, the overall decomposition process seems to be a reaction-controlled phenomena only at lower temperatures. There is also a corresponding increase in the values of heat transfer coefficient until 550 ºC, after which it remains steady at ca. 180 W/m^2K. The value of convective heat transfer coefficient estimated from optimization is ca. four times smaller than theoretical predictions that were calculated to be ca. 700 W/m^2K.

In order to compare the relative scale of the statistical error (S.E) to the experimental error (E.E), standard deviations were calculated for the replicate runs at 511 ºC. It could be seen from Figures 3.16 and 3.17, and Table 3.5 that the experimental errors are higher than the statictical error. This difference could be mainly attributed to the sampling size over which the total errors are averaged. While the S.E is based on ca. 3000 sample points, the E.E is averaged upon three individual experimental runs with slight variations in temperature and sample mass.

The activation energy values reported in this study are much lower than the ones reported in literature [3.2] for EPS decomposition process. This is because most of the kinetic data presented in literature were obtained from conventional thermal instruments

Table 3.5: Standard deviations of kinetic parameters, heat transfer coefficient, and reactor volume based on statistical error (S.E) and experimental error (E.E).

	Average	**S.E**	**E.E**
E	38295	329	3728
h_c	158.6	2	19
V_r	0.029	0.0002	0.002

where the heating rate is usually on the order of 50 to 100 K/min. In the present study, the heating rate calculated based on the particle temperature is as high as 1200 K/min and is on the order of 1000 K/min on an average, see Figure 3.18. This value was computed from the slopes during the non-isothermal heating period. However, it has been predicted that the heating rate in LFC environment is possibly on the order of a few thousand degrees per second [3.11]. It is a challenging task to design and fabricate a laboratory scale reactor that is capable of delivering such high heating rates as encountered in metal castings. Nevertheless, it could be noticed from the experimental yield curves, see Figure

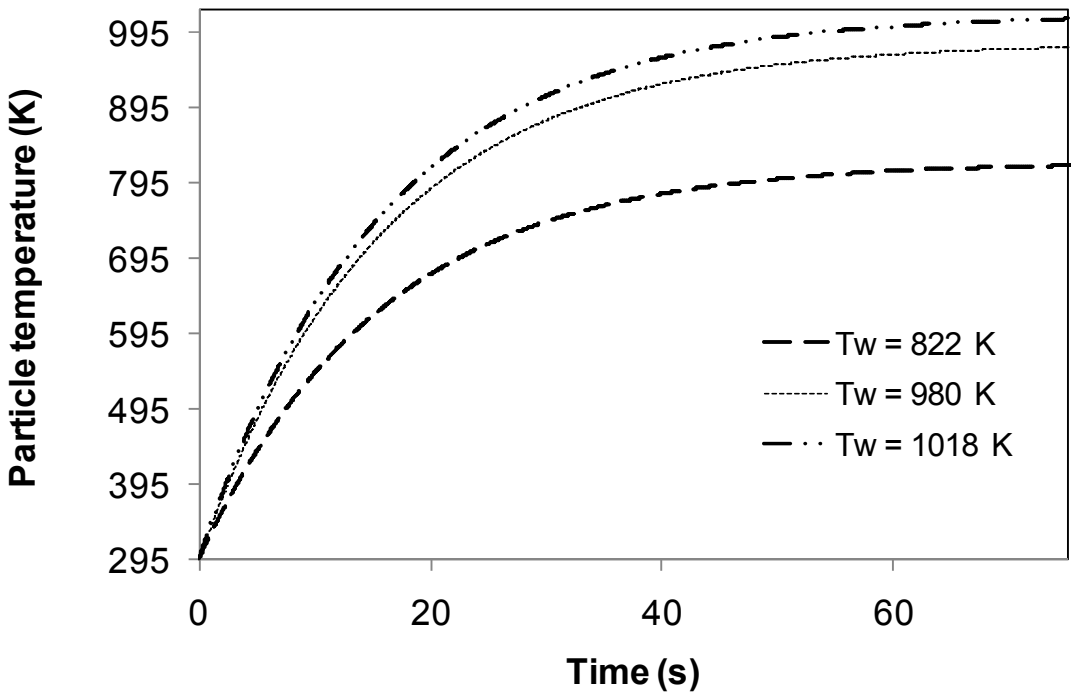

Figure 3.18: EPS sample temperature at various times during the reaction process for various constant reactor wall temperatures.

3.10 that the reaction seems to proceed at a constant rate after a certain temperature, which is also indicated by very low activation energies at these temperatures.

Finally, based on the reactor *effective* volume, the length of the actual reaction zone was estimated to be around 1 cm. This scale indicates that the EPS vaporization is very localized and located near the Fiberfrax insulation plug. This reduces the effects of any temperature variations that might be present along the axial length of the heater tube.

3.6. Conclusions

This study demonstrates a technique to study *fast* pyrolysis of EPS in a laboratory-scale environment. The entire experimental setup, including the reactor designed in this study seems a viable and reliable apparatus for collecting experimental data at elevated temperature conditions with very little influence of the lower temperature regions. Furthermore, a methodology for obtaining kinetic parameters, including activation energy and pre-exponential constant for EPS pyrolysis has been successfully demonstrated. Finally, by accounting for the heat transfer coefficients and volumetric capacitance, the external effects on the kinetic parameters were minimized.

3.7. ENDNOTES

3.1. T. Liliedahl and K. Sjostrom, AIChE Journal, 40 (1994) 1515.

3.2. P. Kannan, J. J. Biernacki and D. P. Visco Jr., J. Anal. App. Pyrolysis, 78 (2007) 162.

3.3. C.E. Bates, J. Griffin and H. Littleton, Expendable Pattern Casting-Process Manual, AFS publication, 1 (1994) p. 75.

3.4. W. J. Kuipers and J. Muller, J. Micromech. Microeng., 18 (2008) p. 7.

3.5. W. L. McCabe, J. C. Smith, and P. Harriott, Unit Operations of Chemical Engineering, McGraw-Hill, NY, (2001), p. 343.

3.6. W. L. McCabe, J. C. Smith, and P. Harriott, Unit Operations of Chemical Engineering, McGraw-Hill, NY, (2001), p. 364.

3.7. W. L. McCabe, J. C. Smith, and P. Harriott, Unit Operations of Chemical Engineering, McGraw-Hill, NY, (2001), p. 426.

3.8. W. L. McCabe, J. C. Smith, and P. Harriott, Unit Operations of Chemical Engineering, McGraw-Hill, NY, (2001), p. 422.

3.9. W. L. McCabe, J. C. Smith, and P. Harriott, Unit Operations of Chemical Engineering, McGraw-Hill, NY, (2001), p. 427.

3.10. L. S. Fan and C. Zhu, Principles of Gas-Solid Flows, Cambridge University Press, London, (1998), p. 148.

3.11. T. Molibog, Experimental Modeling of the Metal/Pattern Exchange Mechanism in the Lost Foam Casting Process, M. Eng. Thesis, University of Alabama, Birmingham, (1999).

3.8. APPENDIX 3.1

For a heat transfer controlled process, the rate of volatile generation is given by:

$$\frac{dm_v(t)}{dt} = \frac{h_c S}{\Delta H_r}\left(T_g - T_p\right) \tag{1}$$

where ΔH_r is the endothermic heat of the reaction, S is the surface area of the particle, h_c is the heat transfer coefficient, $m_v(t)$ is the mass of the volatiles at any instant t, T_g is the gas temperature and T_p is the particle temperature. In terms of yield fraction (Y), this can be written as

$$\frac{dY}{dt} = \frac{h_c \Delta T}{\Delta H_r}\frac{4\pi R_p(t)^2}{m_0} \tag{2}$$

where $R_p(t)$ is the radius of the particle at any instant t, and m_0 is the initial mass of the sample.

Also,

$$R_p(t) = R_0 Y \tag{3}$$

where R_0 is the initial radius of the particle. Substituting for $R_p(t)$ in terms of Y in Equation (2) yields

$$\frac{dY}{dt} = K'(1-Y)^2 \tag{4}$$

where the constant K' is equal to $\frac{3h_c\Delta T}{R_0\ \Delta H_r \rho_p}$.

Hence, for a heat transfer controlled process, a plot of (Y/(1-Y)) against t should yield a straight line. Figure A shows poor linearity for such a relationship for three different temperatures of 463, 478 and 651 ˚C.

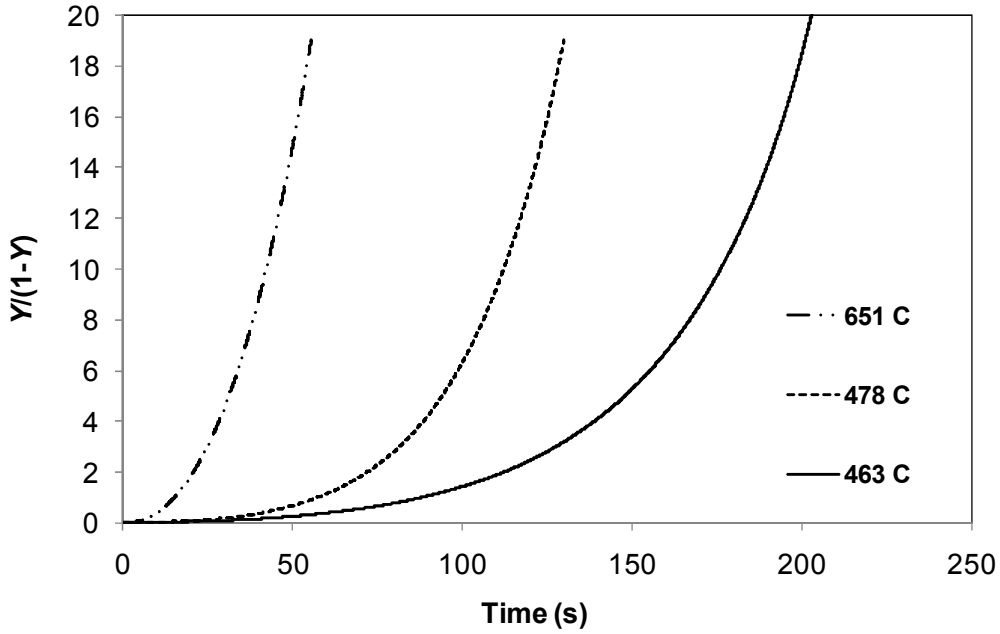

Figure A: Linearity test plot for a heat transfer controlled process.

PART 4

A SIMPLE MULTI SCALE TECHNIQUE FOR DETERMINING GAS DIFFUSIVITY THROUGH EPS FOAMS

4.1. Overview

A simple multiscale model was developed and used to predict gas diffusivities through expanded polystyrene foam at *near* standard temperature and pressure (STP) conditions. The technique involves measuring gas diffusivities at various length scales then combining them using an electrical analogy for parallel resistances to construct an effective property. A commonly used experimental technique, the *continuous flow* method, was used to obtain diffusivity data for argon through polystyrene films and foams. While a simple Fickian mathematical model was able to predict diffusivities through films, a simple "coarse" multiscale model that accounts for the morphological features was developed for the foam.

4.2. Introduction

Expanded foam patterns are characterized by a complex, cellular and porous heterogeneous structure, and hence foam properties such as diffusivity and thermal conductivity are macro-scale apparent parameters. Figure 4.1 is a conceptual illustration of the multi-scale nature of gas diffusion through EPS foam pattern. Gas molecules,

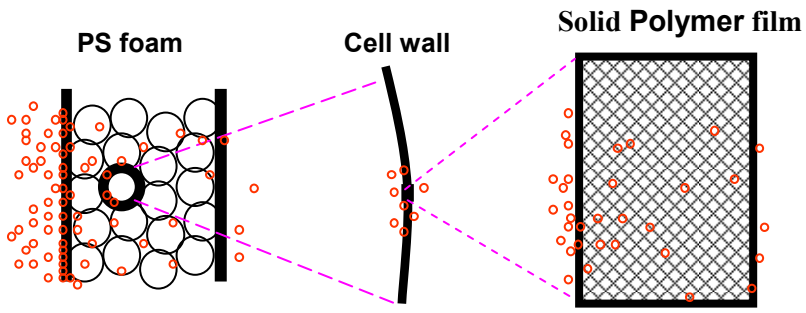

Figure 4.1: Schematic representation of the gas diffusion process in EPS foams.

diffusing from one side of the foam "pattern" to the other, transit through many individual polystyrene beads and the voids present between them. Each polystyrene bead is made up of numerous dodecahedral polymeric film cellular structures of different wall thickness that depends on various processing factors during the pre-expansion step [4.1]. The diffusing gas, within each of these polymeric membranes, first gets adsorbed on the cell surface, dissolves in the solid polymer constrained by its solubility limit, diffuses through the polymer by molecular diffusion, desorbs (detaches) from the other side of the membrane, transports through the gas phase by conduction and possibly convection and the process continues until the gas diffuses out of the bead and ultimately out of the pattern. Apart from the beads, there also exists a pathway between poorly fused beads that may contribute significantly to the overall gas transfer process. Such is expected to result in higher effective diffusion rates through the foam. Prior investigations [4.2] assume that the entire diffusion phenomenon is controlled by gas diffusion through the solid polymeric cell wall, since the gas penetration through the polymer is very slow when compared to the flux through the gas phase inside the bubble, and totally ignore

interconnected voids. This work is an attempt to clarify the differences in the existing theories in the literature and propose a possible and improved model for gas transport in EPS foams.

Figure 4.2 illustrates the *multiscale* nature of the morphology of expanded polystyrene foam. Figure 4.2a shows an SEM micrograph of a single pre-expanded polystyrene bead at 200x magnification. The term "pre-expanded" means that the PS has been partially expanded, having been processed in a pre-expander during post-synthesis processing [4.3]. Figure 4.2b is a micrograph of the cut section of an expanded PS foam pattern at 50x magnification and Figure 4.2c is a micrograph of a cut section of single expanded bead at 200x magnification. These figures clearly depict the various morphological features of the foam, including individual cells, voids (where there is no bond between the beads), and struts (fused bead walls).

Information regarding gas diffusion through polymeric foams is useful in many applications, including building and spacecraft insulation, food packaging, and metal casting. A common metal casting technique, for example, is the *lost* foam casting (LFC) process wherein knowledge of gas diffusion through expanded polystyrene (EPS) foam may lead to new and improved practices. Foundry trials have shown that when the foam is purged with helium before casting, the foam pyrolysis efficiency and the quality of the cast part is improved significantly [4.4]. However, the role of the gaseous environment in purging and during casting is not yet understood. These and similar challenges form the basis and motivates the present research on diffusion in EPS foam. The objective of this

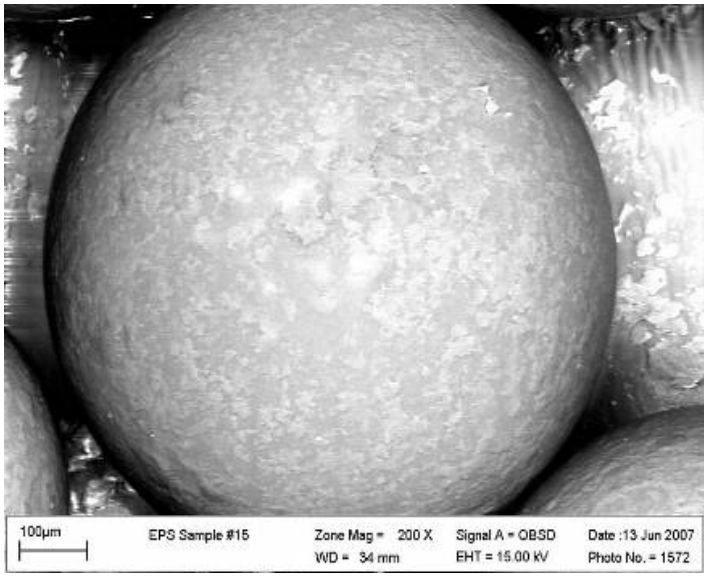

Figure 4.2a: A single pre-expanded PS bead (before molding)

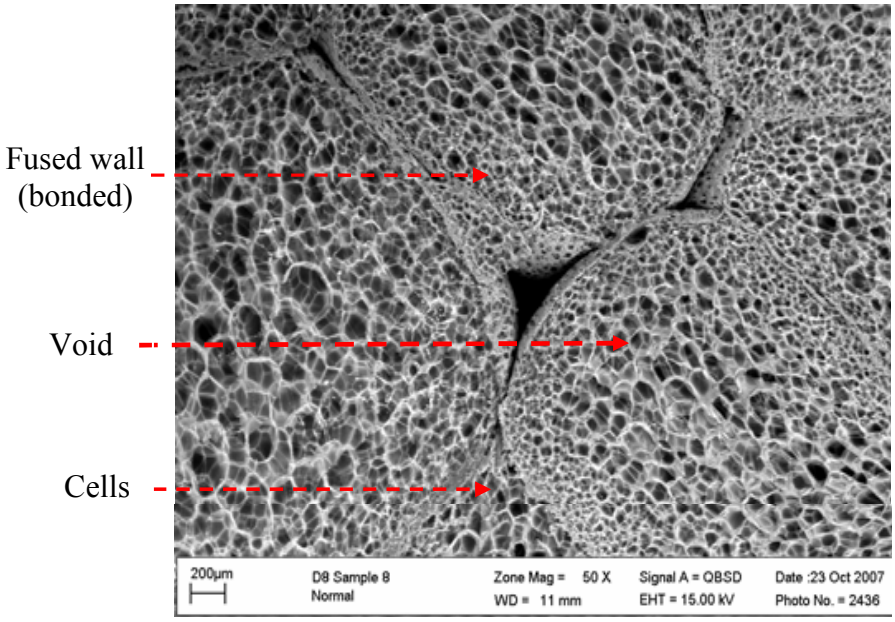

Figure 4.2b: Expanded PS pattern (normal fusion level)

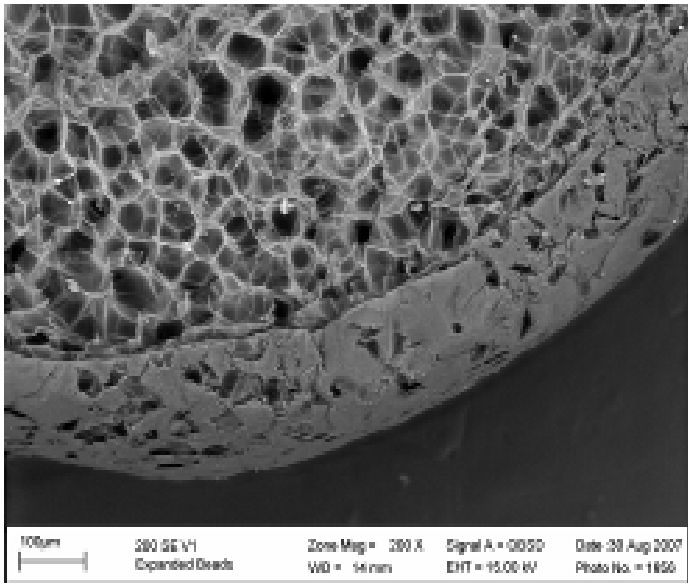

Figure 4.2c: Interior of an expanded bead showing cell structure

Figure 4.2 (4.2a to 4.2c): A multi-scale representation of the morphology of expanded polystyrene beads [4.3].

diffusion study is to extend the use of multi-scale techniques for predicting foam diffusivities.

4.3. Literature Review

An extended review of experimental techniques for gas-solid diffusion in polymer membranes is available elsewhere [4.5], and only a few of which are pertinent to the current work are discussed briefly below. This section also summarizes various techniques that have been presented in the literature for predicting gas diffusivities through complex structures, including porous materials and polymeric foams.

Many researchers, including Haraya et al. [4.6] and Ganesh et al. [4.7], have used "free volume" theory to predict gas diffusion rates in polymeric membranes. This theory assumes that the gas diffusion occurs only through the free volume of the polymer i.e., volume that is not occupied by the polymer molecules. This concept was developed in an attempt to unify and incorporate some critical polymer-gas inherent factors that affect the diffusion process [4.6]. The most typical expression that relates diffusivity to fractional free volume is given by the Doolittle expression:

$$D = A\exp\left(\frac{-B}{V_f}\right) \tag{4.1}$$

where A and B are constants characteristic of the polymer-penetrant system and V_f is the specific free volume of the polymer, e.g. the difference between the specific volume of polymer (V) and occupied volume (V_o). While V is determined from bulk density measurements, V_o is calculated using the relationship $V_o = 1.3V_w$ where V_w is the van der Waals volume and is approximated using Bondi's group contribution method [4.8]. Lee [4.9] calculated the specific free volume of polystyrene using the above method and the value was found to be ca. 99 cc/mol. Using the values for the two Doolittle constants A and B for argon reported by Haraya [4.6], the theoretical diffusivity for the argon – polystyrene system was calculated here to be 5.8 E-09 m^2/s. However, values for Doolittle constants are not always readily available in the literature, and hence the concept of "free volume" has been restricted to only a few diffusion studies. In such cases, the theoretical calculations are insufficient and diffusivity values had to be determined experimentally.

Two standard measurement methods have previously been used to obtain diffusivity values for gas-polymer systems: (1) gravimetric method (based on weight change) and (2) permeation method (based on either pressure or concentration change). These techniques have been demonstrated earlier for determining diffusivities in both polymeric film and foam samples with little or no modifications. In the gravimetric sorption method, as employed by Booth et al. [4.10], the foam sample is first degassed and then flooded by the diffusant gas. The weight change of the polymer sample during sorption is continuously recorded. This approach is quite effective only when studying diffusion through individual polystyrene beads, and is not accurate when a non-homogeneous foam sample is tested. The effective bead surface area with which the diffusant gas makes contact (before adsorption) is affected by the percolated pathways and voids present in the foams. The permeation method involves an experimental technique that either measures the amount of gas that diffuses through the material due to a concentration gradient, or the pressure change in the downstream volume side due to gas permeation as a function of time. Because the pressure differential method requires detailed and accurate design considerations to prevent leaks, an ambient pressure gas flow method seems better suited for diffusion studies. Furthermore, if interconnected pathways are present between poorly fused beads, the pressure gradient would produce a convective flux as well as diffusive flux of mass. Pasternak et al. [4.11] employed a pressure differential technique to study gas diffusion in low-density polyethylene (LDPE) films and Felder et al. [4.12] studied diffusivity of sulfur dioxide in a polytetrafluroethylene (PTFE) tube. While Pasternak's technique involved continuous

thermal conductivity monitoring of the diffusant gas, Felder utilized an electrochemical transducer SO_2 detector to track the rate of gas permeation through the membrane.

The type of data analysis chosen to determine gas diffusivities through polymers depends on the experimental technique employed in the study. In some cases, only a part of the entire data set is used for determining diffusivity while other methods necessitate utilization of the complete data set for accurate predictions. A comprehensive review of the theoretical models used to describe transport of small gas molecules through polymer membranes has been summarized elsewhere [4.13]. The most common methodology for predicting polymer film diffusivities involves utilizing "processed" experimental data for solving the transient diffusion equation under appropriate boundary and initial conditions. One of the other most frequently used techniques to obtain film diffusivity values from permeation data is the time lag method [4.14] originally developed by Barrer. Time lag is interpreted as the time taken by the diffusant molecules on the upstream compartment to transit through and exit the membrane at a constant rate. This method requires experimentally measured values of the time lag (θ) for a corresponding membrane thickness (L) and is given by the following expression:

$$D = \frac{L^2}{6\theta} \tag{4.2}$$

where D represents the diffusivity of the gas-polymer system. The problem in applying this method for polymeric foams is that it takes significantly longer time for the sample to establish steady state conditions thereby necessitating unreasonably long experimental times. Furthermore, extending this method for foam diffusivity predictions may result in

erroneous information because it does not account for the cracks and holes present in the foam network.

Models describing gas diffusion in polymeric foams can be generally categorized into continuous diffusion models and discrete diffusion models [4.15]. While the continuous models, including that of Cuddihy [4.16], Mehta [4.17], and Svanstrom [4.18], treat the foam as a continuous homogeneous polymer medium, discrete models, including those of Norton [4.19], Alsoy [4.15], Pilon [4.2], and Booth [4.10], predict effective foam diffusivity as a function of both polymer diffusivity and morphological parameters. One of the biggest challenges in developing an accurate discrete model for complex polymer structures lies not only in predicting gas diffusivity through the component polymer, but also in incorporating the real morphological structure of an EPS sample. The most characteristic and common feature of all discrete models is the basic representation of the complex polygonal cell structure as a simple cubic array of uniformly distributed cells. One such model developed by Pilon et al [4.2] appears to be the most recent and exhaustive discrete approach. This model relates the foam diffusivity (D_{eff}) to the film diffusivity (D_f), and morphological parameters, including porosity (ϕ) and foam thickness:

$$D_{eff} = G(\phi, n) D_f \tag{4.3}$$

Here, G, the geometric factor is a function of foam porosity (ϕ) and the number of equivalent cubic cells (n) that comprises the foam:

$$G(\phi, n) = \frac{1}{n}\left[1 + \frac{\phi}{1 - \sqrt[3]{\phi}}\right] \tag{4.4}$$

where n is the ratio between the foam thickness (T_f) and the unit cubic cell thickness. The film diffusivity is assumed to follow an Arrhenius relationship with corresponding activation energy of E_f.

In conclusion, it is obvious that the structural parameters of the foam dictate the manner in which the individual diffusivities have to be combined in order to predict the effective diffusivity values. These models were primarily built on two characteristic parameters: a bulk foam morphological parameter that includes porosity and cell size, and a thermo physical parameter that is mainly comprised of the polymer membrane diffusion coefficient. These models focus primarily on ways to best represent the foam architecture in order to capture effective foam morphological parameters, and to an extent have been quite successful. The accuracy of these models depends on literature diffusivity data for a particular gas-polymer, which is sometimes not readily available. In such cases, it becomes imperative to conduct appropriate diffusion experiments to determine those missing values. Most importantly, all the previous works described above neglect gas diffusion through the cracks or holes that are present in the foam. Depending on the size of these pores, other mechanisms such as Knudsen diffusion might play a significant role in the overall diffusion process.

Since there is ca. five orders of magnitude difference in time scales between various diffusion steps, as shown later in this work, this problem could benefit from the use of a multiscale approach. The goal of the present study was to combine experimental

and modeling techniques to form a more distributed description of diffusion through polystyrene foams, which incorporates a multiscale approach. The outline of the methodology is illustrated in Figure 4.3 and could be viewed as two steps. In the first step, experimental diffusivity values were estimated by using a continuous diffusion model. Other diffusivities, including Knudsen and molecular diffusivities were also calculated from theory. Subsequently, the individual diffusivity values, along with the discrete multiscale model, were utilized to estimate values of geometrical factors and fractional contribution of component diffusivities.

4.4. Experimental Procedure

Two types of polystyrene samples were used in this study, film and foam**.** Polystyrene films prepared by a film blowing technique of thickness ranging from 30 to 270 microns were obtained from Plastics Suppliers Inc. In the laboratory, samples of ca. 5 cm diameter were cut using a knife. Polystyrene foam boards processed by steam molding of expandable polystyrene beads were supplied by Foseco Plc. For all foam studies, samples of ca. 1 cm thickness and 3.75 cm diameter were cut from the boards using a sharp metal die. The term “sample”, appearing throughout this manuscript, is a collective term used to represent polystyrene film and polystyrene foam types.

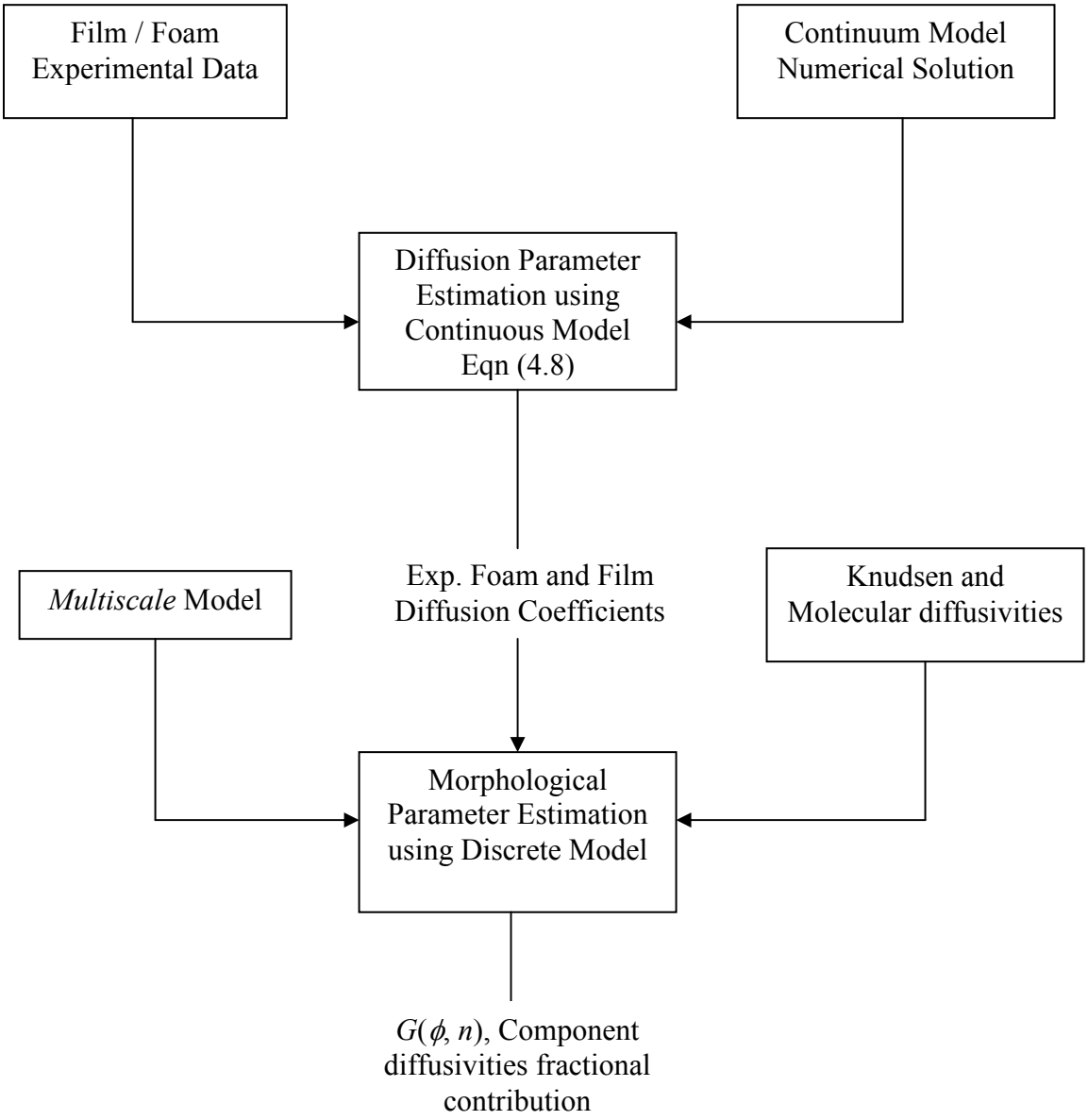

Figure 4.3: Overall methodology of the multiscale technique employed in this study.

4.4.1. Continuous Flow-Zero Net Pressure Gradient Diffusion Experiment

A simple diffusion apparatus (refer Figure 4.4) comprised of two built-in chambers, a purge chamber and a sampling chamber, fitted with entrance and exit gas ports, was built for obtaining diffusion experiment data. The entire diffusion experiment was carried out in two steps: First, a concentration gradient was established between the two chambers separated by the polymer sample. Second, the concentration change of

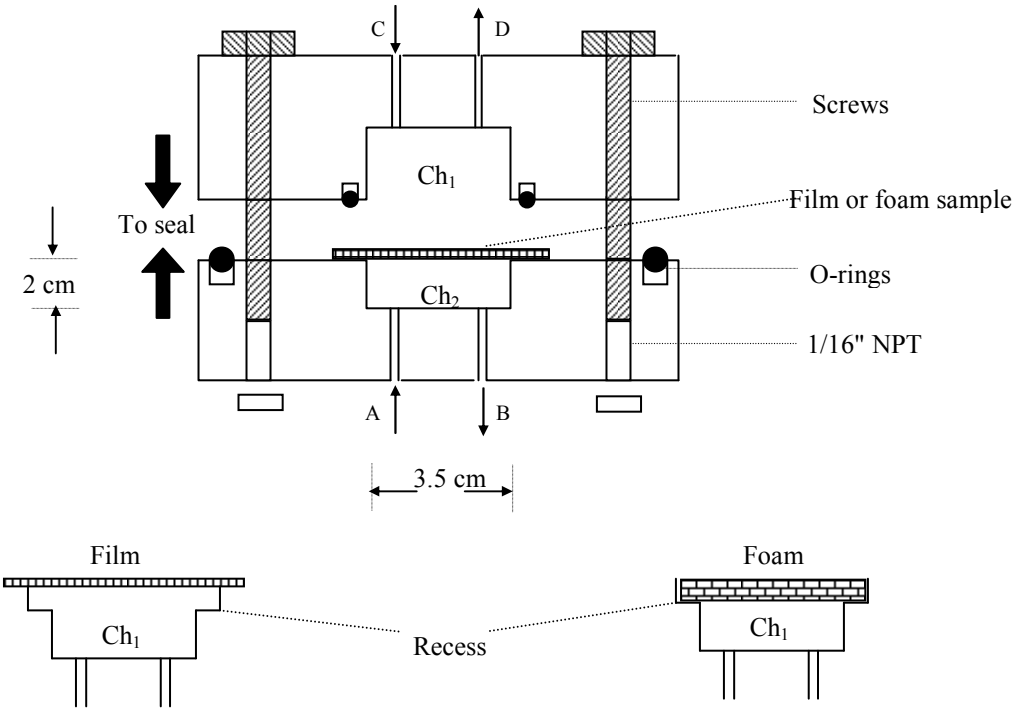

Figure 4.4: A view of the diffusion cell (Notations: A – carrier gas in, B- carrier gas out to mass spectrometer, C – diffusant in, D – diffusant out, Ch_1 – Purge chamber, Ch_2 – sampling chamber). Position of film and foam samples is also shown in the figure.

the neutral gas in the sampling chamber was continuously monitored using a mass spectrometer while the other chamber was left purging with the diffusant gas. To accomplish this, the sample to be tested was glued between the two chambers using a silicone gel, and sealed tightly with a pair of O-rings and screws. Details regarding positioning of the samples have been depicted in Figure 4.4. Initially both chambers (Ch_1 and Ch_2) were purged with a neutral carrier gas (nitrogen) until other contaminant gases were removed from the system. The volume of the sampling chamber (V_2) and purge chamber (V_1) were about 9.6 cm^3 and 20 cm^3, respectively. Once a baseline concentration was attained, the three-way valve control located on the purge chamber gas line was changed in order to allow the diffusant gas (argon) into Chamber 1, and the corresponding time was initialized to zero. The flow rate of the diffusant gas into Chamber 1 (F_1) was high so that V_1/F_1 was on the order of 16 s. The carrier gas (nitrogen) transports any purge gas that diffuses through the sample (membrane) to the mass spectrometer for continuous compositional analysis. The advantage of this experimental technique over other previously described methods is that it facilitates prediction of more *realistic* diffusivity values by permitting the sample to be tested under the conditions of possible counter-diffusion as encountered in practical applications. The details of the experimental setup are illustrated in Figure 4.5.

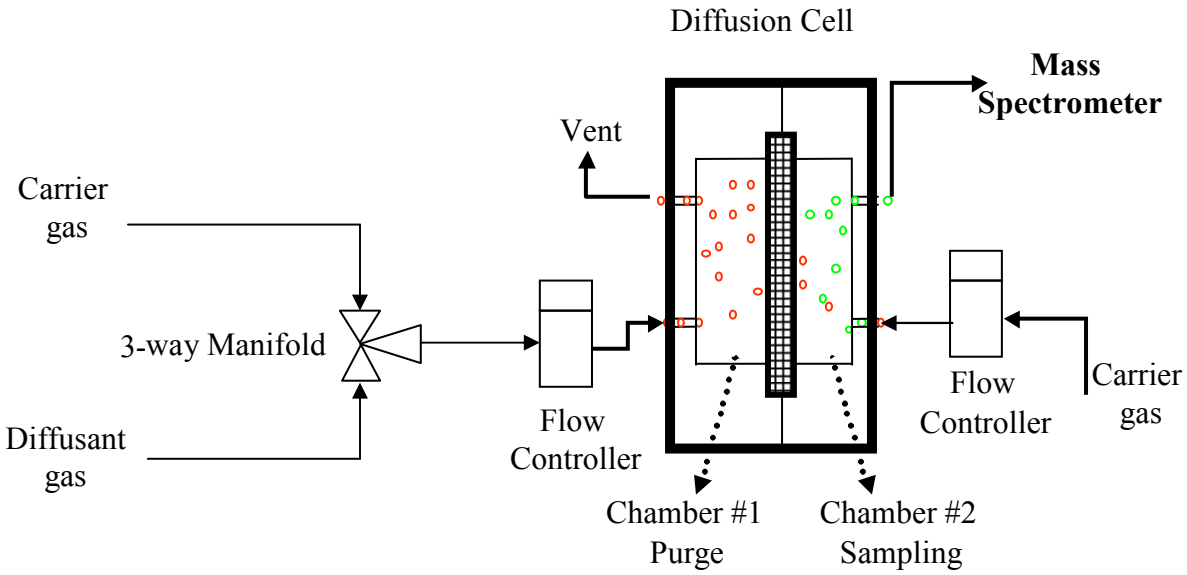

Figure 4.5: Continuous Flow–Zero net pressure gradient diffusion experimental setup. (Red circles represent purge gas and green ones represent carrier gas).

A simple diffusion experiment was performed to test for the presence of gas leaks in the diffusion cell. As a control, a thin aluminum foil was placed between the two chambers rather than a polymer film and the experiment was performed. Results showed no appreciable concentration change for argon in the sampling chamber for the entire experiment time, and hence it was concluded that the purge gas from Chamber 1 could enter Chamber 2 only through the membrane and not by convective leaks via O-ring seals or significant diffusion through the elastometric O-rings.

In order to minimize the effects of time lag in the purge gas transmission line and Chamber 1 volumetric capacitance, a series of diffusion experiments were carried out with varying diffusant gas flow rates. No appreciable changes in the dynamics of the

diffusion curve at flow rates of 50 sccm and above were noted. Hence, for all diffusion runs performed in this study, the diffusant gas flow rate was maintained constant at 75 sccm throughout the experiment. The carrier gas flow rate on the sampling side was maintained at 10 sccm in order to have low signal to noise ratio.

4.5. Mathematical Modeling

Data collected using the external mass spectrometer reflects the capacitance of the sample and Chamber 2. Hence, the mathematical model should incorporate both the sample and Chamber 2 dynamics. A simple mass balance equation was written over Chamber 2 for the diffusing gas assuming continuous-stirred-tank conditions. The gaseous diffusant enters Chamber 2 primarily by diffusive flux through the polystyrene sample and by convective transport of the carrier gas since a trace amount of diffusant is present in the carrier gas as contaminants. In the case of foam, in addition to molecular diffusion through the solid polymer membrane, the diffusant also transits through numerous interconnected percolated pathways present inside the foam, see Figure 4.2b.

At time t = 0, the concentration in Chamber 2 was set equal to the diffusant concentration in the carrier gas which is very small, on the order of a few ppm's. As the gas diffuses through the membrane and enters Chamber 2, it mixes with the carrier gas stream and exits Chamber 2 by convective carrier gas flow. This forms the basis for the following mole balance equation:

$$\textbf{Accumulation}_{Ch2} = \textbf{Moles } \textit{In}_{\text{ carrier}} + \textbf{Moles } \textit{In}_{\text{ Diffusion}} - \textbf{Moles } \textit{Out}_{\text{ Carrier}} \quad (4.5)$$

and is described by the following differential equation:

$$\frac{dC_2(t)}{dt} = F_{in}C_{in} - AD\left[\frac{\partial C}{\partial x}\right]_{x=L} - F_{out}C_2(t) \tag{4.6}$$

where L refers to the sample thickness, C is the concentration of the diffusant argon in the film, F_{in} is the flow rate of carrier gas into Chamber 2, C_{in} is the concentration of argon in the carrier gas, A is the cross-sectional area of diffusion, D is the diffusivity, F_{out} is the flow rate of gas from Chamber 2, and $C_2(t)$ is the concentration of argon inside Chamber 2 at any time t.

As noted earlier in Section 4.2, diffusion through polymers is usually interpreted by solving the time-dependent diffusion equation with appropriate boundary and initial conditions and is often referred to as the "continuous diffusion" model in the literature [4.15]. Analytical solutions to the diffusion equation for various conditions can be found in the literature [4.20]. Because of the nature of the *current* experimental setup, the boundary conditions are more complex and hence only a numerical solution has been provided. The diffusive flux term in Equation (4.6) (second term on right-hand side) is obtained by solving the transient Fick's diffusion model shown below. This equation was coupled with the above mass balance equation, from which the diffusivities were then estimated.

$$\frac{\partial C}{\partial t} = D\frac{\partial^2 C}{\partial x^2} \tag{4.7}$$

The initial and boundary conditions are $C = 0$ at $t = 0$, $C = H_0C_1$ at $x = 0$ and any t, and $C = H_LC_2(t)$ at $x = L$ and any t. Here, C_1 is the concentration of gas in Chamber 1, $C_2(t)$ is the concentration of gas in Chamber 2 at any time t, H_0 is the Henry's constant at $x = 0$, and H_L is the Henry's constant at $x = L$. In the case of foams, D would represent an effective diffusion coefficient, symbolized as D_{eff} throughout this manuscript.

The concentration of the diffusant on the sample boundaries is expressed in terms of the chamber gas concentrations just outside the film, related using Henry's solubility law. Upon discretization, Equations (4.6 and 4.7) yield a solution for the Chamber 2 gas concentration and profile within the polymer sample. Using the experimental and simulated data, diffusivity values for film and foam could be obtained by minimizing the objective function, $\gamma = \sum_t \left(C_2{}^M - C_2{}^E\right)^2$, where $C_2{}^M$ refers to the concentration predicted using Equations (4.6 and 4.7) and $C_2{}^E$ is the experimental data.

In order to estimate experimental foam diffusivity values, a discrete multiscale model including the gas phase molecular diffusivity, Knudsen diffusivity, membrane phase molecular diffusivity, and morhphological parameters was formulated. In the development of this model, the fused portion of the foam network is described using Pilon et al.'s structure for an *idealized* foam [4.2]. In addition, the presence of cylindrical intercellular pores that tunnel through the foam from one end to the other were included to account for the voids, see Figure 4.6. The pores are assumed to be straight and extend throughout the length of the foam (T_{fo}).

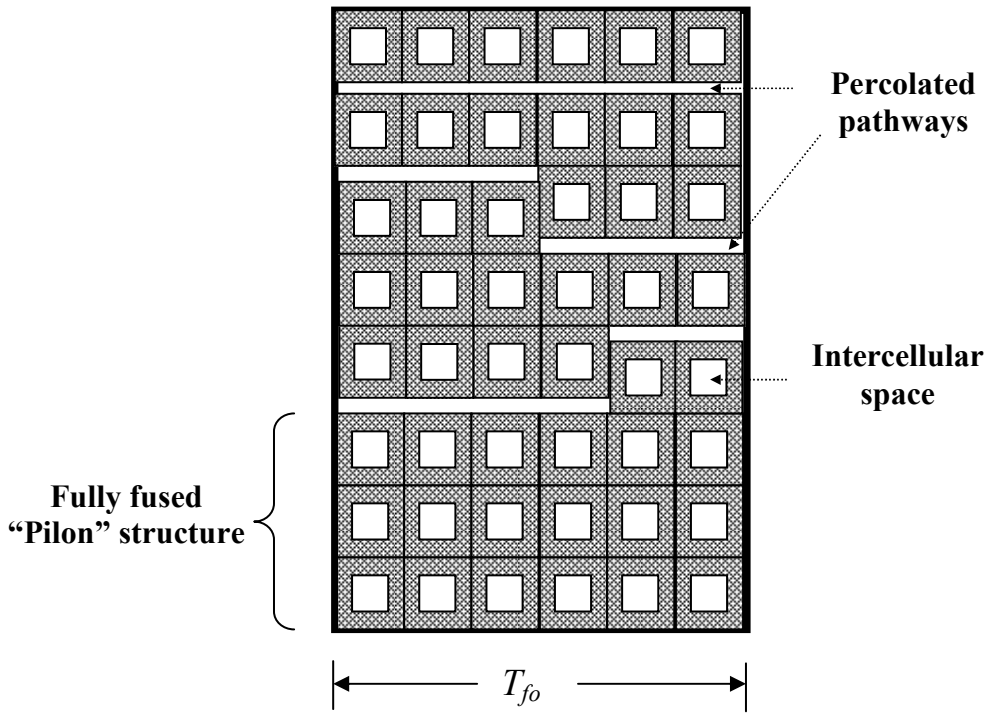

Figure 4.6: Schematic of a simplified model of foam architecture proposed in this study.

Depending on the size of the pore, Knudsen diffusion (D_k) and/or gas phase molecular diffusion (D_{AB}) might control diffusive transport through the intercellular pores. D_k is related to the pore radius using the following relationship:

$$D_k = \frac{2}{3} R_p \sqrt{\frac{8RT}{\pi M}} \tag{4.8}$$

where R_p is the radius of the cylindrical pore, and M is the molecular weight of the diffusant, argon in this case. Knudsen diffusion is pre-dominant when pore sizes are of the order of diffusing gas mean-free path. Hence, the contribution from Knudsen type diffusion to the overall diffusion is negligible. Since observed pores are much larger than

the mean-free path at the experimental temperature and pressure. On the other hand, gas phase molecular diffusivity accounts for collisions between molecules and could be estimated from the Chapman–Enskog formula [4.22]:

$$D_{AB} = 1.858 \times 10^{-3} T^{3/2} \sqrt{\frac{M_A + M_B}{M_A M_B}} \frac{1}{P \sigma_{AB}^2 \Omega_D} \tag{4.9}$$

where M refers to the molecular weight of the compound, subscripts A an B refer to the two gases argon and nitrogen, T is the temperature in K, P is the pressure in atmospheres, σ_{AB} is the characteristic length (collision diameter) in Angstroms, and Ω_D is the dimensionless diffusion colision integral. Details including parameter values for argon and nitrogen† could be found in the literature [4.21]. The gas molecular diffusivity for the argon-nitrogen system was thus calculated to be ca. 1.93E-05 m^2/s.

By using an electrical analogy of parallel resistances as demonstrated by Ostrogorosky [4.22] and Pilon [4.2], the effective foam diffusivity (D_{eff}) could be written as

$$D_{eff} = D_p f_p + D_{AB} f_{AB} \tag{4.10}$$

where D_p refers to the effective diffusivty predicted from Pilon's model, refer to Equation (4.3), D_{AB} refers to the gas phase molecular diffusivity of argon in nitrogen, and the "f" terms represent the corresponding fractional contributions of each diffusivity. These individual fractional diffusion contributions could *best* be described as the

fractional cross-sectional areas normal to diffusion that corresponds to that particular diffusion type. Substituting Equations (4.3 and 4.9) in the above equation, the effective diffusion coefficient could be written in terms of morphological and individual diffusivities as shown below.

$$D_{eff} = \left(G(\phi, n) D_f\right) f_p + \left[1.858 \times 10^{-3} T^{3/2} \sqrt{\frac{M_A + M_B}{M_A M_B} \frac{1}{P \sigma_{AB}^2 \Omega_D}}\right] f_{AB} \qquad (4.11)$$

Using the experimental values and the above-mentioned multiscale model in conjunction with Equation (4.7), values for effective foam diffusivity, Henry's parameters, and fractional contributions for each diffusivity type was estimated.

4.6. Results and Discussion

Figures (4.7 (normalized data with model predictions) and 4.8 (raw data)) show a series of gas diffusion curves for various polystyrene film thicknesses where diffusant concentrations were plotted as a function of diffusion time. The dimensionless concentration values are the raw data collected from diffusion experiments and the normalized values for each thickness were calculated by using their corresponding minimum and maximum values. As it can be seen from Figure 4.7, the model fits well to the experimental data when the three parameters, namely the diffusivity (D), time delay (an empirical factor), and the two Henry's parameters (H_0 and H_L) were optimized, see values reported in Table 4.1. The average film diffusivity value (4.5E-12 m^2/s, not

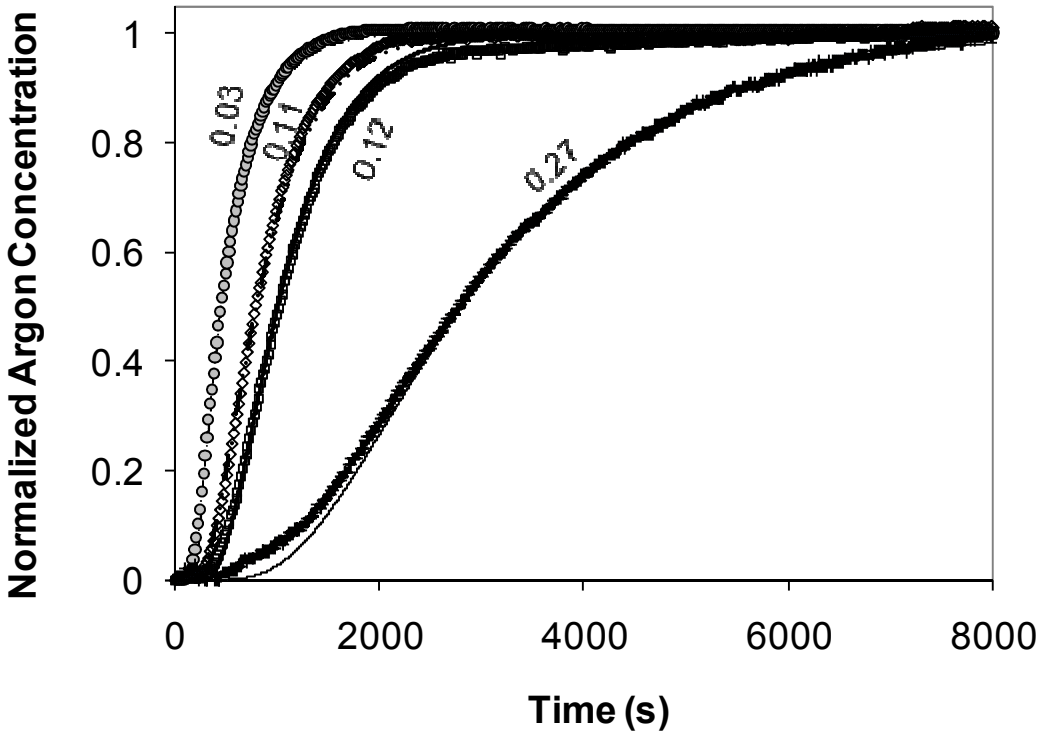

Figure 4.7: Argon gas diffusion through PS films of various thicknesses of 0.03, 0.11, 0.12, and 0.27 mm. Experimental values are characterized by symbols and model predictions by solid lines.

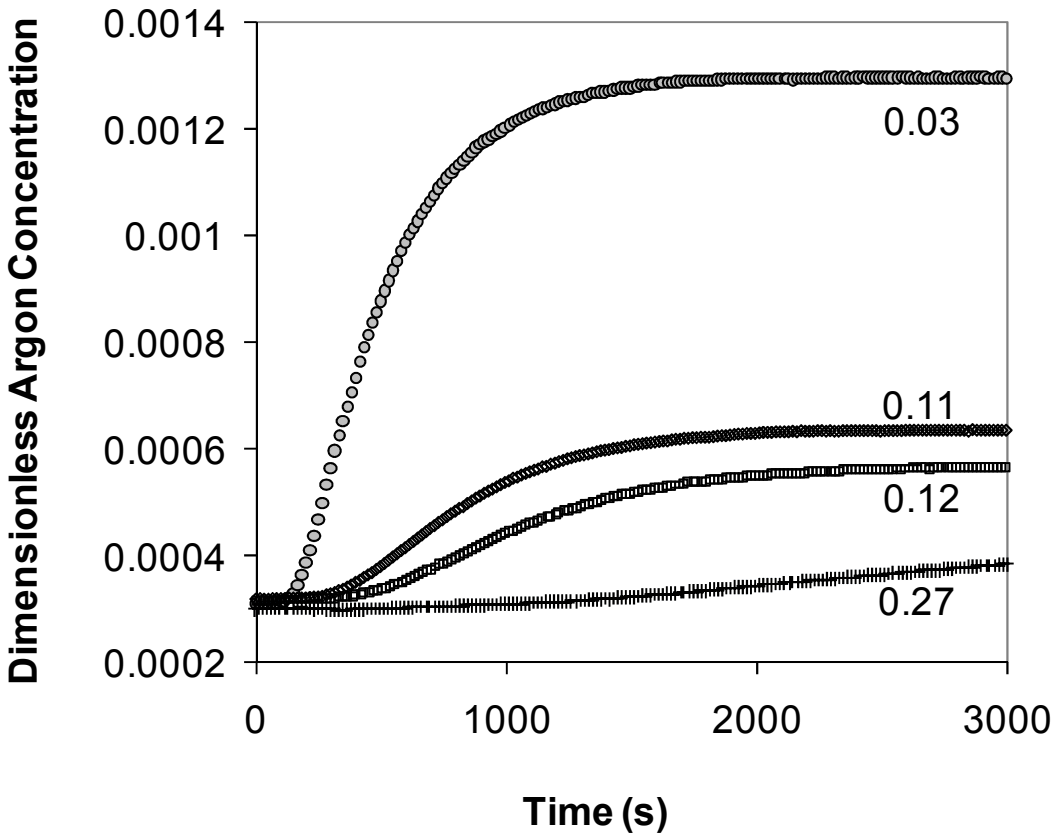

Figure 4.8: Dimensionless gas concentration versus time through PS films of thicknesses, 0.03, 0.11, 0.12 and 0.27 mm.

Table 4.1: Experimental diffusivity values of argon diffusion in polystyrene films

Sample	Thickness (mm)	D (m^2/s)	σ_D	H_0 (cc.atm/g)	σ_{H0}
PS film	0.03	7.5E-12	9.11E-14	0.081	0.003198
PS film	0.11	4.98E-12	1.24E-13	0.136	0.005792
PS film	0.12	4.36E-12	4.51E-13	0.143	0.012142
PS film	0.27	4.40E-12	2.71E-13	0.171	0.004811
EPS foam	10	5.40E-07	4.97E-07	2.796	0.45286

including the 0.03 mm film) is in good agreement with the only other known experimental value of 4.1E-12 m^2/s for argon in polystyrene [4.6], wherein argon diffusion was observed through a 40 μm thick cast film. The reason for relatively higher diffusivity value reported for 0.03 mm film is not clear at this point. However, it is notable that all experimental values distinctly differ from the theoretical diffusivity of 5.8E-09 m^2/s calculated using "free volume" theory, refer to Section 4.2. The value of the Henry's parameter on the sampling side of the film (H_L) was found to be nominally zero (and hence is not reported), likely because the partial pressure of argon in Chamber 2 is small when compared to that of Chamber 1, whereas the values of H_0 seems to be in good agreement with the literature values of about 0.09 cc(STP)-atm/g reported by Durrill et al. [4.23] for molten polystyrene films.

Figure 4.9 shows a plot of dimensionless argon concentration as a function of time for a 1 cm EPS foam test sample. The model curve is simulated using a similar optimization technique that was demonstrated earlier for films, and the values are reported in Table 4.1. All the standard deviations reported in Table 4.1 are based on multiple experimental runs using different samples. It could be seen from the reported values that the variations between individual runs are very minimal and, hence defines the accuracy of the values. This is also evidenced in Figures 4.10 and 4.11 where reproducibility of the diffusion experiments has been illustrated for film and foam respectively.

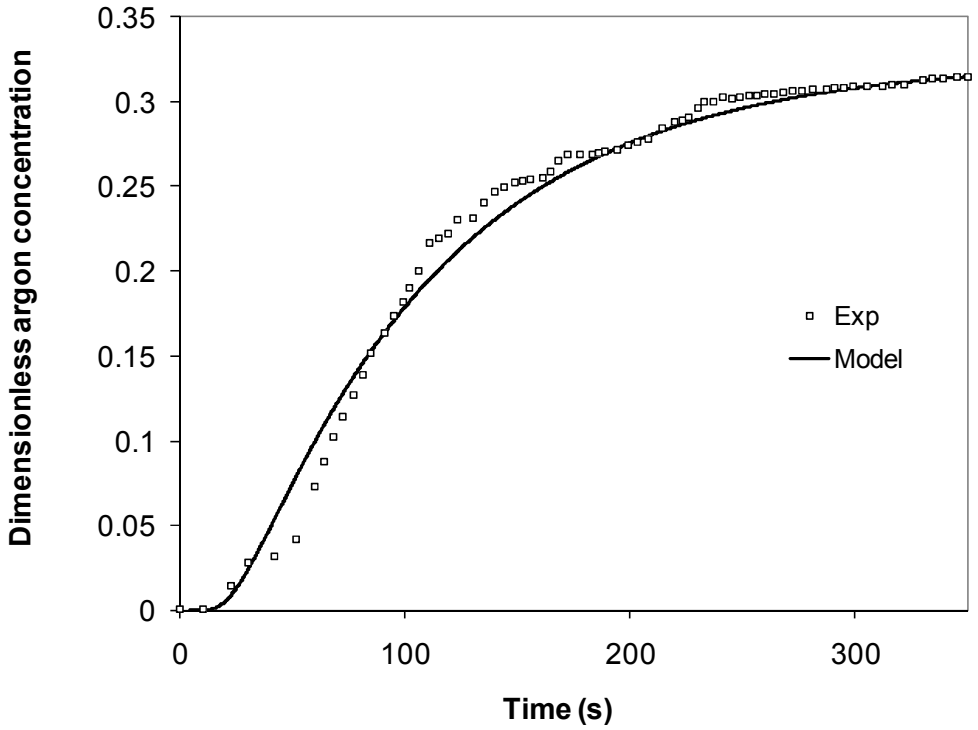

Figure 4.9: Argon gas diffusion through 1 cm thick EPS foam – Comparison of experimental vs. model predictions.

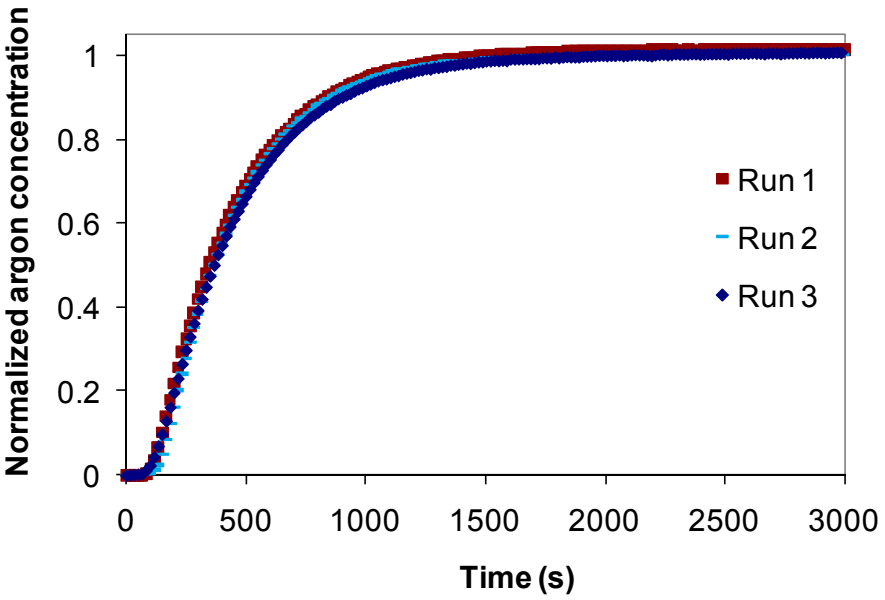

Figure 4.10: Reproducibility test for film experiments using 0.03 mm film at three individual runs.

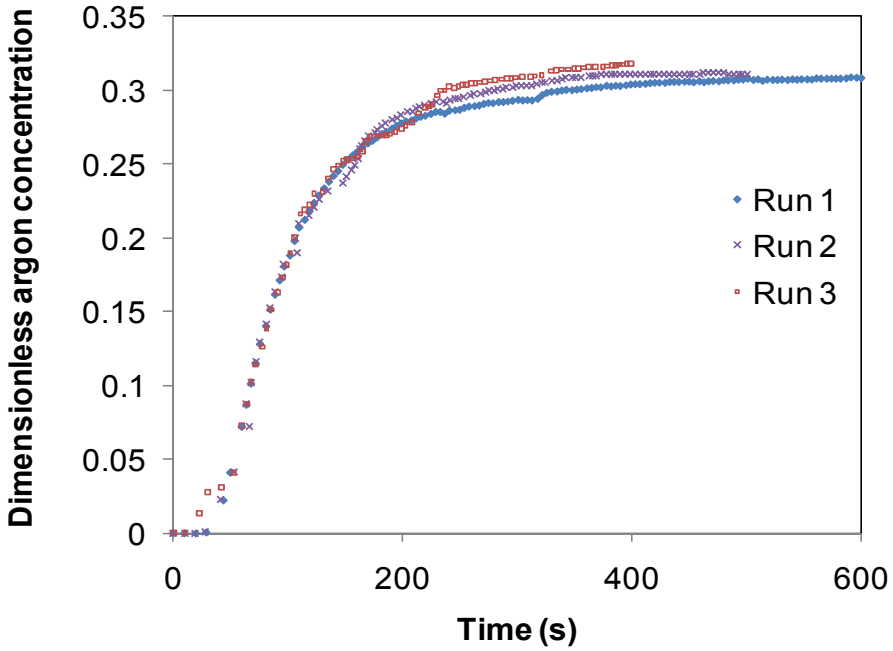

Figure 4.11: Reproducibility test for foam experiments using a 1 cm thick EPS sample.

It could be noticed from Figures 4.8 and 4.9 that the concentration of diffusant is much higher for foam samples than any of the films. Such a huge mass flux within the foam network seems clearly impossible, if the foam is represented as a simple arrangement of cubic cells similar to Pilon's model [4.2]. In other words, such high fluxes cannot be achieved only through molecular diffusion in the polymer membrane. There seems to be significant contribution from other diffusion types occurring in the pore region that is discussed in the following section. Hence, pore diffusion appears to play a major role in gas transport phenomena through these foams. It could be noticed from Figure 4.2 that the size of the pores could be as large as 1000 μm, and distributed randomly throughout the foam network. The size and pore distribution depends on the bead fusion level during the molding process [4.4]. Thus, the effective diffusion coefficient depends on the size and number of such pores present in the sample.

From diffusion experiments, the value of effective diffusivity was estimated to be 5.4E-07 m^2/s. Since both film diffusivity (~10^{-12} m^2/s) and geometric factor (~17 (for n = 1) to 0.017 (for n = 1000)) are relatively small, the fraction contributed by Pilon's diffusivity (~10^{-11} to 10^{-14}) is negligible. The value of "Pilon's structure" volume, refer Figure 4.6, was found to be 97% and, hence, the void volume is equal to 3%. These values imply that ca. 97% of the foam cross-sectional area is accounted in cells and the rest, 3% constitutes the intercellular area comprised of empty interconnected pores and channels. It has been reported in literature [4.4] that the void volume between beads is in the range of 0.5 to 1% of the total volume. Considering the heterogeneity of the foam sample, it is very difficult to measure the void volume experimentally and, hence, the deviation is not so significant. Therefore, the effective foam diffusivity estimated using

the multiscale model proposed in this study reflects the apparent foam diffusivity. The value of Henry's parameter for foams reported in Table 4.1 is much higher than that of the films. This might be due to a larger polymer exposed area in foams due to the porous nature of the cells.

Finally, it can be seen from Figures 4.9 and 4.11 that the shape of the experimental curves is not smooth, and seems to be perturbed. This is possibly due to the heterogeneous nature of the foam network that provides alternate pathways for diffusion. The random distribution of the percolated pathways present within the foam network, see Figure 4.6, *short circuits* the diffusing molecules, thereby distorting the Fick*ian* flow. Thus, the diffusion dynamics is significant in understanding the microstructure of the foam pattern.

4.7. Conclusions

The unique methodology that utilizes both the continuous and discrete multiscale diffusion models has been successfully demonstrated for predicting effective foam diffusivities and morphological parameters. A continuous gas flow experimental method was developed for obtaining gas diffusion information through monolithic polystyrene films and expanded polystyrene foams. More importantly, the experimental method permits to conduct diffusion experiments and collect data under conditions that are encountered in practical situations. Although the theoretical foam diffusivity value was validated by experimental technique, the morphological parameters were validated with

the available, yet limited literature data. The effective diffusivity values estimated in this study are realistic than values reported in literature as it accounts for the intercellular defects present in the foam. This study also illustrates the significant effect of other possible multiscale diffusion mechanisms, and a technique to formulate and bridge them together to predict effective foam diffusivity. Better characterization of the foam morphological parameters using high-resolution microscopic techniques will help to validate the multiscale model estimates. Furthermore, a real multiscale technique, such as cellular automaton would serve as an effective tool for studying such complex heterogeneous materials.

4.8. ENDNOTES

4.1. C.E. Bates, J. Griffin and H. Littleton, Expendable Pattern Casting-Process Manual, AFS publication, 1994.

4.2. L. Pilon, A. G. Fedorov, and R. Viskanta, J. Cellular Plastics, 36 (2000) p. 451.

4.3. K. Currie, G. Walford, M. Abdelrahman, F. Vondra, and M. Renfro, AFS Transactions, 05-102 (2005) p. 1.

4.4. G. V. Walford, J. J. Frafjord, and S. P. Dekanvich, Inframation Proceedings, ITC 126 A, (2008).

4.5. S. S. Dhingra, Mixed gas transport study through polymeric membranes: A novel technique, Ph.d dissertation, Virginia Polytechnic Institute and State University (1997).

4.6. K. Haraya and S. T. Hwang, J. Membrane Sci., 71 (1992) p.13.

4.7. K. Ganesh, R. Nagarajan, and J. L. Duda, Ind. Eng. Chem. Res., 31 (1992) p. 746.

4.8. A. Bondi, J. Phys. Chem., 68 (1964) p. 441.

4.9. W. M. Lee, Polymer Engineering and Science, 20 (1980) p. 65.

4.10. J. R. Booth and T. J. Holstein, J Thermal Insul. And Bldg. Envs., 16 (1993) p.246.

4.11. R.A. Pasternak, J.F. Schimscheimer, and J. Heller, J. Poly. Science, 8 (1970) p. 467.

4.12. R. M. Felder, R. D. Spence, and J. K. Ferrell, J. App. Poly. Science, 19 (2003) p. 3193.

4.13. T. M. Aminabhavi, U. S. Aithal and S. S. Shukla, Macromol. Chem. Phys., C28 (1988) p. 421.

4.14. R. Gendron, Thermoplastic foam processing: Principles and Development, CRC Press LLC, New York (2005).

4.15. S. Alsoy, J. Cellular Plastics, 35 (1999) p. 247.

4.16. E. F. Cuddihy and J. Moacanin, J. Cellular Plastics 3 (1967) p. 73.

4.17. B. S. Mehta, and E. A. Colombo, Society of Plastics Engineers, Annual National Technical Conference. 24 (1978) p. 689.

4.18. M. Svanstrom, O. Ramnas, M. Olsson, and U. Jarfelt, Cellular Polymers, 16 (1997) p. 182.

4.19. F. J. Norton, J. Cellular Plastics, 18 (1982) p. 300.

4.20. J. Crank, The mathematics of diffusion, Oxford University Press, London (1975).

4.21. R. C. Reid, J. M. Prausnitz and T. K. Sherwood, The properties of gases and liquids, McGraw-Hill Book Company, U.S.A. (1977).

4.22. A. G. Ostrogorsky and I. R. Glicksman, J. Cellular Plastics, 24 (1988) p. 215.

4.23. P. Durrill and R. Griskey, AIChE Journal, 12 (1966) p. 1147.

SUMMARY

EPS pyrolysis and gas diffusion phenomena through polymeric foams synthesized with EPS were investigated in this study. Laboratory-scale kinetic experiments (both *low* and *high* heating rates) were carefully designed to collect pyrolysis data that were later used to estimate values for kinetic parameters, including activation energy and pre-exponential constant. During the course of this study, a simple, yet effective, *fast* pyrolysis technique has been demonstrated for studying decomposition kinetics of various materials, including polymers and bio-mass. Diffusion studies focused towards understanding the gas diffusion behavior through expanded polymeric foams from a *multiscale* perspective. An experimental technique was developed to collect gas transmission data for both monolithic polymer films and expanded foams. An existing coarse multiscale model available in the literature was further developed to account for the diffusion anomalies due to certain morphological features of the foam. The experimental data was utilized to validate the multiscale behavior and estimate the fractional contribution of the individual diffusion mechanisms. Results highlight the significance of the multiscale model in exploring and understanding the microstructure of the foam.

The findings from these works could be collectively used in conjunction with the LFC overall process models for process development resulting in energy savings and better quality castings.

VITA

Pravin Kannan was born in Salem, India, on April 1, 1978. He completed his schooling from Vijay Vidyalaya Higher Secondary School in May 1995. Soon after that he joined Annamalai University, Chidambaram, and graduated in May 1999 with a Bachelor of Engineering and Technology degree in Chemical Engineering.

He joined the graduate program in Chemical Engineering at Tennessee Technological University, Cookeville, Tennessee, in August 2000 where he completed his Master of Science degree in August 2002. As part of the program, he undertook a co-op assignment with Packaging Corporation of America at Counce, TN. Later, he joined back into the graduate program at Tennessee Technological University in June 2004 and received his Doctorate of Philosophy in Engineering in May 2009.